DIFFERENTIAL ANALYSIS OF GPCR-INDUCED DYNAMIC CONFORMATIONAL CHANGE IN β-ARRESTIN1 AND 2

Vergleichende Untersuchungen zu GPCR-induzierten dynamischen Konformationsänderung in β-arrestin1 und 2

Dissertation

Zur Erlangung des akademischen Grades

Doctor rerum naturalium (Dr. rer. nat.)

Vorgelegt dem Rat der medizinischen Fakultät
der Friedrich-Schiller-Universität Jena

von Raphael Silvanus Haider, M.Sc.

geboren am 28.04.1991 in Linz, Österreich

Gutachter *(akademischer Grad, Vor- und Nachname sowie Wirkungsort)*

1. **Prof. Dr. Carsten Hoffmann, Universitätsklinikum Jena**

2. **Prof. Dr. Stefan Schulz, Universitätsklinikum Jena**

3. **Prof. Dr. Meritxell Canals Buj, University of Nottingham**

Tag der öffentlichen Verteidigung: 15.03.2022

Table of contents

Abbreviations

AC	adenylate cyclase
ACh	acetylcholine
ACKR3	atypical chemokine receptor 3
ADGRL1	latrophilin-1
ANOVA	analysis of variance
AP2	adaptor protein 2
AU	arbitrary units
BRET	bioluminescence resonance energy transfer
cAMP	cyclic adenosine monophosphate
Cas9	CRISPR-associated protien 9
CFP	cyan fluorescent protein
CRISPR	clustered regularly interspaced short palindromic repeats
CyOFP1	cyan-excitable orange fluorescent protein 1
cyro-EM	cryo-electron microscopy
Da	Dalton
DAG	diacyl glycerol
DAMGO	[D-Ala^2, N-MePhe^4, Gly-ol]-enkephalin
dFLR	deleted finger loop region
DMEM	Dulbecco's modified Eagle medium
DMSO	dimethyl Sulfoxide
EC_{50}	half maximal effective concentration
EDT	ethan-1,2-dithiol
EDTA	ethylenediaminetetraacetic Acid
ER	endoplasmic reticulum
ERK1/2	exctracellular signal-regulated kinase 1/2
EV	empty vector (pcDNA3)
FCS	fetal calf serum
FDA	food and drug administration
FlAsH	fluorescine aresenical hairpin-binder
FLR	finger loop region
FRET	Förster resonance energy transfer
FZD1	frizzled-1
GDP	guanosine diphosphate
GEF	guanine nucleotide exchange factor
GFP	green fluorescent protein
GPCR	G protein-coupled receptor
GRK	G protein-coupled receptor kinase
GTP	guanosine triphosphate
HEK293	human embryoinc kidney 293
HEPES	hydroxyethylpiperazine ethane sulfonic acid
HTTP	high throughput
IP_3	inositol triphosphate
Iso	isoproterenol
k_{cat}	enzymatic rate constant
kDa	kilo Dalton
LB	lysogeny broth
M1R	muscarinic acetylcholine receptor M1
M2R	muscarinic acetylcholine receptor M2
M3R	muscarinic acetylcholine receptor M3
M4R	muscarinic acetylcholine receptor M4
M5R	muscarinic acetylcholine receptor M5
MAPK	mitogen-activated protein kinase
MEK	mitogen-activated protein kinase kinase
mGluR1	metabotropic glutamate receptor 1
MOP	μ-opioid receptor

N/A	not available
NanoLuc	nano Luciferase
NCBI	National Center for Biotechnology Information
NMR	nuclear magnetic resonance
ns	not significant
NTSR1	neurotensin receptor 1
PBS	phosphoate-buffered saline
PCR	polymerase chain reaction
PD	phosphorylation deficient
PDB	protien data bank
PEI	polyethylenimine
Pi	inorganic phosphate
PIP_2	phosphoatidylinositol 4,5-bisphosphate
PKA	protein kinase A
PKC	protein kinase C
PLCβ	phospholipase Cβ
pp	phosphopeptide
P-R	phosphorylated inactive receptor conformation
P-R*	phosphorylated active receptor conformation
PTH	parathyroid hormone
PTH1R	parathyroid hormone receptor 1
PTHrP	parathyroid hormone related peptide
R	inactive receptor conformation
R*	active receptor conformation
Ras	rat sarcoma
Rho	rat sarcoma homologue
Rho	rhodopsin
rLuc	renilla luciferase
RTK	receptor tyrosine kinase
S_0	ground quantum state
S_1	excited quantum state
SEM	standard error of the mean
shRNA	short hairpin ribonucleic acid
siRNA	short interfering ribonucleic acid
SMO	smoothened
TasR1	taste receptor type 2 member 1
V2R	Vasopressin receptor 2
WT	wild type
YFP	yellow fluorescent protein
β1ADR	$β_1$ adrenergic receptor
β2ADR	$β_2$ adrenergic receptor
βarr1	β-arrestin1
βarr2	β-arrestin2
ΔGRK2	HEK293 with GRK2 knockout
ΔGRK2/3	HEK293 with GRK2/3 knockout
ΔGRK2/3/5	HEK293 with GRK2/3/5 knockout
ΔGRK2/3/6	HEK293 with GRK2/3/6 knockout
ΔGRK2/5/6	HEK293 with GRK2/5/6 knockout
ΔGRK3	HEK293 with GRK3 knockout
ΔGRK3/5/6	HEK293 with GRK3/5/6 knockout
ΔGRK5	HEK293 with GRK5 knockout
ΔGRK5/6	HEK293 with GRK5/6 knockout
ΔGRK6	HEK293 with GRK6 knockout
ΔQ-GRK	HEK293 with GRK2/3/5/6 knockout

Summary

G protein-coupled receptors (GPCRs) constitute the largest family of membrane receptors in human physiology, comprising more than 800 different genes. They sense diverse extracellular signals and initiate intracellular signaling responses via the activation of specific G proteins. The downregulation of GPCR signaling is mediated by four ubiquitously expressed GPCR kinases (GRK2, 3, 5, and 6) and two β-arrestin isoforms (β-arrestin1 and 2). GRKs phosphorylate intracellular domains of active receptors to facilitate high-affinity β-arrestin-binding. Depending on the specific GPCR–β-arrestin interaction, β-arrestins undergo different conformational changes to mediate receptor desensitization, internalization, and mitogen-activated protein kinase (MAPK) signal-amplification. However, the impact of individual GRK isoforms on these processes has not been comprehensively assessed until now. Moreover, whether β-arrestin1 and 2 undergo different conformational changes upon binding to the same GPCR is still unknown.

The first part of this thesis focusses on the elaboration of GRK isoform-specific aspects of GPCR signaling. For this, a panel of elven in-house created combinatorial HEK293 knockout cell clones, lacking GRK2/3/5/6 (including four single, two double, four triple, and a quadruple GRK knockout cell line), was extensively used. To investigate GRK isoform-specific β-arrestin recruitment, a NanoLuc–HaloTag-based BRET system was established and combined with the unique possibility to vary individual GRK expression levels using different ΔGRK knockout cell lines. Hence, the GRK-specificity of β-arrestin-binding was assessed with two different strategies: first, utilizing the triple GRK knockout cell lines, featuring the endogenous expression of only one GRK isoform (ΔGRK3/5/6, ΔGRK2/5/6, ΔGRK2/3/6, ΔGRK2/3/5), and additionally by re-introduction of a single GRK isoform in the quadruple GRK knockout cell line (ΔQ-GRK). These experiments revealed that different GPCRs require certain levels of GRK expression for high-affinity arrestin-binding. The overexpression GRK2 facilitated stable β-arrestin recruitment for all tested receptors. Yet, the endogenous expression level of GRK2 in the ΔGRK3/5/6 cell line was able to induce β-arrestin-binding at the parathyroid hormone 1 receptor (PTH1R) but failed to mediate this interaction for the β_2 adrenergic receptor (β2ADR).

By analysis of GRK-specific β-arrestin1 and 2 interactions for ten different GPCRs, two main receptor subsets were identified: GRK2/3-regulated and GRK2/3/5/6-regulated

receptors. Interestingly, also receptors that are primarily regulated by other intracellular kinases can be identified using this strategy, as they do not show significant differences between the kinase-specific conditions. Two model receptors that show differential GRK-specificity, namely, the PTH1R (regulated by GRK2, 3, 5, and 6) and the muscarinic acetylcholine receptor 5 (m5AChR, regulated by GRK2 and 3) were furthermore assessed using confocal microscopy. This analysis confirmed the initially found GRK-specificity of GPCR regulation and disclosed that receptor internalization is dependent on the same GRK isoforms as β-arrestin recruitment. Additionally, the established system provides the unique opportunity to assess the subtype-specificity of pharmacological GRK inhibitors in living cells.

In the second part of this thesis, an advanced set of NanoLuc/FlAsH-based β-arrestin1 and 2 biosensors was created. These sensors revealed the comprehensive signature of conformational changes for both isoforms when bound to the PTH1R (P-R*). Analysis of these conformational “fingerprints” disclosed crucial differences between the two β-arrestin isoforms in multiple positions, especially within their phosphorylation-sensing N-domains and the so-called C-edge regions. This approach was expanded to assess β-arrestin conformational changes that are induced by two phosphorylation-deficient PTH1R variants and in the absence of GRKs (R*). These measurements allowed for the differentiation between β-arrestin conformational changes induced by the P-R* or R* receptor states, and further discloses the impact of site-specific GPCR phosphorylation on arrestin-coupling. As a functional correlate, proximal receptor phosphorylation was shown to modulate β-arrestin-mediated receptor internalization and trafficking, whereas distal receptor phosphorylation was identified as the key factor to enable β-arrestin-facilitated MAPK signaling. Moreover, the conducted experiments provide evidence that β-arrestin1 is better suited to form a “hanging” complex, in comparison to β-arrestin2, which seems to prefer the formation of tight “core” complexes.

This study demonstrates that the GPCR phosphorylation state not only regulates differences in affinity between β-arrestin1 and 2 but also translates into specific conformational rearrangements that determine the functional diversity between the two isoforms.

Zusammenfassung

G-Protein-gekoppelte Rezeptoren (GPCRs) bilden mit ihren über 800 verschiedenen Rezeptoren die größte Familie von Membranrezeptoren im menschlichen Körper. Dabei nehmen sie unterschiedlichste extrazelluläre Signale wahr und übersetzen diese in intrazelluläre Signalantworten durch die Aktivierung von spezifischen G-Proteinen. Anschließend wird die GPCR-Signalgebung durch vier ubiquitär exprimierte GPCR-Kinasen (GRK2, 3, 5 und 6) und zwei β-arrestin Isoformen (β-arrestin1 und 2) reguliert. GRKs phosphorylieren intrazelluläre Domänen aktiver Rezeptoren, um schließlich die Bindung von β-arrestin zu ermöglichen. Durch diese Interaktion werden spezifische Konformationsänderungen in β-arrestin induziert, welche schließlich die Desensibilisierung, Internalisierung und mitogen-activated protein kinase (MAPK)-Signalgebung des Rezeptors beeinflussen und koordinieren.

Der erste Teil dieser Arbeit behandelt GRK Isoform-spezifische Aspekte der GPCR Regulierung. Hierfür wurden mehrere HEK293 basierte GRK2/3/5/6 Knockout Zellklone generiert (einschließlich vierer einfach-, zweier doppel-, vierer dreifach- und einer vierfach GRK Knockout Zelllinie) und in verschiedenen Versuchsaufbauen verwendet. Um zunächst die GRK Isoform-spezifische β-arrestin Rekrutierung verschiedener Rezeptoren zu untersuchen, wurde ein NanoLuc-HaloTag basiertes BRET System etabliert. Mit Hilfe der verschiedenen ΔGRK Knockout Zelllinien konnten nun die individuellen GRK Expressionsniveaus kontrolliert beeinflusst werden. Hierfür wurden zwei unterschiedliche Strategien angewandt: Erstens, unter Verwendung der dreifach GRK Knockout Zelllinien. Da diese Zelllinien lediglich die endogene Expression einer GRK Isoform aufweisen (ΔGRK3/5/6, ΔGRK2/5/ 6, ΔGRK2/3/6, GRK2/3/5) konnten somit die spezifischen Einflüsse endogen exprimierter GRKs untersucht werden. Zweitens wurden, durch Überexpression einzelner GRK Isoformen in der vierfach GRK Knockout Zelllinie (ΔQ-GRK), die molekularen Fähigkeiten dieser Kinasen, bei anzunehmender Sättigung des Systems, charakterisiert. Diese Experimente zeigten, dass verschiedene GPCRs unterschiedliche GRK Expressionsniveaus benötigen um stabile Komplexe mit β-arrestinen einzugehen. Durch die Überexpression von GRK2 konnte die β-arrestin Rekrutierung für alle getesteten Rezeptoren ermöglicht werden. Das endogene GRK2 Expressionsniveau der ΔGRK3/5/6 Zelllinie war, interessanterweise, ausreichend, um diese Interaktionen

für den Parathormon-1-Rezeptor (PTH1R) zu vermitteln, jedoch nicht für den β_2 adrenergen Rezeptor (β2ADR).

Durch die Analyse von β-arrestin1- und 2 Interaktionen mit zehn verschiedenen GPCRs konnten zunächst zwei Untergruppen identifiziert werden: GRK2/3-regulierte und GRK2/3/5/6-regulierte Rezeptoren. Zwei Modellrezeptoren mit unterschiedlicher GRK Spezifität, nämlich der PTH1R (reguliert durch GRK2, 3, 5 und 6) und der muskarinische Acetylcholin-Rezeptor 5 (m5AChR, reguliert durch GRK2 und 3), wurden weitergehend mit Hilfe konfokaler Mikroskopie untersucht. Dieser Versuchsaufbau bestätigte die GRK Spezifität dieser Rezeptoren und zeigte zusätzlich, dass deren Internalisierung von den gleichen GRK Isoformen vermittelt wird, die auch deren β-arrestin Kopplung ermöglichen.

Im zweiten Teil dieser Arbeit wurden neuartige, NanoLuc-FlAsH basierte β-arrestin1 und 2 Biosensoren entwickelt, um umfassend die Konformationsänderungen beider β-arrestin Isoformen für die Bindung an PTH1R (P-R*) zu charakterisieren. Durch diese Experimente konnten wesentliche Unterschiede zwischen den beiden β-arrestinen in mehreren strukturellen Positionen gefunden werden. Insbesondere innerhalb ihrer Phosphorylierungs-bindenden N-Domänen und den sogenannten C-edge Regionen unterscheiden sich die Konformationsänderungen zwischen β-arrestin1 und 2 demnach stark. Zusätzlich wurde dieser Ansatz erweitert, um Konformationsänderungen in β-arrestinen zu untersuchen, welche durch zwei phosphorylierungsdefiziente PTH1R Varianten, sowie in Abwesenheit von GRKs (R*), induziert werden. Diese Messungen ermöglichten erstmalig die Zuordnung von Konformationsänderungen, die durch die P-R*- oder R* Rezeptorzustände induziert wurden. Außerdem zeigte dieser Versuchsaufbau den Einfluss spezifischer GPCR-Phosphorylierung auf die β-arrestin Kopplung auf. Schließlich werden weiterführende Experimente präsentiert, die nahe legen, dass die proximale PTH1R Phosphorylierung primär die Internalisierung und den Transport von GPCRs moduliert, während die distale Rezeptor Phosphorylierung bestimmend für die β-arrestin ermöglichte Erhöhung des MAPK-Signals ist.

Zusammenfassend zeigt diese Studie, dass der GPCR Phosphorylierungszustand nicht nur über Affinitätsunterschiede zwischen β-arrestin1 und 2 entscheidet, sondern auch in spezifische Konformationen übersetzt wird, welche die funktionelle Diversität zwischen den beiden Isoformen bestimmen.

1. Introduction

Cells are some of the most fundamental entities of life. As one of their central features, they must separate themselves from their environment. Almost all organisms achieve this by employment of a phospholipid bilayer that keeps molecules from diffusing freely in and out of cells. This mechanism is especially important since cells operate with defined sets of functional molecules that require specific concentrations of salts, ions, and organic compounds. For cells to be able to respond to their environment, a multitude of different membrane proteins evolved. These large biomolecules are anchored at or incorporated in the cell membrane to facilitate the perception of extracellular stimuli or regulate the amounts of soluble components of the cytoplasm (Singer und Nicolson 1972).

As all mammalian proteins, they are composed of 20 different amino acids that are assembled at ribosomes in a specific sequence via peptide bonds. This process of protein biosynthesis gives rise to macromolecular structures that may contain up to several thousand amino acids. Characterized by their primary sequence, proteins fold due to the natural properties of the incorporated amino acid side chains or assisted by specific binding partners, chaperones, or post-translational modifications. The resulting natural shape, or conformation of a protein enables its specific functions. Importantly, proteins can adopt different conformations. These conformational states may enable or disable the functionality of the protein, but always exist side-by-side in a certain equilibrium (Vaidehi und Kenakin 2010, Gurevich und Gurevich 2017).

1.1 GPCRs and their intracellular signaling machinery

Cell surface receptors are membrane proteins that sense extracellular stimuli in order to invoke an intracellular response. The largest superfamily of cell surface receptors is constituted by G protein-coupled receptors (GPCRs), with more than 800 different genes encoded in the human genome (Fredriksson et al. 2003). They share a common structure that consists of an extracellular N-terminus, seven transmembrane helices that are connected by three intracellular and three extracellular loops, and an intracellular C-terminus. Due to these distinct structural features, GPCRs are often also referred to as seven-transmembrane (Pierce et al. 2002) or heptahelical receptors (Lefkowitz 2000).

The sheer number of different GPCRs that are present in human physiology directly reflects on the number of different stimuli that they perceive. These activating ligands, or stimuli include but are not limited to: photons, odors, neurotransmitters, hormones and chemokines. Thus, GPCR signaling is interlaced with most physiological processes that occur on an organism- or cellular scale. Moreover, GPCR signaling directly enables the sensory functions of vision, smell and taste (Lefkowitz 2013).

After the human genome was fully sequenced (Venter et al. 2001) and became available for researchers, Fredriksson *et al.* phylogenetically analyzed all identified human GPCR sequences. This led to a widely used categorization of GPCRs into 5 main families: glutamate, rhodopsin, adhesion, frizzled/taste2, and secretin, combined as the acronym GRAFS (Fredriksson et al. 2003). Although there are many other classification systems, this thesis will refer to the GRAFS classification unless specifically noted. A compiled list of important features of the different receptor families can be accessed via **Table 1.1**.

Table 1.1 Characteristics of GPCRs, classified by the GRAFS system
The presented information was compiled from Fredriksson *et al.* (2003) and Langstrom and Schioth (2008).

	Glutamate	Rhodopsin	Adhesion	Frizzled	Taste2	Secretin
number of family members	15	701	24	11	13	15
size of N-terminus	**large** ~280 – 580 amino acids	**short peptide stretches**	**very large** ~200 – 2800 amino acids	**large** ~200 amino acids	**short peptide stretches**	**mediocre** ~60 – 80 amino acids
favored type of ligand	amino acids, small organic compounds	nucleotides, small organic compounds, peptides	proteins	proteins	small organic compounds	peptides
prominent members	metabotropic glutamate receptor 1 (mGluR1)	rhodopsin, adrenergic-, adenosine-, muscarinic receptors	latrophilin-1 (ADGRL1)	frizzled-1 (FZD1) smoothened (SMO)	taste receptor type 2 member 1 (TAS2R1)	parathyroid hormone receptor 1 (PTH1R)

With 241 non-olfactory GPCRs and a total of 701 receptors, the rhodopsin family constitutes the largest group. Similar to the light-sensitive receptor rhodopsin itself, most rhodopsin-like receptors feature a small N-terminus (Fredriksson et al. 2003,

Lagerstrom und Schioth 2008). Grouping GPCRs in this classification can be useful to identify larger patterns, similarities or differences between the receptor families and emerging mechanisms that might hold true for all GPCRs. Nonetheless, even closely related GPCRs can exhibit very different characteristics, especially regarding their intracellular signaling. For a detailed evaluation, every GPCR must be seen and approached as an individual gene, evolved to fulfill specific tasks in a cellular context.

Due to their involvement in virtually all vital functions of the human body and since they are expressed at the cell membrane and readily associate with suitable small molecule ligands, GPCRs can be utilized as excellent drug targets. More than one third of all food and drug administration- (FDA) approved drugs target GPCRs directly (Hauser et al. 2017, Santos et al. 2017). These diverse active compounds act on GPCRs to modulate many different pathologies. They are widely used to relieve hypertension, allergic reactions or pain, but are also employed to tackle neurodegenerative disorders like Parkinson's and Alzheimer's disease or metabolic disturbances like diabetes and obesity (Hauser et al. 2017). However, still more than half of all non-olfactory GPCRs have not been addressed by specific therapeutic agents. This highlights the potential of basic and pharmaceutical GPCR research to further improve human health.

At the beginning of this ongoing pharmacological success story stands, of course, the elucidation of the basic functionality of GPCRs, their structural features and the modality of how their activity is regulated. To honor the most recent scientific achievements that shaped our understanding of the GPCR structure-function relationship, two inspiring scientists, namely Robert J. Lefkowitz and Brian K. Kobilka, were awarded the Nobel Prize in chemistry in 2012. Sections of their work and contributions of many other biologists, chemists and pharmacologists are compiled in the next chapters to appropriately introduce the functionality of GPCRs and some of their most prominent intracellular binding partners, β-arrestins.

1.1.1 GPCR structure-function relationship

Upon GPCR activation, which most commonly happens via binding of an agonist, the receptor undergoes large conformational changes (**Figure 1.1**). A side-by-side comparison of the inactive- (Cherezov et al. 2007) and active structure (Rasmussen et al. 2011) of the β_2 adrenergic receptor (β2ADR), as a prototypical GPCR of the rhodopsin family, is shown in **Figure 1.1 A**.

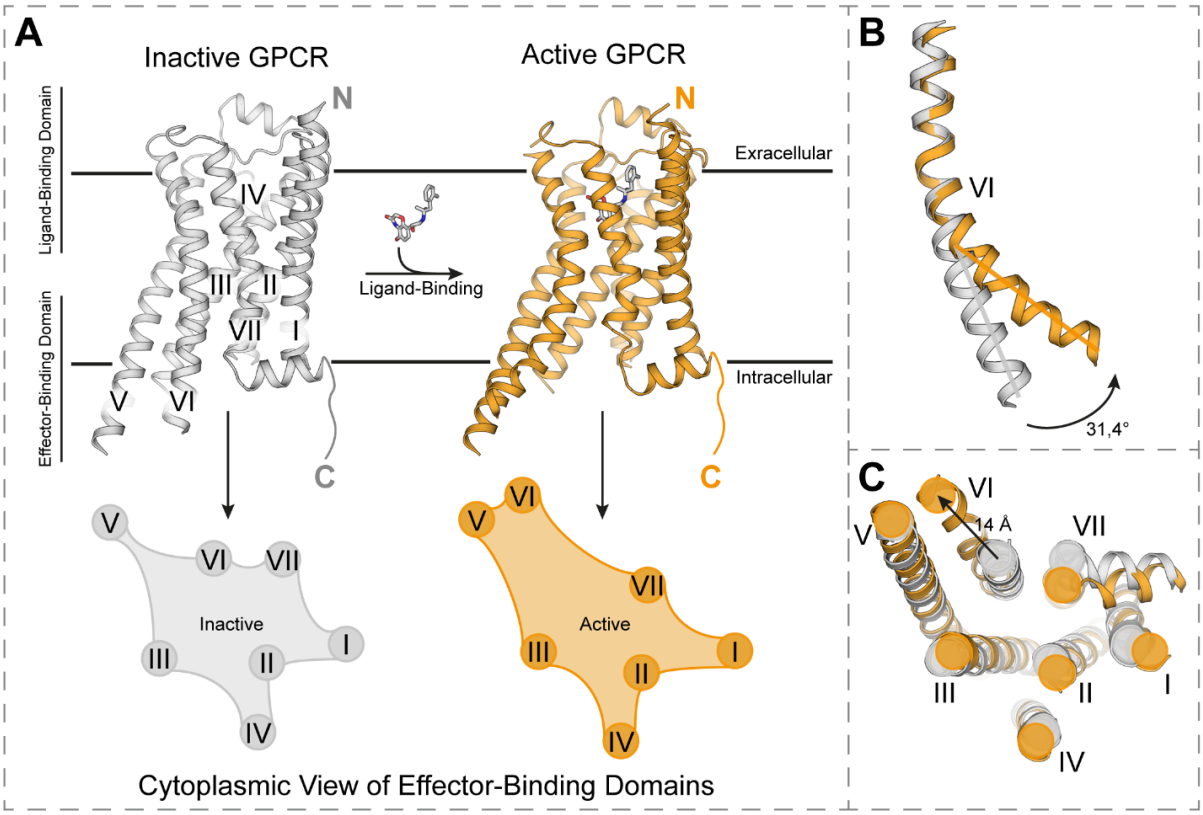

Figure 1.1 Structural consequences of GPCR activation

GPCRs are central signaling proteins that consist of seven α-helices, vertically embedded in cell membranes. **A** Shown are inactive (PDB: 2RH1) and active (ligand-bound, PDB: 3SN6) structures of the β_2 adrenergic receptor (β2ADR), as a prototypical GPCR of the rhodopsin family. The receptor domains facing the extracellular side can be considered canonical ligand-binding domains, whereas the intracellular receptor domains are responsible for effector-binding. Ligand-induced conformational changes of the receptor alter the geometry of the intracellular cavity, formed by the transmembrane helix bundle, to allow for high-affinity effector binding. This is schematically depicted below the respective GPCR structure. **B** Upon GPCR activation helix 6 undergoes large conformational changes. For the β_2ADR this results in a 31,4° outward movement. **C** Cytoplasmic view of an alignment of both crystal structures, visualizing the conformational changes of all helices upon ligand-binding. The most prominent movement (14 Å) is again found for helix 6.

With the help of the conformational changes that occur during the transition from an inactive to an active receptor state, GPCRs convey extracellular stimuli across the membrane. The seven transmembrane helixes of GPCRs are embedded in the plasma membrane and form a barrel-like structure. The extracellular side-facing part of GPCRs can be considered their canonical ligand-binding domain. With contributions of all seven transmembrane helices as well as the N-terminus and extracellular loops 1-3, GPCRs recognize and form tight interactions with their ligands. As these receptors have evolved to recognize a plethora of different stimuli, their ligand-binding domains also feature the highest amount of structural diversity between GPCR families (Katritch et al. 2012). This is especially highlighted as the N-terminus of most rhodopsin-like receptors only features a small unstructured peptide stretch, whereas GPCRs of other

families exhibit large globular domains (see also **Table 1.1**), often-times stabilized by disulfide bonds between cysteine residues located in the N-terminus and extracellular loops. During the association process between a receptor and its ligand, they (mostly) engage in reversible polar, hydrophobic, or hydrogen-bond interactions. Both binding partners mutually influence their conformations and relative orientations until a minimum of free energy is reached and a rigid receptor–ligand complex is formed (Alhadeff et al. 2018).

The conformational changes that occur in the ligand-binding domain during the formation of this complex are rather subtle when compared to the global conformational changes that happen in the protein. Especially, the intracellular side-facing part of the GPCR dramatically changes its geometry during activation. The sequence and structure of this canonical effector-binding domain is less diverse between GPCR families (Katritch et al. 2012), as GPCRs only operate with a limited amount of intracellular binding partners, in contrast to the large variety of extracellular stimuli they have to perceive.

Consequently, the smaller conformational changes that are induced near the ligand-binding domain are transmitted along the receptor molecule and finally evoke an opening of the barrel-like structure at the intracellular side. For the activation of most GPCRs, the largest movement of any structural feature is registered for transmembrane helix 6 (Katritch et al. 2013). The N-terminal cytosolic tip of helix 6 effectively bends away from the receptor core at a ~30° angle and performs an outward movement of up to more than 14 Å (**Figure 1.1 B, C**). This increases the accessible intracellular surface area of the receptor and creates a cavity, which is subsequently engaged by effector proteins to mediate intracellular signaling. To aid visualization of this process, a cytoplasmic view of the inactive and active receptor structure after alignment is shown in **Figure 1.1 C**. Additionally, schematic representations of the cytoplasmic surface areas with exact positions of the intracellular termini of helix 1-7 are shown for both respective receptor structures in **Figure 1.1 A**.

Interestingly, not only the outward movement of helix 6 seems to be strikingly well conserved across all GPCR families, but also the way it is achieved. Two integral “microswitches”, namely the D[E]RY and NPxxY motifs, aid in the stabilization of inactive and active configurations of the transmembrane helix bundle and feature amino acid positions that are up to 96% conserved among GPCRs (Katritch et al.

2013). The arginine residue of the D[E]RY motif (located in helix 3) can form salt bridges that stabilize the inactive positions of helix 3 and 6 relative to each other (Vogel et al. 2008). This interaction is also termed “ionic lock”, as it breaks apart during GPCR activation and further facilitates G protein-coupling of the active receptor (Rasmussen et al. 2011).

The NPxxY motif is located near the cytosolic end of helix 7 and facilitates stabilizing interactions with helix 1 and 2 in the inactive state of the receptor. Upon GPCR activation, the conserved tyrosine residue changes its rotamer conformation to rigidify the opening of the intracellular GPCR cavity via interactions with helix 3 and 6 (Katritch et al. 2013).

1.1.2 Signaling mediated by intracellular effectors and binding partners

The described transition process of GPCRs, as they change their conformation from an inactive to an active state, is the basis for our understanding of GPCR functionality. Whereas this binary model of a receptor “turning on and off” might hold true for snapshots of a single GPCR molecule, the reality of how different conformational states persist in a cellular context is highly dictated by probabilities.

The abundance of an individual protein in a given cell may range from a few molecules to up to more than 10^4 copies (Budnik et al. 2018, Ho et al. 2018). Each individual receptor molecule may probe for inactive or active conformations spontaneously and by now it is even clear, that a single receptor may adopt different inactive conformations (Manglik et al. 2015). Following this, the entirety of expressed GPCRs exists in a conformational equilibrium. This equilibrium strongly favors inactive receptor conformations in absence of activating stimuli, but the application of an agonist can shift the conformational equilibrium towards specific active states of the receptor (Vaidehi und Kenakin 2010, Gurevich und Gurevich 2017).

As GPCRs become more accessible at their intracellular side after activation, they will associate with different signaling proteins. Complex-formation again induces specific conformational changes in both binding partners, as they mutually influence their conformational states. The most prominent “cornerstones” of the GPCR conformational landscape are depicted in **Figure 1.2** in the context of cellular signaling.

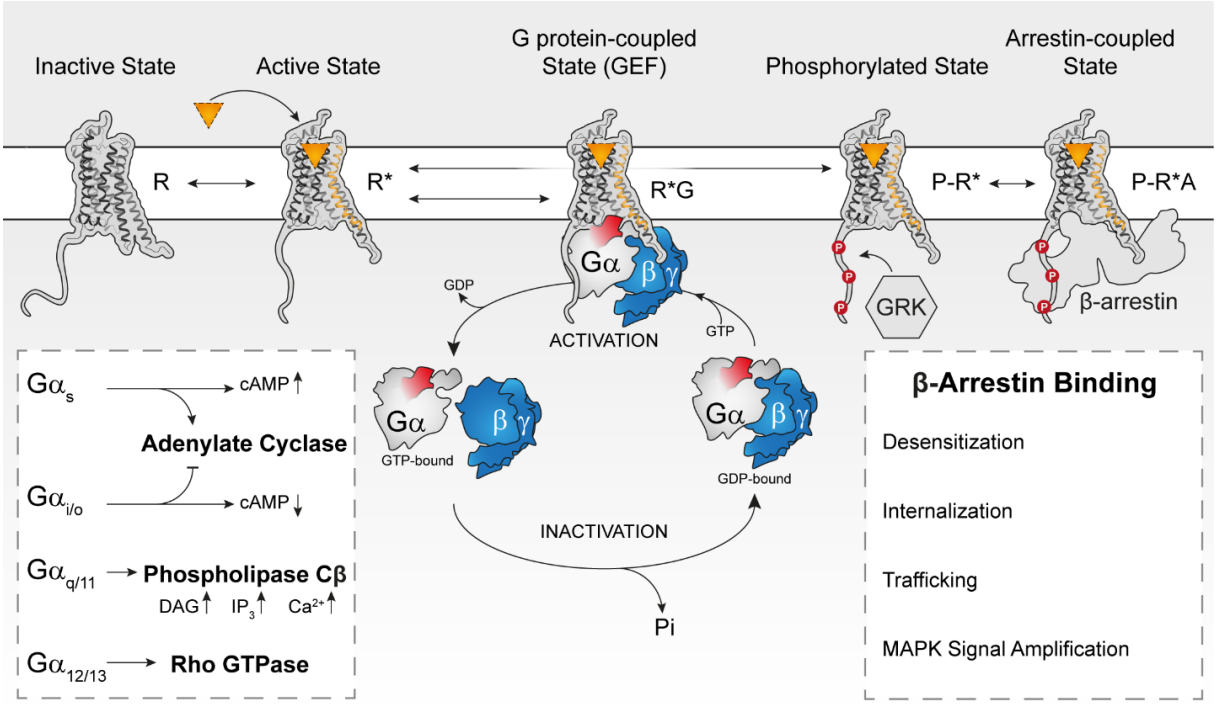

Figure 1.2 GPCR conformational landscape and canonical signaling cascade

GPCRs can adopt different conformational states that persist in a certain equilibrium (indicated by black two-sided arrows). While most receptor molecules adopt an inactive conformation (R, PDB: 2RH1) in the absence of activating stimuli, this equilibrium can be shifted to favor active receptor conformations (R*, PDB: 3SN6) by application of an agonist. In the R* state, GPCRs specifically couple to guanosine diphosphate- (GDP) bound trimeric G proteins (Gαβγ). As this functional GPCR–G protein complex is formed (R*G state), they facilitate the rapid exchange of GDP for guanosine triphosphate (GTP). This mechanism qualifies GPCRs as guanine nucleotide exchange factors (GEFs) and leads to a dissociation of the G protein from the receptor and into two active subunits: Gα and Gβγ. Active Gα subunits drive the intracellular second messenger response. Depending on their signaling, they are classified into four different groups: $G\alpha_s$, $G\alpha_{i/o}$, $G\alpha_{q/11}$, and $G\alpha_{12/13}$. The main consequences of their induced signaling are depicted as a box on the left. As Gα subunits have an intrinsic GTPase activity, they automatically return to their GDP-bound state, as they release a molecule of inorganic phosphate (Pi) before re-assembly of the Gαβγ trimer. The active GPCR can additionally be phosphorylated by GPCR kinases (GRKs) (P-R*), which increases the binding affinity of β-arrestins. The formation of a GPCR–β-arrestin complex (P-R*-A) canonically desensitizes the receptor and leads to internalization, intracellular trafficking, and a possible amplification of G protein-induced mitogen-activated protein kinase (MAPK) signaling (depicted in a box on the right).

As inactive GPCRs (R-state) are activated (R*-state) via extracellular application of an agonist, they are engaged by trimeric G proteins. These primary signal transducers consist of different Gα, Gβ, and Gγ subunits. In its inactive state, the Gα subunit of the trimer is bound to guanosine diphosphate (GDP). Upon formation of a GPCR–G protein complex (R*G-state), the receptor acts as a guanine nucleotide exchange factor (GEF), and facilitates the exchange of GDP to guanosine triphosphate (GTP) at the Gα subunit (Oldham und Hamm 2008). This, in turn, leads to a dissociation of the G protein from the receptor and separates the G protein trimer. Thus, the two active components, GTP-bound Gα and the free Gβγ heterodimer, can individually kick off

specific signaling cascades. Due to their intrinsic GTPase activity, Gα subunits terminate the duration of their activity themselves. Presumably, after induction of their specific signaling pathway, GTP is cleaved, and they return to their inactive GDP-bound state. At this point the G protein trimer can assemble again, primed to be activated via binding of another active GPCR (**Figure 1.2**).

Human physiology features a sizeable amount of G protein subunits, with 21 Gα, 6 Gβ, and 12 Gγ subunits (Downes und Gautam 1999) that are differentially expressed in specific cell types. Thus, the theoretical number of G protein trimer subunit combinations is comparable to the total number of human GPCRs. Notably, not all G protein combinations occur in nature, as some subunits might be structurally incompatible or simply not expressed in the same cell at the same time (Clapham und Neer 1997). Although the Gβγ heterodimer is signaling-competent in its own right, G proteins are divided into four classes depending on the sequence of implemented Gα subunits: $G\alpha_s$, $G\alpha_{i/o}$, $G\alpha_{q/11}$, $G\alpha_{12/13}$ (**Figure 1.2**). After activation, the different classes elicit specific intracellular second messenger responses. $G\alpha_s$ proteins activate adenylate cyclase (AC) to drive cyclic adenosine monophosphate (cAMP) production. cAMP is responsible for a variety of different cellular effects, most prominently it activates cAMP-gated ion channels and protein kinase A (PKA). $G\alpha_{i/o}$ proteins fulfill the exact opposite function, as they inhibit AC and effectively reduce intracellular cAMP levels. $G\alpha_{q/11}$ subunits lead to an activation of phospholipase Cβ (PLCβ), which catalyzes the hydrolysis of phosphatidylinositol 4,5-bisphosphate (PIP_2, an integral part of eukaryotic cell membranes) into diacyl glycerol (DAG) and inositol trisphosphate (IP_3). The soluble IP_3 induces the release of stored Ca^{2+} from the endoplasmic reticulum (ER) via activation of IP_3 sensitive Ca^{2+} channels. DAG, on the other hand, stays membrane-bound and activates protein kinase C (PKC). $G\alpha_{12/13}$ proteins activate rat sarcoma (Ras) homologue (Rho) GTPases, another class of membrane-bound G proteins, that are important for the dynamic remodeling of the cytoskeleton (Oldham und Hamm 2008).

GPCRs are traditionally also classified by their primary G protein-coupling preference. In fact, some GPCRs very specifically couple to only one family of Gα subunits (e.g. $G\alpha_s$-coupling of the vasopressin receptor 2 (V2R)). On the other hand, most GPCRs can activate multiple different Gα subunits to different extents (Inoue et al. 2019).

The R*-state of GPCRs additionally serves as an excellent substrate for GPCR kinases (GRKs, **Figure 1.2**). GRKs have been shown to be catalytically activated by active GPCRs (Boguth et al. 2010). These serine/threonine kinases phosphorylate intracellular sites of the receptor, most importantly residues of the unstructured C-terminus and intracellular loop 3. Notably, also second messenger kinases like PKA and PKC can phosphorylate GPCRs, albeit usually at different positions and presumably with different effects on downstream functions (Seibold et al. 2000). Phosphorylation primes the GPCR for desensitization and internalization, two processes that canonically reduce agonist-induced GPCR signaling. As GPCRs are important for the activation of GRKs and second messenger kinases, this system establishes a negative feed-back loop that terminates receptor signaling.

In their phosphorylated and active state (P-R*), GPCRs are eligible for high-affinity arrestin-binding (**Figure 1.2**). This implies a multi-step binding mechanism, as in contrast to G proteins and GRKs, arrestins not only sense the active conformation of the receptor, but also its phosphorylation state. When bound to a GPCR (P-R*-A), arrestins mediate desensitization, internalization, trafficking, and the amplification of mitogen-activated protein kinase (MAPK) signaling (DeWire et al. 2007). As a major focus of this thesis, the functionality of GRKs and arrestins will be discussed in more detail in the following chapters.

1.1.3 Competition at the intracellular GPCR cavity

Interestingly, all three discussed GPCR interaction partners, namely G proteins, GRKs, and arrestins, share overlapping binding interfaces, as they all engage the opened intracellular receptor cavity (**Figure 1.3 A**). For G proteins and arrestins, the interaction interface with multiple GPCRs has been elucidated in the form of complex crystal structures or via cryo-electron microscopy (cryo-EM) (Rasmussen et al. 2011, Zhao et al. 2019, Kang et al. 2015, Huang et al. 2020). G proteins bind to active GPCRs via insertion of an α-helix formed at the C-terminus of the Gα subunit. This interaction interface is also the most important factor that determines the G protein-coupling preference of GPCRs (Conklin et al. 1993, Conklin et al. 1996).

Arrestins use a similar “lock in key” mechanism to associate with the active conformation of GPCRs. Via insertion of the finger loop region (FLR) into the intracellular GPCR crevice, they form a binding interface that overlaps with the

receptor-bound Gα C-terminus (**Figure 1.3 A**). This is also how arrestins are thought to mediate receptor desensitization, as the G protein-binding interface is occluded if arrestin is bound to the GPCR in such a tight manner. Although the FLR appears unstructured in inactive crystal structures of arrestins, binding of a GPCR might induce the formation of an α-helix (Kang et al. 2015).

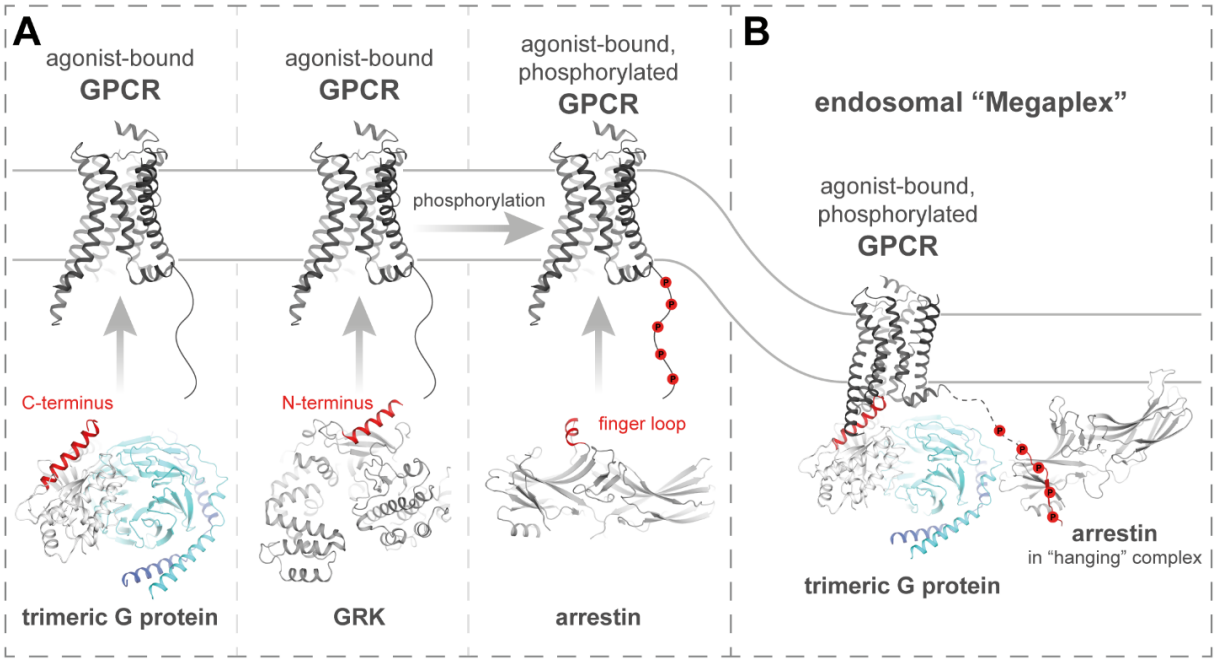

Figure 1.3 Central effectors compete for the cytoplasmic GPCR cavity – most of the time

Active agonist-bound GPCRs (PDB: 3SN6) accommodate effector proteins with their intracellular cavity. The topography of this binding interface is dictated by the primary GPCR sequence and its conformational state. **A** G proteins (PDB: 3SN6), GRKs (PDB: 3NYN) and arrestins (PDB: 5DGY) share similar structural features (red) to engage active GPCR folds. In case of G proteins, specific receptor-coupling is facilitated by the α-helical C-terminus of the Gα subunit, while GRKs are thought to interact with GPCRs via their α-helical N-terminus. The arrestin finger loop region (FLR) might adopt a similar α-helical structure upon GPCR-binding. Thus, these mediators and regulators of GPCR signaling must compete for binding at the intracellular GPCR cavity. **B** Arrestins are also able to interact with the phosphorylated receptor C-terminus in a so-called "hanging" complex, allowing further G protein-activation. Thus, some combinations of GPCRs, G proteins and arrestins can form non-canonical "Megaplexes" (PDB: 6NI2), which may drive GPCR signaling even from endosomal compartments. (Figure was similarly published in Matthees et al. (2021) and reproduced according to the Creative Commons Attribution 4.0 International License)

Just recently, the first crystal structure of GRK1 in complex with rhodopsin was published (Chen et al. 2021). This structure reveals that GRK1 features a prominent α-helix which inserts into the seven transmembrane region of active rhodopsin to stabilize this specific interaction. Previous studies have shown that this N-terminal α-helix is also crucial for activation of the GRK kinase function (Palczewski et al. 1993, Beautrait et al. 2014, Boguth et al. 2010). Still, the mechanisms that other GRK isoforms utilize to achieve GPCR-coupling are less well characterized (Cato et al.

2021). Computational analyses of binding interfaces between different GRK isoforms and GPCRs suggest that the formation of multiple different complex configurations might be possible (Cato et al. 2021). Here, it cannot be ruled out that these distinct complexes are able to induce differential receptor phosphorylation states and regulatory processes. Nevertheless, the main hypothesis of how GRKs interact with GPCRs, is via insertion of their N-terminal α-helix into the open GPCR cavity (**Figure 1.3 A**). More structural evidence is needed to complete our understanding of GRK-binding, although the notion that GRKs interact with active GPCR conformations in a similar fashion as G proteins and arrestins is highly attractive.

As the three major effector proteins compete for binding at the intracellular cavity of active GPCRs, the receptor molecules interact with G proteins, GRKs and arrestins in a specific equilibrium. This equilibrium can be shifted towards arrestin-binding via phosphorylation of the receptor, favoring arrestin-mediated functions at the later stages of agonist-induced signaling (DeWire et al. 2007).

Interestingly, recent studies have shown that arrestin-binding does not necessarily need to compete with G protein-binding. Given that enough negative charges are present at the GPCR C-terminus, arrestins may also omit their FLR-dependent binding interface and form a complex that relies only on the interaction between the GPCR C-terminus and arrestin N-domain (Shukla et al. 2014). This so-called “hanging” complex has been shown to be functionally active and able to drive receptor internalization, while still allowing further activation of G proteins (Cahill et al. 2017). A cryo-EM structure of an active GPCR simultaneously bound to a trimeric G protein and β-arrestin1 has been recently published (Nguyen et al. 2019) and is depicted in **Figure 1.3 B**, showing a snapshot of the so-called endosomal “Megaplex”. Notably, the mentioned studies that characterized the “hanging” complex or endosomal “Megaplex” all utilized the C-terminal tail of the V2R. As this peptide seems to have evolved in order to facilitate very stable GPCR–arrestin interactions (Oakley et al. 1999), it is unlikely that all GPCRs are able to form these specific complexes.

1.2 β-arrestins and their importance as universal GPCR adaptor proteins

The human genome encodes for four different arrestin isoforms. Two of them are only functionally expressed in the retina to regulate corresponding photoreceptors in rod- (arrestin-1) or cone cells (arrestin-4). The remaining two isoforms, namely β-arrestin1

and β-arrestin2, are broadly expressed but vary in their tissue distribution (Matthees et al. 2021). They are hypothesized to mediate specific downstream functions for all non-visual GPCRs. β-arrestin1 and 2 share 78% sequence identity and a remarkably similar overall structure. In line with this observation, mice featuring a singular knockout of either β-arrestin1 or 2 show only mild phenotypes (Conner et al. 1997, Bohn et al. 1999), whereas the double knockout of both β-arrestin isoforms is embryonically lethal (Kohout et al. 2001). This highlights the importance of β-arrestin functionality on an organism level, but also suggests that the two isoforms can substitute for each other to a certain extent.

Interestingly, arrestin-mediated functions for different GPCRs are at least as diverse as their primary G protein signaling. In case of the G proteins, this diversity is adequately explained as different receptors preferably couple to specific combinations of G protein trimers (Inoue et al. 2019) to convey their characteristic signaling. This contrasts with the modality of arrestin-mediated GPCR regulation, as binding of the same interaction partner has different consequences for different receptors. For some GPCRs, arrestin-binding mediates desensitization and immediate recycling, redirecting the receptor back to the membrane after initial internalization (Claing et al. 2002). Certain other GPCRs exhibit prolonged intracellular trafficking which localizes the receptors to specific compartments and may give rise to a second wave of endosomal signaling (Godbole et al. 2017).

Upon binding to the active and phosphorylated GPCR, arrestins undergo major conformational changes. Especially, since arrestins have no enzymatic function, these conformational changes can be seen as hallmarks of arrestin activation. The interaction with different GPCRs differentially influences the active conformation of bound arrestin proteins (Nuber et al. 2016, Lee et al. 2016). Thus, arrestins are able to mediate GPCR-specific functions, as they adopt different active conformations that result from the formed GPCR–arrestin complex (Yang et al. 2015). Moreover, arrestins have been shown to serve as scaffolds for more than 100 intracellular proteins (Xiao et al. 2007). This enables the formation of specific effector-hubs that regulate intracellular trafficking and signaling of active GPCRs, depending on the active conformation of the central arrestin protein.

1.2.1 Arrestin structure-function relationship

Even though arrestins will adopt a specific active conformation for every different GPCR complex, some general information can be extracted from comparing active and inactive structures. **Figure 1.4** shows such a comparison for arrestin-1 in its inactive (Hirsch et al. 1999) and rhodopsin-bound state (Zhou et al. 2017).

Arrestins are soluble proteins that are about 48 kDa in size. Their structure consists of two domains (N- and C-domain) that are each made up of a characteristic β-sheet sandwich. Between the N- and C-domains is the so-called “hinge”-region, which connects the two bulky domains via several unstructured loops. An additional structural feature is the C-terminus of arrestins, which is not resolved in any of the available crystal structures, but shown in **Figure 1.4** as modelled by Dr. Xavier Deupi (Haider et al. 2019b).

The inactive conformation of arrestin is stabilized by multiple intramolecular interactions, namely the three-element interaction, the polar core, and the finger loop lock. These interactions work in tandem to retain two major hallmarks of the inactive arrestin conformation: the relative orientation of N- and C-domain towards each other and association of the arrestin C-terminus with its own N-domain (Haider et al. 2017). Especially the positioning of the C-terminus seems to play an instrumental role in regulating the functionality of arrestins. In its inactive conformation it occludes a conserved positively charged groove in the N-domain which is important for the recognition of the phosphorylated GPCR C-terminus.

Existence of the so-called finger loop lock (**Figure 1.4 a**) was just recently proposed by Sente et al. (2018). This interaction sits on top of the N-domain, as it stabilizes the inactive conformation of the unstructured FLR. Positively charged amino acids of the FLR form polar interactions with negative residues of β-sheets 5 and 6 of the N-domain. Interestingly, the modelled inactive C-terminus of arrestin also provides charged residues that possibly participate in this interaction.

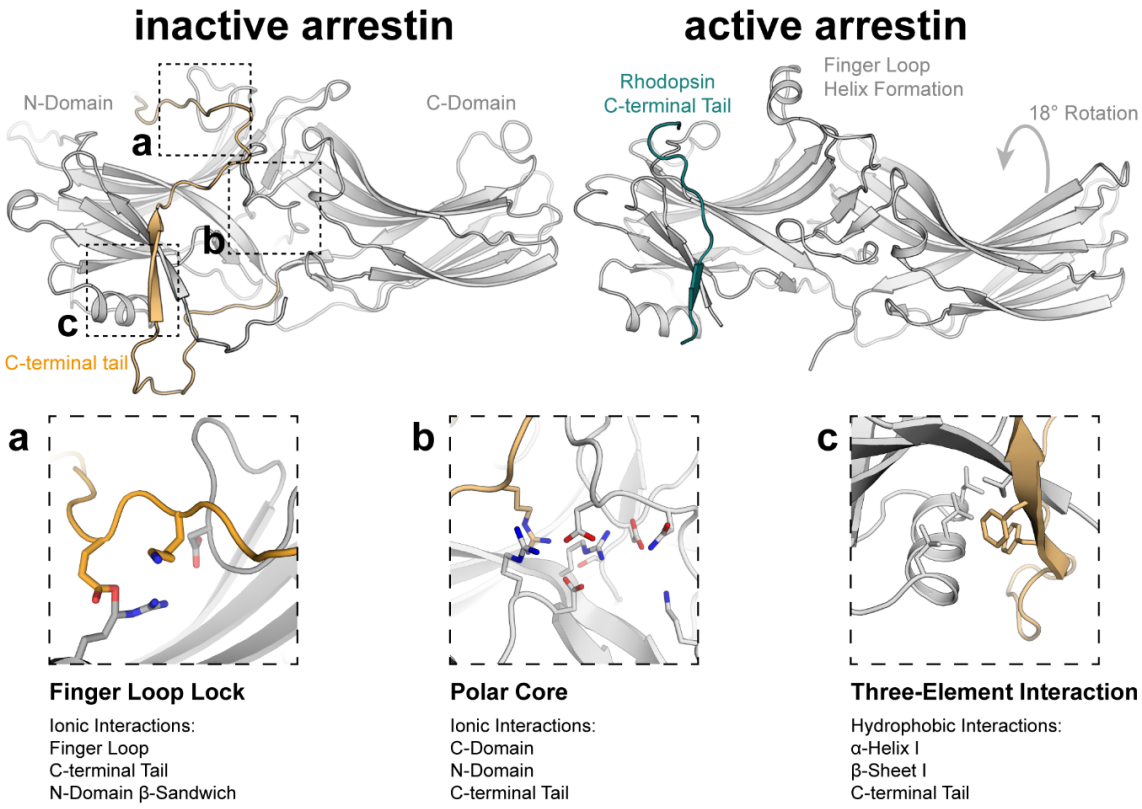

Figure 1.4 Structural hallmarks of inactive and active arrestin conformations

The inactive conformation of arrestin (PDB: 1CF1, with a modeled C-terminus) is stabilized by multiple intramolecular interactions. The arrestin C-terminus has an auto-inhibitory function, as it participates in ionic interactions of the finger loop lock (a), and the polar core (b), as well as in hydrophobic interactions of the three-element site (c). In combination, these interactions fixate the C-terminus on top of the arrestin N-domain and additionally stabilize the relative orientation of the C-domain. Upon arrestin activation (PDB: 5W0P), the phosphorylated GPCR C-terminus associates with a positively charged groove of the arrestin N-domain. This conserved feature is initially obstructed by the arrestin C-terminus which, in turn, dissociates from the N-domain. Termed “C-tail exchange”, this process disrupts the interactions at the finger loop lock, polar core and three-element site. As a hallmark of major structural rearrangements, the arrestin C-domain changes its orientation in respect to the N-domain, rotating approximately 18°. The arrestin FLR can then interact with the intracellular GPCR cavity and might adopt an α-helical fold to stabilize GPCR–arrestin “core”-complexes.

The polar core (**Figure 1.4 b**) consists of a network of salt bridges and hydrogen bonds that is formed between highly conserved residues in the hinge region of arrestin. Additionally, it also features another anchoring point for positive amino acids of the arrestin C-terminus. As it is located in between the N- and C-domains, it is crucial for the preservation of the relative orientation of the two domains (Haider et al. 2017).

The most important interaction that traps the arrestin C-terminus at the N-domain is the three-element interaction (**Figure 1.4 c**). This site features hydrophobic interactions between α-helix 1, β-sheet 1 and phenylalanine residues of the arrestin C-terminus (Haider et al. 2017).

During GPCR-binding and concomitant activation of the protein, arrestin first interacts with phosphorylated residues of the GPCR C-terminus. The unique ability of arrestin to detect and embrace phosphorylated GPCR peptide stretches is mediated by specific phosphate-sensing residues in the N-domain. These phosphate-sensors are uncovered as the collapse of all three described interactions leads to a dissociation of the arrestin C-terminus from the N-domain. The arrestin C-terminus is now sterically replaced by the phosphorylated GPCR C-terminus in a process termed “C-tail exchange”. The manner in which this “C-tail exchange” takes place is highly dependent on the number and location of phosphorylated residues of the GPCR C-terminus (Moore et al. 2007, Yang et al. 2015, Mayer et al. 2019), defining a conformational need for distinct phosphorylation patterns.

A direct consequence of the breakdown of the polar core is the change in orientation between the N- and C-domain of about 18°. This becomes evident, as crystal structures of the pre-active p44 splice variant of arrestin-1 (Kim et al. 2013), as well as V2R C-terminal peptide-bound β-arrestin1 (Shukla et al. 2013) already feature the ~18 - 20° interlobe rotation, even without direct GPCR-binding. Hence, most of the global conformational changes that happen during arrestin activation, are already triggered by association with the phosphorylated GPCR C-terminus.

The release of the arrestin C-terminus is furthermore hypothesized to play a central role in the mediation of arrestin-mediated downstream functions. It harbors binding motifs for adaptor protein 2 (AP2) and clathrin (Laporte et al. 2000, Krupnick et al. 1997, Goodman et al. 1996), additional to a MAPK kinase (MEK) phosphorylation site (Cassier et al. 2017) that enables scaffolding of MAPKs. Accordingly, arrestins are able to facilitate clathrin-dependent GPCR internalization and enhance G protein-induced MAPK signaling, provided that they adopt an appropriate active conformation.

After a successful “C-tail exchange”, arrestin is primed for the formation of a tight “core” complex with the GPCR transmembrane helix bundle. This can also be seen for the two β-sheets leading to and from the FLR. In both pre-active structures (Kim et al. 2013, Shukla et al. 2013), the β-sheets 5 and 6 of the N-domain are elongated for the FLR to practically stretch towards the anticipated GPCR cavity. After the insertion of the FLR into the cytoplasmic receptor core, it adapts its conformation to fit the specific receptor. This leads to the formation of a short α-helix for some GPCR–arrestin complexes (Kang et al. 2015, Huang et al. 2020), but not all of them (Staus et al. 2020).

Taken together, the resulting active conformation of arrestin is influenced by at least three distinct parameters: the overall complex configuration with a GPCR, the specific application of the FLR, and finally the employed electrostatic interactions between the arrestin N-domain and the phosphorylated GPCR C-terminus. These crucial determinants of arrestin conformational changes will be discussed in further detail in the following chapters.

1.2.2 Different binding-modes and complex configurations

Arrestins do not necessarily establish a tight interaction with the intracellular GPCR cavity in order to form a stable complex with the receptor. One can assume that the importance of different binding interfaces is differently weighted for each individual receptor. Hence, different GPCRs may favor distinct arrestin complex configurations, although they are most probably not mutually exclusive and rather employed in a certain equilibrium. Especially since β-arrestins have to service such a staggering number of different GPCRs, it is very conceivable that the presented binding interfaces will differentially facilitate the formation of specific complexes and their stability.

By now, multiple forms of arrestin-activation have been identified (**Figure 1.5 A**). Interestingly, they share a common mechanism as they all require the presence of phosphorylated GPCR C-termini.

After association with the phosphorylated GPCR C-terminus, arrestins may form a stable “core” complex. This configuration was first seen in the crystal structure of the rhodopsin–arrestin-1 complex elucidated by Kang et al. (2015). According to this structure, the complex relies on at least two distinct binding interfaces: the electrostatic interactions with the phosphorylated GPCR C-terminus as well as the insertion of the FLR into the opened GPCR cavity (**Figure 1.5 A**). Arrestins were also found to interact with GPCRs in a “hanging” complex, which just relies on the electrostatic interactions and omits the FLR-based binding interface (Shukla et al. 2014). Both configurations can be found in clathrin-coated structures, as they have been shown to facilitate internalization of the GPCR–arrestin complex (Cahill et al. 2017) (**Figure 1.5 B**).

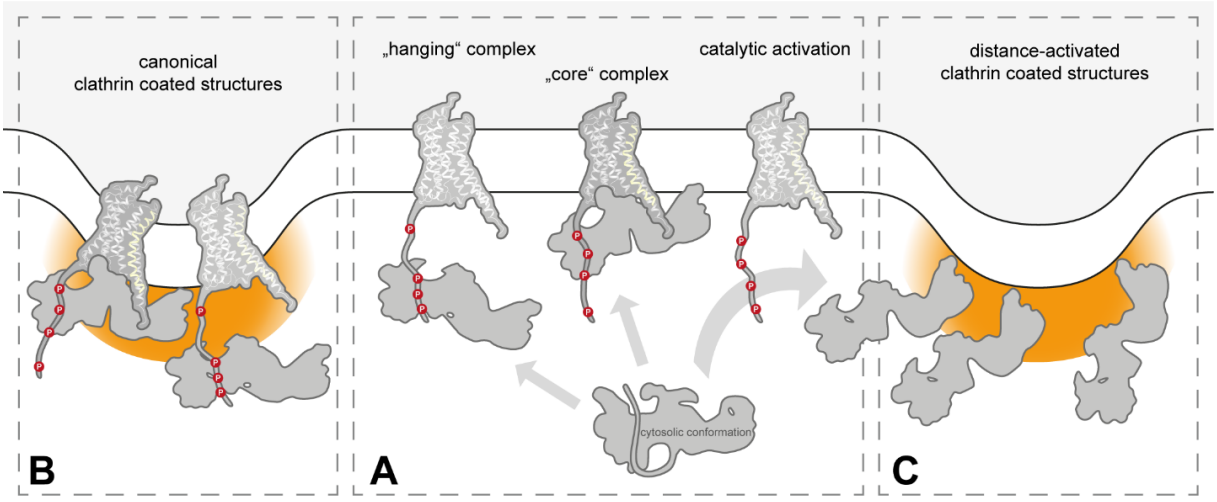

Figure 1.5 Arrestin activation enables the formation of different complex configurations

A In the inactive state, arrestins exhibit an auto-inhibitory conformation that is mostly localized in the cytosol. Active and phosphorylated GPCRs can activate and bind arrestins, forming canonical “core” complexes that rely on the electrostatic interaction with the phosphorylated receptor C-terminus and docking of the arrestin FLR at the intracellular receptor cavity (Kang et al. 2015). Depending on the availability of charged residues, arrestins can interact with the phosphorylated GPCR C-terminus only, forming a “hanging” complex. This configuration omits the binding interface at the receptor core and allows for further activation of G proteins (Shukla et al. 2014). **B** Both complexes facilitate internalization of GPCRs and can be found in clathrin-coated or endosomal structures (Cahill et al. 2017). **C** Recently, arrestins have been shown to retain an active conformation after dissociation of the GPCR–arrestin complex. This catalytic activation of arrestin leads to an accumulation of so-called “distance-activated” arrestins in clathrin-coated structures (Eichel et al. 2018). (Figure was similarly published in Haider et al. (2019a) and reproduced with permission, license ID: 1129681-1)

These complex configurations feature a GPCR-to-arrestin stoichiometry of one-to-one. Interestingly, some receptors also induce a superstoichiometric accumulation of arrestins at the plasma membrane. This observation led to the identification of catalytically activated arrestins (Eichel et al. 2018). They presumably adopt an active conformation after GPCR-induced “C-tail exchange” and accumulate in clathrin-coated structures (**Figure 1.5 C**). The localization of distance-activated arrestins is mostly facilitated by interactions with membranous lipids and clathrin itself. In line with these findings, the FLR plays only a minor role in the catalytic activation of arrestins (Eichel et al. 2018).

1.2.3 Different employment of the “core”-binding interface

Due to immense advances in structural biology, and especially the cryo-EM methodology, we can now appreciate the precise organization of more and more individual GPCR–arrestin complexes. These complex structures are of great value for determining and comparing tight interaction interfaces, but also have their limitations.

To elucidate the structure of such a complex, both binding partners have to be stabilized to a certain extent, which usually involves mutagenesis of residues at critical positions. Additionally, large unstructured regions, like the intracellular loop 3 or GPCR C-terminus, are commonly truncated or exchanged for shorter derivatives. The V2R C-terminus is very commonly used as a substitute for C-terminal domains of other GPCRs. This is due to the relatively small size of the peptide of just 26 amino acids and high density of phosphorylation sites (42% of its residues are either serine or threonine). Thus, it seemingly facilitates very stable β-arrestin interactions and was used in the recently elucidated complex structures of the muscarinic acetylcholine receptor M2 (M2R) and β1 adrenergic receptor (β1ADR) with β-arrestin1 (Staus et al. 2020, Lee et al. 2020).

The overall geometries of different GPCR–arrestin “core” complexes share a high degree of similarities. Especially the employment of both interaction interfaces, the electrostatic interaction between the arrestin N-domain and the phosphorylated GPCR C-terminus, as well as the insertion of the FLR into the transmembrane helix bundle, have been confirmed multiple times by now (Kang et al. 2015, Zhou et al. 2017, Yin et al. 2019, Staus et al. 2020, Lee et al. 2020, Huang et al. 2020).

An example of a “core” complex which shows a strikingly different configuration was established by the groups of Brian Kobilka and Eric Xu almost simultaneously early 2020. Both groups published the structure of β-arrestin1 in complex with the neurotensin receptor 1 (NTSR1). The Huang et al. (2020) structure of the complex is depicted side by side with the prototypical structure of the rhodopsin–arrestin-1 complex (Kang et al. 2015, Zhou et al. 2017) in **Figure 1.6**.

The comparison of side-views of the two GPCR–arrestin complexes reveals that arrestin shows different interactions with the plasma membrane (**Figure 1.6 A**). The rhodopsin-bound arrestin exhibits only a slight tilt, indicating a membrane interaction of the arrestin C-edge (Lally et al. 2017). On the other hand, the NTSR1-bound arrestin is positioned at a dramatically steep angle, that allows for most of the outward loops of the arrestin C-domain to be buried in the membrane. One reason for this apparent difference could also be found in the differently applied structural biology methodologies.

The rhodopsin–arrestin-1 complex was solved via serial X-ray crystallography, which featured the detergent-solubilized and crystalized receptor. The NTSR1, on the other

hand, was reconstituted in micelles and subjected to cryo-EM, which may enable or even enhance β-arrestin1 interactions at such an angle. NTSR1-bound β-arrestin1 also interacts directly with a PIP_2 molecule, protruding from the micelle (not shown). This interaction between the β-sheet sandwich of the β-arrestin1 C-domain and PIP_2 additionally stabilizes its positioning towards the membrane.

The FLRs of these arrestin complexes show a different organization as well, although small α-helical structures are formed in both cases (**Figure 1.6 a, b**). Despite these differences, binding of the phosphorylated GPCR C-terminus happens in an overall similar fashion in both complexes (**Figure 1.6 c, d**).

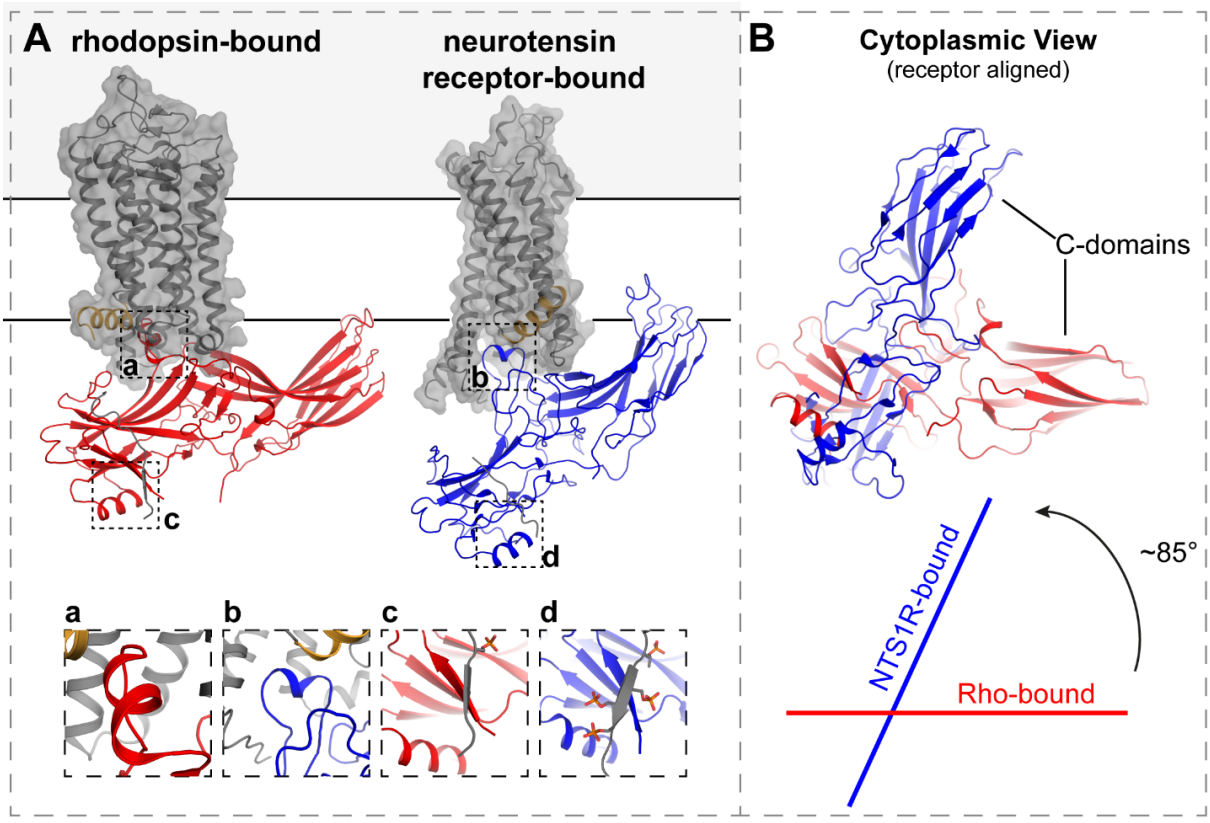

Figure 1.6 Structural diversity of core-bound GPCR–arrestin complex configurations

β-arrestins have to accommodate hundreds of active GPCR conformations and facilitate specific functions. **A** Shown are side-views of rhodopsin in complex with arrestin-1 (red, PDB: 5W0P) and the neurotensin receptor 1 (NTSR1) bound to β-arrestin1 (blue, PDB: 6UP7). This point of view allows for comparison of arrestin interaction with the plasma membrane. The NTSR1-bound β-arrestin1 buries itself deeper into the membrane and at a steeper angle, in comparison to the rhodopsin-bound arrestin-1. Highlighted are close-ups of differently organized FLRs, directly bound to the transmembrane helix bundles of rhodopsin (a) or the NTSR1 (b) and phosphorylated residues of GPCR C-termini bound at the three-element interaction site of arrestin-1 (c) or β-arrestin1 (d). Helix 8 of both receptor structures is colored in ocher to allow for comparison of the different orientation of receptor and arrestin molecules in the respective complex. **B** A view from the cytoplasm, facing the plasma membrane, of both complexes is depicted after receptor alignment (GPCRs not shown). This point of view reveals that arrestin-binding occurs at a rotated angle of approximately 85° in the respective complexes. (Figure was similarly published in Matthees et al. (2020) and reproduced with permission according to the Elsevier copy right agreement)

Moreover, the NTSR1–β-arrestin1 complex structure revealed an alternative orientation of arrestin-binding. In comparison to the rhodopsin-bound state, this new complex shows a ~85° rotation of arrestin relative to the receptor. In **Figure 1.6 B**, a view from the cytoplasm of both complexes is shown after receptor alignment. Notably, every miniscule difference, like the differently organized FLRs, or big configurational changes, like the rotation of arrestin in respect to the receptor, influences the active conformation of arrestin. The comparison of these structures highlights the flexibility of arrestins and the diverse nature of different GPCR–arrestin interactions, even though both discussed configurations have to be considered “core” complexes.

1.2.4. Different associations with phosphorylated peptide stretches

Multiple positively charged residues form a groove inside the arrestin N-domain to facilitate interactions with phosphorylated peptide stretches (**Figure 1.7 A**). Interestingly, these so-called phosphate sensors are differentially spaced between different arrestin isoforms, while the overall shape of the positive crevice seems to be conserved.

By now, multiple structures of arrestins bound to phosphopeptides or even full-length GPCRs with intact phosphorylated C-termini have been elucidated. They all confirm that the principle electrostatic binding interface of arrestins is located in the N-domain, but the individual positioning seems specific for every individual phosphopeptide. As examples, the C-terminal phosphopeptides of the V2R (V2R-pp), the atypical chemokine receptor 3 (ACKR3-pp) and rhodopsin (Rho-pp) are shown in their arrestin co-crystalized structure next to their primary amino acid sequence in **Figure 1.7 B**.

The V2R-pp structure shows electron densities for eight individual phosphorylated serine or threonine residues. Overall, the entire length of the synthetic peptide is associated with β-arrestin1 in the corresponding crystal structure (**Figure 1.7 C**). Interestingly, two amino acids in the middle of the V2R-pp are not resolved and the two resulting parts of the peptide bind the β-arrestin1 N-domain in distinct locations. The amino acids upstream of this unresolved region (proximal) associate with positive amino acids that are located close to the finger loop lock (**Figure 1.7 D**). The distal part of V2R-pp engages in interactions with β-arrestin1 close to the polar core and also reaches the three-element interaction. Thus, the V2R-pp seems to be uniquely able to replace the whole length of the inactive arrestin C-terminus, leading to a complete “C-

tail exchange". In line with this, co-crystalized β-arrestin1 already shows a 20° interlobe rotation.

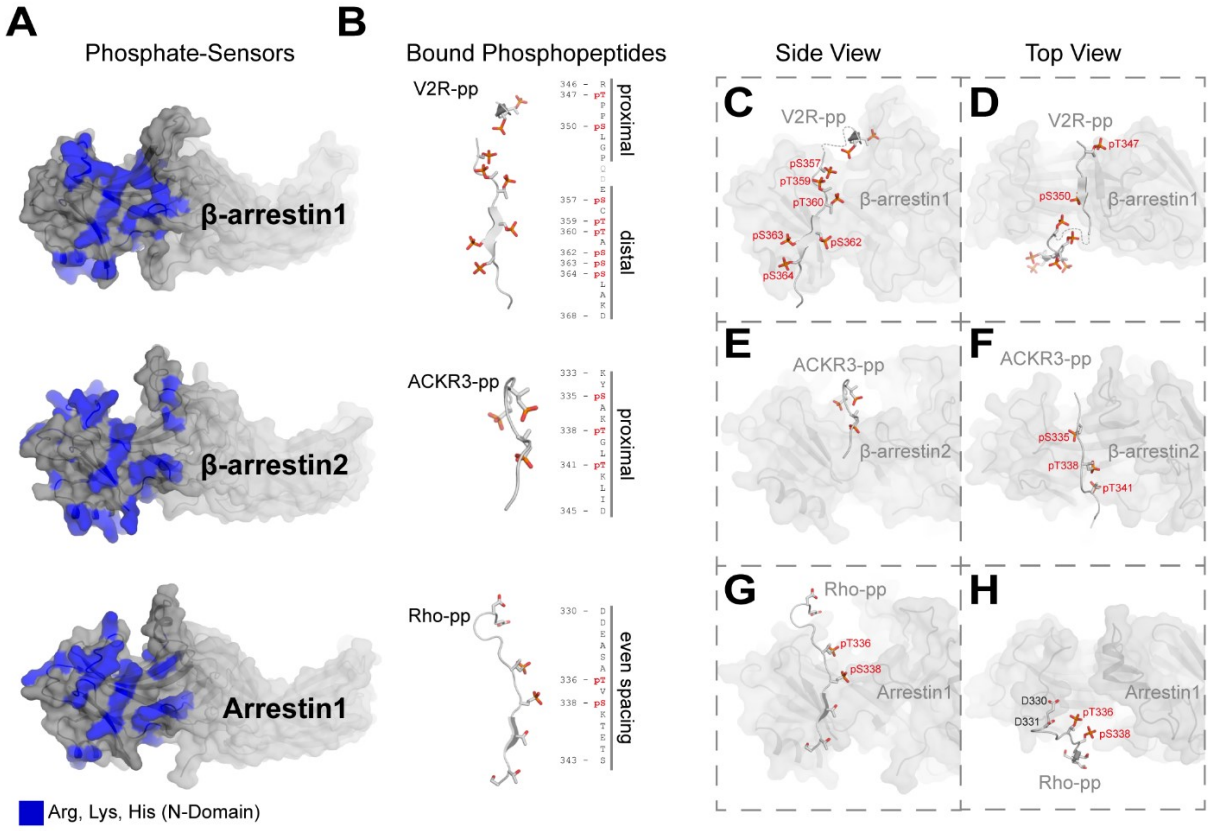

Figure 1.7 Positively charged domains and distinct interactions of arrestins with different phosphopeptides

A The arrestin N-domain features multiple exposed positively charged residues. The location of specific arginine, lysine or histidine residues (blue) is not necessarily identical between different arrestin isoforms, but overall, they make up a conserved positively charged groove. The shape of this crevice is similar for β-arrestin1 (PDB: 4JQI), β-arrestin2 (PDB: 6K3F), and arrestin-1 (PDB: 5W0P). Positively charged amino acids located in this groove can be seen as "phosphate-sensors" as they interact with phosphorylated GPCR C-termini. **B** Structures of individual phosphopeptides (pp) of the vasopressin receptor 2 (V2R), the atypical chemokine receptor 3 (ACKR3) and rhodopsin (Rho), co-crystalized with arrestins are shown as cartoons, with phosphates (and selected aspartic acid residues for Rho) depicted as sticks. Alongside, a sequence indicates the positions of important residues related to the primary sequence of the respective receptor. The distal part of the V2R-pp was shown to interact directly with the positive groove of β-arrestin1, and the three-element site (**C**), whereas the proximal part binds on top of the N-domain, close to the finger loop lock (**D**). The ACKR3-pp was shown to only interact with residues on top of the arrestin N-domain, similar to the proximal part of the V2R-pp (**D**, **E**). In contrast to the V2R- and ACKR3-pps, binding of the Rho-pp appears to be evenly spaced between the finger loop lock and three-element site (**G**, **H**), while neither of these two sites interact directly with the Rho-pp.

The ACKR3-pp–β-arrestin2 structure, on the other hand, only gives coordinates for three phosphorylated residues. These correspond quite nicely with the "proximal"-termed part of the V2R-pp, as they mostly associate with β-arrestin2 near the finger loop lock. The three-element, and to some extent also the polar core, seem to not participate in this interaction (**Figure 1.7 E, F**). This partial occupancy of the β-arrestin2

N-domain only leads to a relatively small inter-domain rotation of about 8°. Notably, the authors provide a modelling of the ACKR3-pp complete sequence bound to β-arrestin2 (Min et al. 2020a).

The Rho-pp associates with arrestin-1 in again another binding mode. It shows interactions with the arrestin-1 N-domain in evenly spaced intervals between the finger loop lock and the three-element site (**Figure 1.7 G**). Some of these interactions also involve negatively charged amino acids of the Rho-pp. Interestingly, there are no interactions that correspond to the very proximal part of the V2R-pp or ACKR3-pp, as the Rho-pp does not enter the crevice adjacent to the finger loop (**Figure 1.7 H**). This might be explained as the arrestin-1 structure was obtained in complex with full-length rhodopsin (not shown). In this tight “core” complex, the FLR directly interacts with the transmembrane helix bundle (**Figure 1.6 A, a**), possibly occupying the proximal binding interface used by the V2R- and ACKR3-pp.

Notably, arrestins also interact with non-GPCR-derived phosphorylated molecules. In a crystal structure, β-arrestin2 was shown to associate with inositol hexaphosphate (IP_6) (Chen et al. 2017). The complex features three IP_6 molecules, one bound near the finger loop lock, one close to the three-element site and one that occupies the same binding site as PIP_2 in NTSR1-bound structure (Huang et al. 2020). Additionally, β-arrestin1 is hypothesized to also form functional complexes with phosphorylated peptide stretches of receptor tyrosine kinases (RTKs) (Girnita et al. 2014).

Taken together, it becomes evident that arrestins use distinct binding interfaces to detect specific patterns of phosphorylated GPCR C-termini. As showcased by the comparison of the V2R-pp and ACKR3-pp co-crystal structures, arrestins respond to these differently spaced negative charges with specific conformational changes (20° or 8° interlobe rotation, respectively). This has also been shown multiple times by nuclear magnetic resonance (NMR) spectroscopy (Yang et al. 2015, Mayer et al. 2019) or computational models (Latorraca et al. 2020).

1.2.5 Measurement of conformational change

As a way to assess the activation state of arrestins, different methods to measure arrestin conformational changes have been established. While co-crystal structures of arrestins provide complete information about molecular rearrangements, they are cumbersome to obtain. Even though cryo-EM studies prove to be less labor-intensive,

these approaches are also not suitable to screen for multiple different parameters that influence arrestin conformational changes. Moreover, structure determination is less meaningful if important binding interfaces are modified to aid stabilization of the purified proteins, as seen in Staus et al. (2020).

NMR spectroscopy approaches share similar pitfalls, as they also analyze conformational changes of purified proteins. Recent NMR studies were able to convincingly quantify conformational changes of arrestin when coupling to different phosphopeptides, but they fail to portray the impact of arrestin-coupling to the full-length GPCR (Yang et al. 2015, Mayer et al. 2019).

To overcome these limitations, different versions of genetically encoded biosensors have been established. These tools allow for the assessment of arrestin conformational changes in living cells and possibly even at a high spatial and temporal resolution. Moreover, the most prominent advantage of the biosensor approach is that arrestin conformational changes can be induced via agonist stimulation of wild type (WT) GPCRs in the presence of all possibly involved intracellular interaction partners. They also enable the screening of different ligand-induced conformational states, as well as the strategic use of mutations to identify specific moieties that induce arrestin conformational changes.

1.2.5.1 Resonance energy transfer

Most of the established biosensor designs rely on the mechanism of intramolecular Förster resonance energy transfer (FRET) or bioluminescence resonance energy transfer (BRET). Both techniques are based on the radiation-less excitation of an acceptor fluorophore by a light-emitting donor molecule, first described by Förster (1948).

A Fluorophore is a molecule that absorbs light and thereby elevates one of its electrons to a higher quantum state. Some of the energy is immediately converted to molecular vibration, but as it relaxes back from its excited state (S_1) to its ground state (S_0), the fluorophore spontaneously emits a photon (**Figure 1.8 A**). This quantum of light has a lower energy than the one that was needed for excitation, hence a higher wavelength and lower frequency. Thus, the color of the emitted light is shifted to the red part of the visual spectrum (Stokes shift) (Wiens und Campbell 2018).

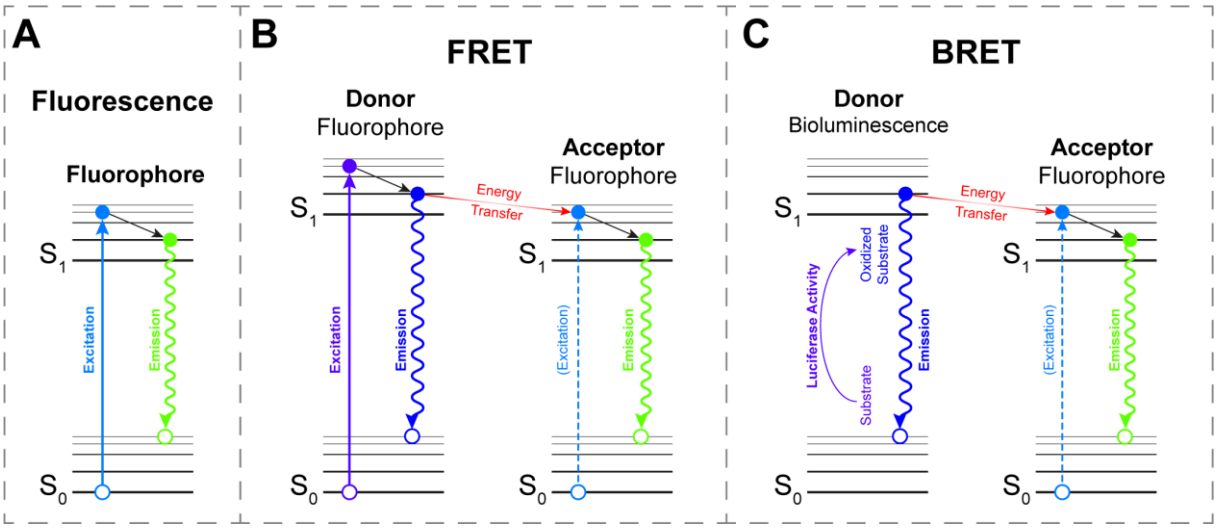

Figure 1.8 Schematic Jablonski representation of energy conversion in fluorescence, FRET and BRET
A Fluorophores in their ground state (S0) absorb photons with high energy (colored straight arrow) to reach an excited state (S1). As some energy is converted internally (black arrow), the fluorophore emits light of lower energy (colored curved arrow) as it relaxes back to its ground state. **B** FRET utilizes two fluorophores that are in close proximity of each other. The donor fluorophore is excited with external light and is subsequently able to excite the acceptor fluorophore via a non-radiative energy transfer. **C** BRET approaches utilize luciferases as energy donors. During the catalytic oxidation of their substrates, light is emitted as a product of this reaction. An energy transfer between the "excited" substrate and an acceptor fluorophore can again occur if both partners are in close proximity of each other.

Both FRET and BRET use fluorophores as acceptor molecules. FRET requires external illumination in order for the donor fluorophore to adopt an excited state (**Figure 1.8 B**), whereas BRET techniques use luciferases to provide the energy which is transferred to the acceptor fluorophore (**Figure 1.8 C**). For a direct energy transfer to take place, both partners of FRET or BRET have to be in close proximity. An efficient energy transfer is usually possible if the donor and acceptor molecules are less than 10 nm apart from each other. Additionally, the two molecules have to exhibit matching dipole moments. The energy transfer is most efficient if the emission dipole moment of the donor is oriented parallel to the absorption dipole moment of the acceptor molecule. Moreover, the donor emission spectrum must overlap with the excitation spectrum of the acceptor (Förster 1948, Lohse et al. 2012).

If these criteria are fulfilled, the donor directly transfers a quantum of energy to the acceptor (resonance energy transfer). The acceptor, in its quantum excited state, relaxes back to its ground state while emitting a photon of a characteristic wavelength. Via the intensity measurement of the donor and acceptor emission, a FRET or BRET ratio can be assessed. This non-dimensional ratio is calculated by division of the acceptor signal by the donor signal. An increased FRET or BRET ratio always results from a more efficient energy transfer in the system. For most systems this is achieved

as the acceptor and donor come into close proximity of each other (Lohse et al. 2012, Wiens und Campbell 2018).

Hence, these techniques are very well suited to measure protein–protein interactions (with the donor or acceptor fused to one of the binding partners, respectively) or the conformational changes of a protein (with both partners of the FRET or BRET pair located in different domains of the same protein).

1.2.5.2 Available conformational change biosensors

The first arrestin conformational change biosensor was conceived by the group of Michel Bouvier (Charest et al. 2005) (**Figure 1.9 A**). This original design used β-arrestin2 with a N-terminal fusion of a *renilla* luciferase (rLuc) as the BRET donor and a C-terminal fusion of a yellow fluorescent protein (YFP). With the help of this sensor, the measurement of agonist-induced arrestin conformational changes was first achieved.

Oishi et al. (2020) improved on this design and exchanged the BRET pair for a Nano Luciferase (NanoLuc) and a red-shifted cyan-excitable orange fluorescent protein 1 (CyOFP1) (**Figure 1.9 B**). This enhanced the signal intensity of the biosensor to enable high throughput (HTP) screening assays. A recent advance, utilizing only a single fluorophore, was established by the insertion of β-arrestin2 into a circular-permutated green fluorescent protein (cpGFP) (**Figure 1.9 C**) by Hoare et al. (2020). Upon translocation of β-arrestin to the stimulated receptor, the fluorescence intensity changes with the conformation of the biosensor. A very versatile tool is the synthetic antibody fragment Fab30, which can be used in approaches with unmodified β-arrestin1 (Ghosh et al. 2019) (**Figure 1.9 D**). Originating from crystallography, Fab30 was first identified to stabilize the active conformation of β-arrestin1. Fluorescently tagged, it can be used to visualize trafficking of the active β-arrestin1 conformation in living cells. Furthermore, Fab30 can be used as part of a FRET or BRET pair.

Some of these tools are excellent to rapidly evaluate arrestin conformational changes, or in the case of Fab30 follow the intracellular fate of the active β-arrestin1 conformation. Still, the biosensors described in **Figure 1.9 A-D** share one disadvantage: they report only from a single point of view. For the N- and C-terminally tagged intramolecular biosensors, different active conformations of arrestin can be identified if a different BRET ratio is recorded. Still, there might be alternative active

arrestin conformations that induce similar BRET changes or do not induce a BRET change for this biosensor at all. Similar to this, Fab30 only recognizes active conformations of β-arrestin1 that are related to the V2R-pp-bound state (Ghosh et al. 2019).

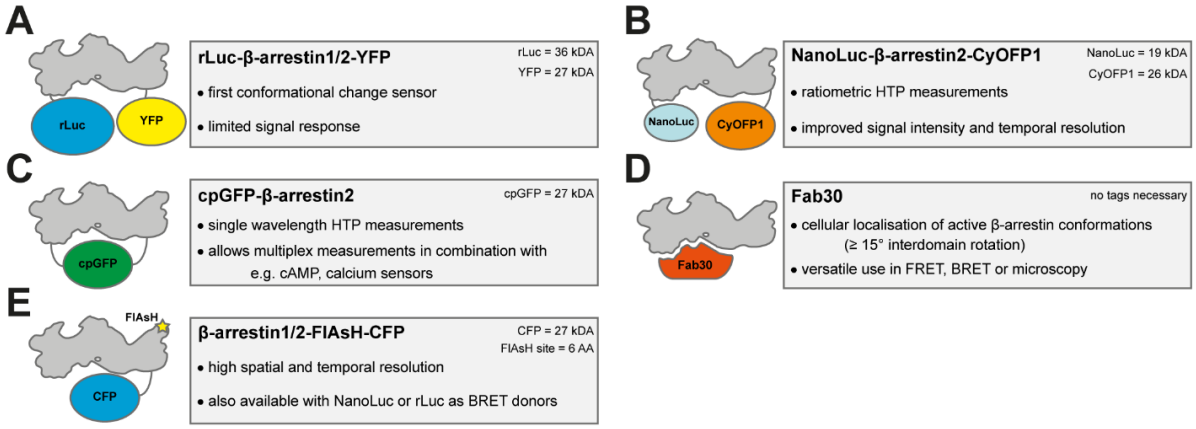

Figure 1.9 Schematic depiction of established β-arrestin conformational change biosensors

The design of different conformational change biosensors is depicted next to their important features (grey boxes). **A** Measurement of β-arrestin conformational changes in living cells was first achieved via introduction of arrestin BRET biosensors featuring a N-terminal *renilla* luciferase (rLuc, BRET donor) and a C-terminal yellow fluorescent protein (YFP, BRET acceptor), as shown in Charest et al. (2005). **B** An improved version of the same measuring principle with a nano luciferase (NanoLuc, BRET donor) and a cyan-excitable orange fluorescent protein1 (CyOFP1) was published by Oishi et al. (2020). **C** Hoare et al. (2020) introduced biosensors that only rely on a single fluorophore, a circular permutated green fluorescent protein (cpGFP). **D** An antibody fragment that specifically recognizes the active conformation of β-arrestin1 (Fab30) was successfully implemented to assess arrestin conformational changes by Ghosh et al. (2019). **E** Nuber et al. (2016) introduced FRET biosensors that report upon change of proximity between a C-terminally tagged cyan fluorescent protein (CFP, FRET donor) and individually introduced CCPGCC sites that are labeled with fluorescein arsenical hairpin binder (FlAsH, FRET acceptor). A similar strategy was realized by Lee et al. (2016) using a N-terminal rLuc as a BRET donor instead of CFP. (Figure was similarly published in Matthees et al. (2020) and reproduced with permission according to the Elsevier copy right agreement)

Hence, Nuber et al. (2016) and Lee et al. (2016) improved on the available biosensor designs to allow for a more comprehensive analysis of β-arrestin conformational changes (**Figure 1.9 E**). This was achieved via the individual introduction of several fluorescein arsenical hairpin binder (FlAsH)-binding motifs in exposed loops of the N- and C-domain of β-arrestin2. When labeled with FlAsH, these sites act as FRET (Nuber et al. 2016) or BRET (Lee et al. 2016) acceptors that allow for the measurement of conformational changes from different vantage points inside the protein. Nuber et al. (2016) used a C-terminal cyan fluorescent protein (CFP) as FRET donor, whereas the Lee et al. (2016) introduced a N-terminal rLuc fusion to enable BRET measurements. Their work showed that different GPCRs might induce similar conformational changes

in some regions of β-arrestin2, while other regions showed a significant difference. When data for all available biosensors are recorded, these so called “finger prints” of β-arrestin2 conformational changes can be used to comprehensively compare different conformational states. An improved version of this biosensor design was used by Reyes-Alcaraz et al. (2018) to show that stimulation of a GPCR with different endogenous ligands induces distinct conformational changes in β-arrestin2. Moreover, Nuber et al. (2016) showed that GPCR–β-arrestin2 interactions precede the induced β-arrestin2 conformational changes, while the protein remains in the active conformation for a prolonged time after agonist wash-out. The biosensor design, which was developed in this thesis, represents the direct evolution of the Nuber et al. (2016) approach and will be explained in more detail in the next chapter.

1.2.5.3 Intramolecular NanoBRET biosensors for β-arrestin1 and 2

In an effort to enhance the signal of measured conformational changes, the C-terminal CFP used in Nuber et al. (2016) was exchanged with a NanoLuc fusion in the novel sensor design (**Figure 1.10**).

Due to its small size (about 19 kDa) and improved brightness (~150 times higher luminescence as compared to firefly luciferase), the NanoLuc represents an excellent protein tag and BRET donor. The enzyme was originally isolated from a deep-sea shrimp, *Oplophorus gracilirostris*, and engineered to achieve higher stability, brightness and an improved signal half-life (Hall et al. 2012). In order to emit photons with an emission peak at about 460 nm, the NanoLuc catalyzes the conversion of its optimized substrate furimazine to furmimamide (**Figure 1.10 A**).

In contrast to firefly luciferase, this reaction is neither dependent on ATP nor Mg^{2+} ions. The emission spectrum of NanoLuc, as well as the excitation- and emission spectra of FlAsH are shown in **Figure 1.10 B**. The overlap between the NanoLuc emission and FlAsH excitation is depicted in blue and sufficient to enable an energy transfer between the two BRET partners, especially considering the improved brightness of NanoLuc. The use of FlAsH as a BRET acceptor has several advantages. Due to its small size (about 700 Da) and the requirement to only introduce six amino acids to facilitate specific labeling, it can be used to tag a protein at different positions without disturbing the fold or providing severe sterical hindrance. The used tetracysteine binding motif (CCPGCC, **Figure 1.10 C**) can be efficiently labeled with FlAsH right before the

measurement. This is suitable even for living cells, due to the membrane permeability of the used non-fluorescent FlAsH–ethandithiol (FlAsH–EDT_2) complex. After association with the CCPGCC binding motif, FlAsH is fluorescently active. Using an optimized protocol that also minimizes the amount of unspecifically bound fluorophores, the recombinant β-arrestin biosensors can be specifically labeled at the desired positions (Hoffmann et al. 2010). The overall sensor design and the position of the individually introduced FlAsH-binding motives are shown in **Figure 1.10 D**.

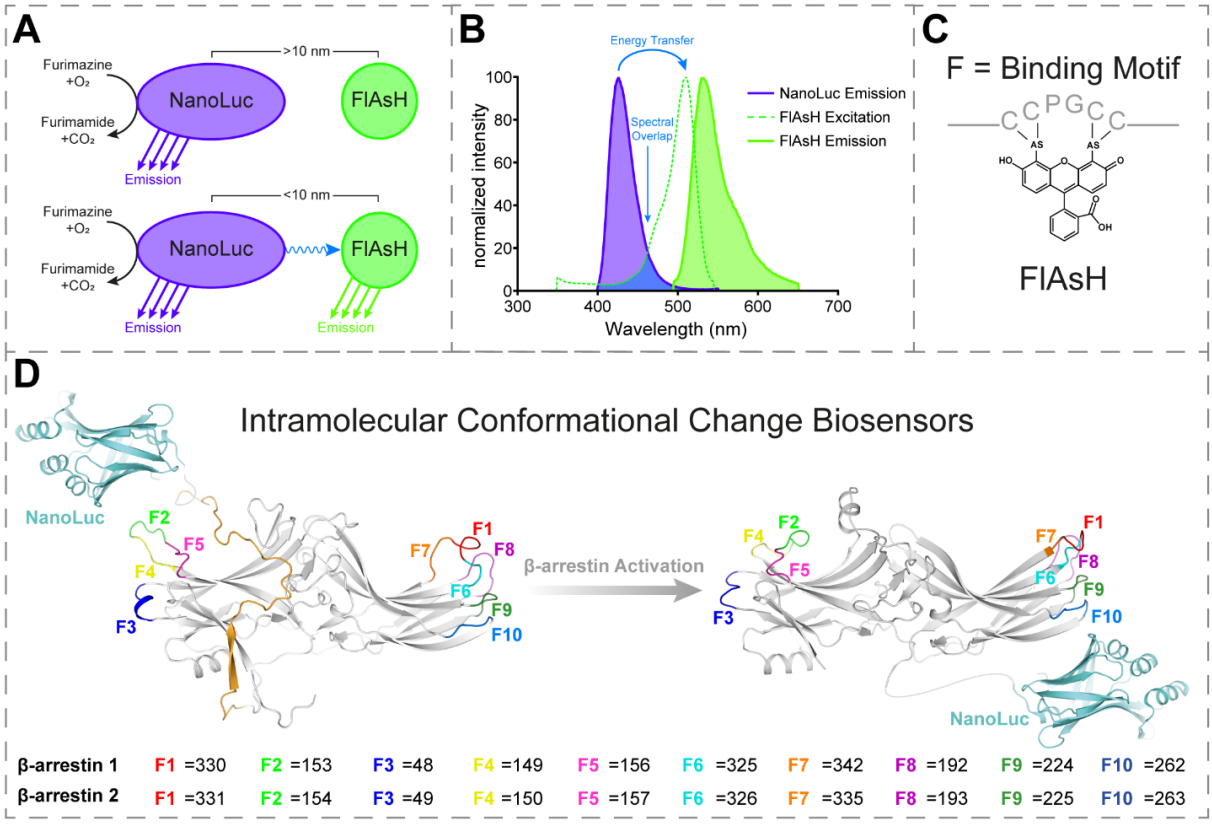

Figure 1.10 Measurement principle, labeling and design of novel β-arrestin1 and 2 FlAsH–NanoLuc sensors

A Schematic depiction of the BRET principle, featuring the used donor (NanoLuc) and acceptor (FlAsH) molecules. NanoLuc is a small protein (19 kDa) that catalyzes the oxidation of furimazine, its commercial substrate. This reaction yields furimamide, CO_2 and light emission. BRET between the NanoLuc and FlAsH occurs if both are in a close proximity of less than 10 nm. FlAsH in its excited state may then emit photons, specific to its emission spectrum. **B** Depicted are the specific emission spectra of NanoLuc (Schihada et al. 2018) and FlAsH, as well as the excitation spectrum of FlAsH (thermofisher.com/spectraviewer). The overlap of the FlAsH excitation and NanoLuc emission spectra is colored in blue. **C** The FlAsH-binding motif consists of six amino acids (CCPGCC) that are genetically introduced at specific positions of arrestin. Via an optimized labeling procedure (Hoffmann et al. 2010), FlAsH can be specifically bound to the thiol side-chains of the cysteine residues in the binding motif. **D** Overall sensor design of intramolecular β-arrestin1 and 2 conformational change biosensors. The NanoLuc BRET donor is genetically fused to the arrestin C-terminus and individual FlAsH-binding motifs are introduced at ten different positions in outward-facing loops of the arrestin N- and C-domains (F1 – F10, colored loops and amino acid sequence positions denoted for β-arrestin-1 and 2). In the inactive state (PDB: 1CF1, with a modeled C-terminus), the NanoLuc is in close proximity of the individual FlAsH-binding motifs, resulting in an efficient energy transfer. Upon GPCR- and subsequent arrestin activation (PDB: 5W0P), the distance between the BRET pair increases, depending on the nature of the conformational change and the specific labeling position.

Keeping in mind these important differences in comparison to the precursory designs of e.g. Charest et al. (2005), the principle of how these sensors report on β-arrestin conformational changes stayed the same. Upon agonist-induced recruitment to the receptor and subsequent β-arrestin activation, the NanoLuc and labeled FlAsH-binding site will change their orientations. This results in a measurable BRET change that is dependent on the assumed active conformation of arrestin, and the individually used FlAsH-binding site.

As another unique feature of the presented biosensor design, the FlAsH-binding motives were introduced for β-arrestin1 and 2 at homologous positions. With ten different biosensors per β-arrestin, each featuring a CCPGCC motif in one of the outward facing loops of the N-domain (F2, F3, F4, F5) or C-domain (F1, F6, F7, F8, F9, F10), this design enables the comprehensive comparison of conformational changes between the two β-arrestin isoforms for the first time.

1.3 GRK-specific GPCR phosphorylation and regulation

In order to phosphorylate intracellular peptide stretches of GPCRs, which is important for the binding and functionality of arrestins, human physiology features seven different GRKs. Two of them, GRK1 and GRK7 are only expressed in the retina to specifically facilitate the downregulation of rhodopsin and cone opsins, respectively. Non-visual GRKs are classified into two families (Gurevich et al. 2012, Homan und Tesmer 2014, Mushegian et al. 2012). GRK2 and GRK3 constitute the GRK2 family and feature a cytosolic expression. Upon GPCR activation, they are recruited to the membrane, facilitated by GPCR- and G protein- complex formation (Tesmer et al. 2005). In contrast, GRK4 family kinases, namely GRK4, 5, and 6, are generally membrane-bound. Four of these kinases (GRK2, 3, 5, and 6) are thought of as ubiquitously expressed and are thus hypothesized to regulate all non-visual GPCRs. These four GRKs, in combination with the two ubiquitously expressed β-arrestin isoforms, can be seen as a functional unit that mediates specific downstream functions for most GPCRs (Matthees et al. 2021).

1.3.1 “barcode” hypothesis

In its most straightforward interpretation, the “barcode” hypothesis states that arrestins react to different phosphorylation patterns via specific conformational changes to fulfill

targeted functions (**Figure 1.11 A**). This adequately explains how individual GPCRs can be differently regulated by arrestins and constitutes a solid foundation for the investigation of these phosphorylation-dependent processes. In line with this hypothesis, arrestins have been shown to undergo specific conformational changes for the coupling with different GPCRs (Lee et al. 2016, Nuber et al. 2016).

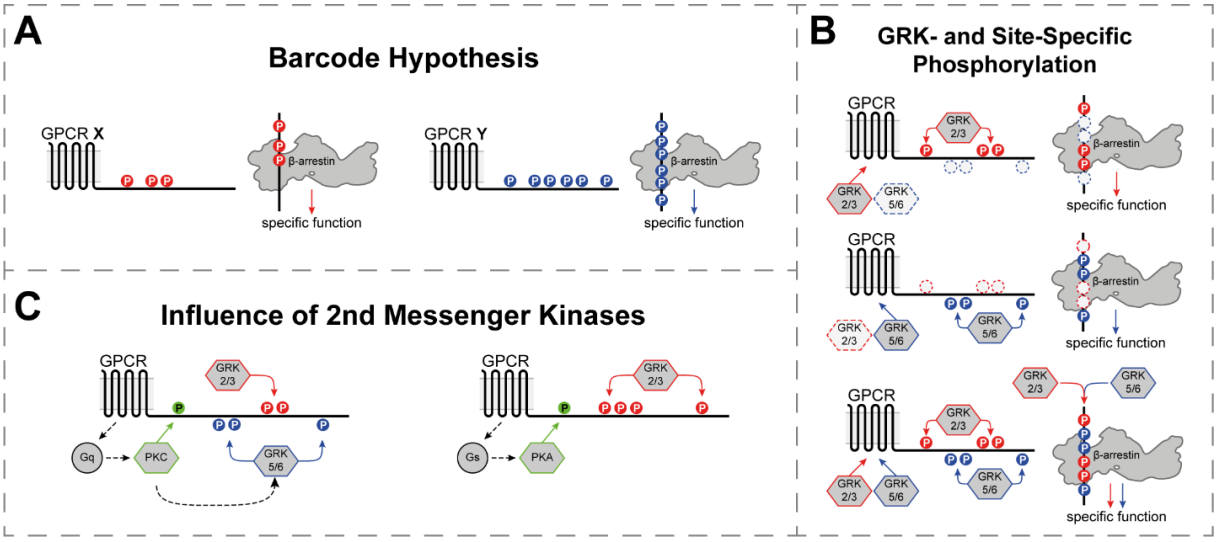

Figure 1.11 The "barcode" hypothesis of how β-arrestins interpret various GPCR phosphorylation patterns

A In its original form, the "barcode" hypothesis describes the fundamental features of β-arrestin mediated GPCR regulation: different GPCRs exhibit different phosphorylation patterns to induce specific β-arrestin functions. **B** GRK families (GRK2/3 or GRK5/6), or even individual GRK isoforms are able to phosphorylate specific serine or threonine residues with variable efficiency (Nobles et al. 2011, Doll et al. 2012, Miess et al. 2018). For different GPCRs this may result in the formation of GRK-specific phosphorylation patterns. As different cells feature distinct expression patterns of GRKs, the same GPCR could induce different β-arrestin functions, depending on the available GRK isoforms. Following this example, GRK2/3-mediated phosphorylation could be responsible for one specific downstream function (e.g. internalization), whereas GRK5/6-mediated phosphorylation could provoke a different reaction (e.g. amplification of MAPK signaling). **C** Not only GRKs, but also second messenger kinases have been shown to phosphorylate GPCRs directly. PKA and PKC are activated by $G\alpha_i$ and $G\alpha_q$ signaling, respectively. Thus, the phosphorylation pattern of a GPCR might also be influenced by its primary G protein coupling preference. (Figure was similarly published in Matthees et al. (2021) and reproduced according to the Creative Commons Attribution 4.0 International License.)

Multiple studies showed that different GRK isoforms preferentially phosphorylate specific sites of the same GPCR (Nobles et al. 2011, Miess et al. 2018, Doll et al. 2012). These findings expand the "barcode" hypothesis, as they suggest that one receptor may feature different phosphorylation states depending on the cellular context and the availability of kinases. For example, the β2ADR has been shown to be differentially phosphorylated by GRK2 or GRK6, resulting in kinase-specific C-terminal phosphorylation patterns (Nobles et al. 2011). From these results, a "site-specific barcode" hypothesis emerged, which suggests that GRK2/3 or GRK5/6 phosphorylate

the receptor at different sites to induce divergent functions (**Figure 1.11 B**). Thus, depending on the available kinases, a GPCR could be phosphorylated at GRK2/3- or GRK5/6-specific sites only, or fully phosphorylated by all four GRK isoforms to induce all possible arrestin-mediated functions.

Indeed, there is evidence that supports this hypothesis. As an example, Yang et al. (2015) linked specific receptor phosphorylation patterns with distinct conformational changes in β-arrestins. The publication also suggests that these defined β-arrestin conformational states mediate differential downstream functions. Interestingly, GRK2/3 phosphorylation was proposed to be the driver of receptor internalization, whereas GRK5/6-mediated GPCR phosphorylation was linked with increased ERK signaling (Yang et al. 2015, Kim et al. 2005, Ren et al. 2005). In contrast to these reports, overlapping or even opposing effects for individual GRK isoforms were identified, depending on the used cellular system and the investigated receptor (Zhu et al. 2013, Tran et al. 2004).

GPCR phosphorylation patterns are also influenced by second messenger kinases, like PKA or PKC (**Figure 1.11 C**). Those kinases are activated via the primary G_s or G_q signaling pathways, respectively, and have been shown to phosphorylate GPCRs directly. Interestingly, PKC also phosphorylates GRKs and is able to modulate their activity (Chuang et al. 1995, Winstel et al. 1996, Pronin und Benovic 1997). Thus, the resulting phosphorylation “barcode” of a GPCR might be changed by direct phosphorylation or via increasing or decreasing the activity of specific GRK isoforms, depending on the individual G protein-coupling preference.

1.3.2 ΔQ-GRK as a novel tool to decipher the impact of individual GRK isoforms

Studies investigating the impact of individual GRK isoforms on GPCR regulation usually rely on short interfering ribonucleic acid (siRNA), short hairpin RNA (shRNA) approaches or GRK inhibitors (Nobles et al. 2011, Doll et al. 2012, Miess et al. 2018). These methods harbor the risk of co-analyzing a remaining expression of targeted GRK(s) in knockdown approaches, or potential off-target effects of pharmacological intervention. Furthermore, the impact of these methods depends on the initial endogenous GRK expression levels, which were not assessed in these studies. As an example, the knockdown or inhibition of GRK2 would have less pronounced effects in a cellular system that genuinely features a low expression of GRK2. Additionally, no

clear consensus sequences have been identified for specific GRK isoforms, and even though GRK2, 3, 5, and 6 are usually thought of as ubiquitously expressed, different tissues feature vastly different expression levels of individual GRKs.

In an effort to overcome these limitations, Dr. Julia Drube created a comprehensive panel of eleven different human embryonic kidney 293 (HEK293) GRK knockout cell lines by utilization of the clustered regularly interspaced short palindromic repeats (CRISPR)/CRISPR-associated protein 9 (Cas9) technology. A representative western blot analysis, confirming the functional knockout of targeted GRKs is shown in **Figure 1.12**. Notably, single and double knockouts of individual GRK isoforms have been utilized before (Moller et al. 2020).

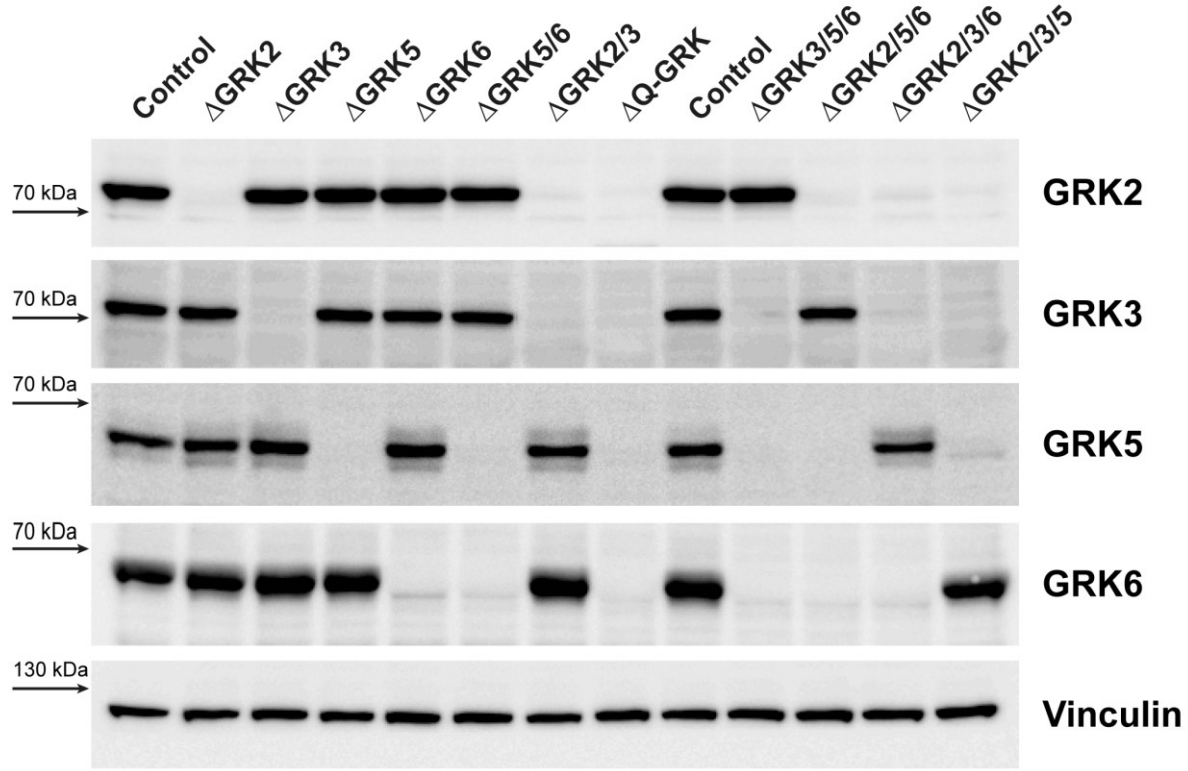

Figure 1.12 Western blot analysis and confirmation of functional GRK knockout

Western blot analysis of all targeted GRK isoforms (GRK2, 3, 5, 6) to confirm functional knockouts at a protein level. Single (ΔGRK2, 3, 5, 6), double (ΔGRK2/3 or 5/6), triple (ΔGRK3/5/6, 2/5/6, 2/3/6, 2/3/5), and quadruple (ΔQ-GRK) cells were generated using the CRISPR/Cas9 technology and established as single cell HEK293 clones. Additionally, the viability of the obtained clones was confirmed via cell proliferation assays and their morphology was normal, as assessed by phase-contrast microscopy (data not shown). (A pre-print of this figure was similarly published in Drube et al. (2021), cell lines and analysis were kindly provided by Dr. Julia Drube)

These cell lines comprise all single knockouts of ubiquitously expressed GRKs (ΔGRK2, 3, 5, 6), the two family knockouts of either GRK2 and 3 (ΔGRK2/3) or GRK5

and 6 (ΔGRK5/6) and all possible triple knockouts, namely ΔGRK3/5/6, ΔGRK2/5/6, ΔGRK2/3/6, ΔGRK2/3/5. These cell lines opened the possibility to investigate the impact of a single GRK at endogenous expression levels. Most importantly, the panel also includes a quadruple GRK knockout, also called ΔQ-GRK. This cell line, devoid of endogenous GRK2, 3, 5, or 6 expression, is an excellent tool to investigate the cellular effects of GRK phosphorylation. Especially with the possibility to reintroduce a single GRK isoform, ΔQ-GRK is an ideal measuring system. Assessing the effects of overexpressed kinases in ΔQ-GRK also has another great advantage, as the cell line provides a suitable “negative” control in form of a condition without any added GRKs.

These cell lines were extensively used throughout this thesis to investigate GRK-specific effects on GPCR regulation. In fact, the first part the thesis is a major contribution to the functional characterization of the established knockout clones.

1.4 PTH1R as a model receptor to investigate β-arrestin functions

Since arrestins are hypothesized to service all human GPCRs, the investigation of arrestin functions always demands the choice of a model system, or in this case, a model receptor. Historically, the rhodopsin–arrestin-1 system was extensively used to elucidate the structure and function of arrestins. One reason for this, is the availability of native rhodopsin, as it can be purified from bovine retinas in large quantities. Thus, biochemists are not limited to the use of recombinant receptors for their assays, which accelerated the progress in the field. Especially scanning mutagenesis approaches were successful to predict important arrestin-1 residues even before their structural confirmation by using native rhodopsin (Ostermaier et al. 2014, Peterhans et al. 2016, Haider et al. 2019b). The rhodopsin–arrestin-1 system is still the most important comparison for all other arrestin research, as conformational states (Mayer et al. 2019) and complex structures (Kang et al. 2015, Zhou et al. 2017) are very well defined. However, studies using this system do not always allow for generalized conclusions. As the visual system evolved to feature photoreceptors and separate arrestin genes, in an almost compartmentalized fashion, arrestin-1 only needs to service one specific GPCR to fulfill its role on an organism scale. Thus, experiments conducted with β-arrestins are anticipated to produce different results, as they have to mediate targeted functions for 800 different GPCRs.

As this thesis aims to elucidate differences between the two β-arrestin isoforms, many different model receptor systems could have potentially been applied. Moreover, it was even crucial to include multiple different GPCRs for the identification of GRK-specific arrestin interactions. The central experiments of this thesis, however, were conducted with the parathyroid hormone 1 receptor (PTH1R). This is due to the interesting features of the PTH1R, as it exhibits extended periods of intracellular trafficking and a robust interaction with β-arrestin1 and 2 (Vilardaga et al. 2002).

1.4.1 PTH1R sequence, signaling and physiology

The PTH1R is instrumental for multiple effects in human physiology. Its unique features, key signaling properties, and physiological roles are summarized in **Figure 1.13.** As a secretin-family GPCR, it features a rather large N-terminus that is essential for the recognition of its hormone ligands. The protein sequence is additionally led by a signal peptide that localizes the receptor efficiently to the membrane (**Figure 1.13 A**).

For PTH1R interactions with β-arrestins, especially the receptor C-terminus is of highest interest. Using different receptor mutations and mass spectrometry Zindel et al. (2016) identified two phosphorylation clusters of the PTH1R C-terminus that are important for β-arrestin2 recruitment (**Figure 1.13 A**). The proximal phosphorylation cluster is located exactly downstream of helix 8 and features five serine residues (amino acid positions 497-503). The distal phosphorylation cluster comprises four phosphorylatable amino acids and is located in close proximity (amino acid positions 509-514). Interestingly, an AP2-binding motif can be found between the two phosphorylation clusters, which possibly presents a way for the receptor to facilitate internalization in an arrestin-independent manner.

The cellular signaling of the PTH1R is depicted in **Figure 1.13 B** and can be seen as rather unique. In human physiology, the PTH1R is activated differently via two endogenous ligands, the parathyroid hormone (PTH), with its active component that comprises 34 amino acids (PTH(1-34)), and the PTH related peptide (PTHrP), which comprises 36 amino acids. Both ligands originate from much larger pro-hormones, which are excreted by the parathyroid gland (PTH) or neighboring cells (PTHrP) and subsequently cleaved by macrophages, in a process that involves the protease cathepsin D, to yield either PTH(1-34) or PTHrP(1-36) (Hendy et al. 1995).

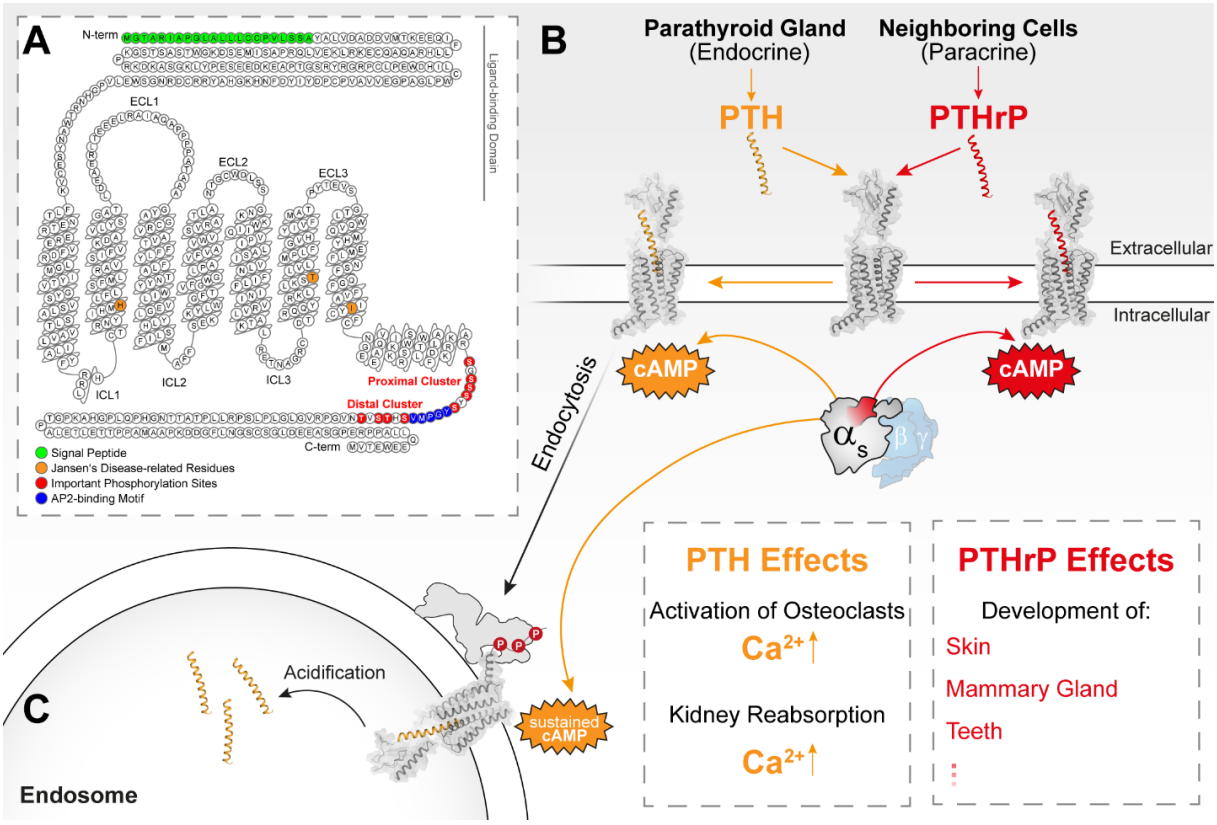

Figure 1.13 PTH1R physiology and key receptor domains

A Depicted is a snake-plot representation of the PTH1R (gpcrdb.org/protein/pth1r_human), highlighting important amino acid positions. The protein sequence features a signal peptide (green) in its rather big extracellular N-terminal ligand-binding domain. Orange-colored amino acids represent sites that are subject to mutation in Jansen's disease (Schipani et al. 1996), leading to a constitutive activation of the receptor. Red serine and threonine residues have been found to be important phosphorylation sites that enable high-affinity β-arrestin2 binding (Zindel et al. 2016), grouped in a proximal and distal cluster. An AP2-binding motif is located between the two phosphorylation clusters and colored in blue (Vilardaga et al. 2011). **B** The parathyroid hormone (PTH), is excreted by the parathyroid gland as a reaction to low blood Ca^{2+} levels and reaches its target cells via the endocrine system. When bound to the $G\alpha_s$-coupled PTH1R, PTH induces an immediate cAMP response at the membrane. Subsequently, the receptor is internalized via strong interactions with both β-arrestin isoforms. These processes enable a sustained cAMP production, as G proteins are further activated from endosomal compartments (Cheloha et al. 2015) (**C**). In kidney, PTH-mediated signaling leads to reabsorption of Ca^{2+}. In a synergistic manner, PTH activates osteoclasts in bone tissue, which also release Ca^{2+}. The secondary natural ligand is termed PTH related peptide (PTHrP), which leads to a similar cAMP response at the cell membrane, but does not induce sustained cAMP production from intracellular compartments. PTHrP acts in a paracrine manner, and regulates the formation of organs like skin, mammary glands and teeth.

Both ligands induce an active PTH1R conformation, which is able to mediate G protein activation. Hence, the $G\alpha_s$-coupled receptor is able to mediate an increase in cAMP at the cell membrane after binding to either PTH(1-34) or PTHrP (Cheloha et al. 2015).

The two natural agonists also bind the receptor in a very similar manner, but show substantial differences regarding their dissociation from the receptor. PTH(1-34) forms very stable complexes with the receptor, whereas PTHrP seems to rapidly and fully dissociate from the PTH1R after its initial activation (Ferrandon et al. 2009). Thus,

PTH(1-34) induces further internalization and trafficking of the receptor, via phosphorylation and interaction with β-arrestins. Most of the PTH1R–PTH(1-34) complexes also remain stable until they are redirected towards lysosomes, at which point the ligand dissociates due to low pH values (**Figure 1.13 C**).

The longevity of these PTH1R–PTH(1-34) complexes enables the receptor to induce sustained cAMP production. Interestingly, the extensive trafficking and robust β-arrestin interactions do not necessarily terminate the primary $G\alpha_s$ signaling of the PTH1R, as the receptor has been shown to mediate these prolonged cAMP responses specifically from endosomes (Sutkeviciute und Vilardaga 2020).

Accordingly, the two natural agonists of the PTH1R also mediate different physiological processes. Active PTH is released via the endocrine system as a reaction to low Ca^{2+} levels in the blood. After reaching the targeted cells, PTH-mediated signaling leads to reabsorption of Ca^{2+} in kidneys and activates osteoclasts in bone tissue. These cells also release Ca^{2+} via bone remodeling processes, which in combination leads to the restoration of physiological blood Ca^{2+} levels (Vilardaga et al. 2011). PTHrP, on the other hand, acts in a paracrine manner. It most prominently regulates the differentiation of cells, as it is released from adjacent cells of the same tissue. The signaling mediated by PTHrP seems to play a key role in the formation of organs like skin, mammary glands and teeth (Vilardaga et al. 2011).

Especially because of its robust interactions with both β-arrestin isoforms when activated with PTH(1-34), the PTH1R poses as an excellent model receptor to investigate differential conformational changes of β-arrestin1 and 2.

2. Aim of the thesis

Recent advances in structural biology established the cornerstones of our understanding of GPCR–arrestin interactions and the arrestin structure-function relationship. Nevertheless, these structural studies mostly present snapshots of the highly dynamic arrestin activation process. Hence, crucial questions regarding the role of GRKs, and distinct active arrestin conformations remain to be disclosed.

The first part of this project aimed to assess the influence of individual GRK isoforms on β-arrestin1 and β-arrestin2 interactions with different GPCRs. Additionally, these experiments were meant to provide a first functional characterization for the newly established GRK knockout cell lines. The main goals of this project are outlined below:

- *Establishment of a reliable BRET-based assay to characterize GRK-specific GPCR–β-arrestin interactions via the utilization of various GRK knockout cell lines.*
- *Characterization of GRK-specific β-arrestin recruitment for ten different receptors.*
- *Assessment of GRK-specific GPCR internalization, early trafficking, and β-arrestin co-localization.*

The second part of this thesis aimed to disclose differences between β-arrestin1 and β-arrestin2 conformational changes for the coupling to the same GPCR. The main objectives are again listed below:

- *Design and development of novel NanoLuc/FlAsH-based intramolecular conformational change biosensors for β-arrestin1 and 2.*
- *Establishment of an intramolecular BRET assay to study β-arrestin conformational changes, suitable for high-throughput screening.*
- *Differential analysis of β-arrestin1 and 2 conformational changes for coupling to the PTH1R.*
- *Assessment of phosphorylation-dependent and -independent β-arrestin1 and 2 conformational changes by utilization of phosphorylation deficient PTH1R variants and the ΔQ-GRK cell line.*
- *Characterization of differently formed PTH1R–β-arrestin complex configurations.*
- *Investigation of PTH1R–β-arrestin complex functionality in regards to internalization and MAPK-signaling.*

Taken together, this thesis aimed to provide crucial missing pieces in our understanding of arrestin-mediated GPCR regulation. With a focus on β-arrestin conformational changes and the functionality of individual GRK isoforms, the main ambition was to identify the different determinates for β-arrestin1 and 2 to adopt specific active conformations.

3. Materials and Methods

All chemicals, reagents and substances used in this thesis are listed in **Table 3.1** next to their corresponding manufacturer and article identifier.

Table 3.1 Used substances and corresponding manufacturers

Substance	Alias or Abbreviation	Manufacturer	Article identifier
Acetylcholine	ACh	Sigma-Aldrich	A6625
Agarose	–	Biozym	840000
C5a	C5a agonist	AnaSpec	AS65121
CaCl2	–	Merck	1.023.820.500
CMPD101	–	Tocris	15777006
cOmplete protease inhibitor cocktail	–	Roche	04693132001
[D-Ala^2, N-MePhe^4, Gly-ol]-enkephalin	DAMGO	Tocris	1171
Dulbecco's Modified Eagle Medium	DMEM	Sigma-Aldrich	d6429
Dimethyl Sulfoxide	DMSO	Sigma-Aldrich	D8418
Effectene transfection reagent	–	Qiagen	301427
Ethane-1,2-Dithiol	EDT	Sigma-Aldrich	02390
Ethylenediaminetetraacetic Acid	EDTA	Sigma-Aldrich	E-9884
Epinephrine Hydrochloride	–	Sigma-Aldrich	E4642
Fetal Calf Serum	FCS	Sigma-Aldrich	f7524
Fluorescein Arsenical Hairpin Binder	FlAsH-EDT$_2$	Toronto research chemicals	F335200
Fluoromount		Invitrogen	00-4958-02
Furimazin	NanoLuc Substrate	Promega	N1663
Gibson Assembly Mastermix	–	New Engalnd Biolabs	E2611
Glucose	–	Merck	8337
Halo Tag(618)	–	Promega	N1663
HCl	–	Roth	4625.1
hydroxyethylpiperazine ethane sulfonic acid	HEPES	AppliChem	A1069,0500
isoproterenol	Iso	Sigma-Aldrich	I5627
KCl	–	Sigma-Aldrich	P9541
KOD polymerase	–	Merck	71086
Lysogeny Broth	LB	Roth	X968.2
MgCl2 x 6 H2O	–	Roth	HN03.1
Plasmid plus midi kit	–	Qiagen	12945
NaCl	–	Roth	3957.2
NaOH	–	Roth	9356.1
NP-40 (alternative)	–	Merck	492016
Norepinephrine hydrochloride	–	Sigma-Aldrich	74488
P44/42 (ERK1/2) mouse mAb		Cell Signaling	9107
Phosphate-Buffered Saline	PBS	Sigma-Aldrich	P4417
Phospho-p44/42 (ERK1/2) mouse mAb	–	Cell Signaling	9106
PhosSTOP phosphatase inhibitor cocktail	–	Roche	04906845001
Polyethylenimine	PEI	Sigma-Aldrich	408727
Penicillin/Streptomycin	–	Sigma-Aldrich	P0781
Pindolol	–	Sigma-Aldrich	P0778
Poly-D-Lysine hydrobromide	–	Sigma-Aldrich	P6407
Parathyroid Hormone (1-34) acetate	PTH(1-34)	BACHEM	4011474
Sodium deocycholate	–	Sigma-Aldrich	D6750
Tris	–	Roth	5429.3
Trypsin EDTA	–	Gibco	25300
Vinculin mouse mAb	–	BIOZOL	BZL03106

3.1 Cell culture

Furthermore, all functional data presented in this study was acquired using the cell lines described in **Table 3.2**. HEK293 cells were cultured at 37°C with 5% CO2 in Dulbecco's modified Eagle medium (DMEM), supplemented with 10% fetal calf serum (FCS) and 1% penicillin and streptomycin. The adherent cells were passaged twice a week with all experiments being conducted using cultures that were passaged less than 30 times with an optimal confluency between 70 and 90%.

Table 3.2 Utilized cell lines and their origins

Cell line	species	parental line	reference
HEK293	human	–	Graham et al. (1977)
Control	human	HEK293	Drube et al. (2021)
ΔGRK2/3/5/6	human	HEK293	Drube et al. (2021)
ΔGRK2/3	human	HEK293	Drube et al. (2021)
ΔGRK5/6	human	HEK293	Drube et al. (2021)
ΔGRK3/5/6	human	HEK293	Drube et al. (2021)
ΔGRK2/5/6	human	HEK293	Drube et al. (2021)
ΔGRK2/3/6	human	HEK293	Drube et al. (2021)
ΔGRK2/3/5	human	HEK293	Drube et al. (2021)
β-arrestin1/2 KO	human	HEK293F	O'Hayre et al. (2017)

3.2 Molecular cloning

All featured overexpression experiments were conducted using the recombinant plasmids specified in **Table 3.3**.

β-arrestin2 conformational change biosensors were created on the basis of constructs described in Nuber et al. (2016). To enable BRET measurements, the CFP-tag was exchanged with the NanoLuc gene (Promega, (Hall et al. 2012)). For FlAsH insertions at position F9 and F10 homologous positions as described in Lee et al. (2016) (their position F4, F5, respectively) were used. β-arrestin1 constructs were designed homologously. A detailed alignment and comparison of insertion sites for FlAsH-binding (CCPGCC) for all utilized β-arrestin conformational change biosensors is shown in the appendix of this thesis (**Appendix Figure 1**).

The C-terminal tags of PTH1R constructs previously described in Zindel et al. (2016) were exchanged with the Halo-tag gene (Promega, (Los et al. 2008)). For this and all other constructs that required an exchange in biological tags, the isothermal assembly

reaction was used as described by Gibson et al. (2009). To generate fragments with suitable overhangs to facilitate this reaction, the primer design software provided by New England Biolabs (NEBuilder: https://nebuilder.neb.com/) was used. Fragments were synthesized using KOD polymerase and the cloning procedure was performed according to the New England Biolabs isothermal assembly protocol.

Table 3.3 Utilized DNA constructs

Backbone	Gene of interest	source	cloning strategy or reference
pcDNA3	β-arrestin1-Nluc	Ulrike Zabel (AG Hoffmann)	–
pcDNA3	β-arrestin2-Nluc	Ulrike Zabel (AG Hoffmann)	–
pFN21K	HaloTag-β-arrestin1	Promega	–
pFN21K	HaloTag-β-arrestin2	Promega	–
pcDNA3	β-arrestin1-F1-10-Nluc	Ulrike Zabel (AG Hoffmann)	–
pcDNA3	β-arrestin1-dFLR-F5-Nluc	self-made	site-directed mutagenesis
pcDNA3	β-arrestin2-F1-10-Nluc	Ulrike Zabel (AG Hoffmann)	–
pcDNA3	β-arrestin1-YFP	Cornelius Krasel	Krasel et al. (2005)
pcDNA3	β-arrestin2-YFP	Cornelius Krasel	Krasel et al. (2005)
pcDNA3	β-arrestin1-dFLR-YFP	self-made	site-directed mutagenesis
pcDNA3	β-arrestin2-dFLR-YFP	self-made	site-directed mutagenesis
pcDNA3	GRK2	Julia Drube (AG Hoffmann)	Drube et al. (2021)
pcDNA3	GRK3	Julia Drube (AG Hoffmann)	Drube et al. (2021)
pcDNA3	GRK5	Julia Drube (AG Hoffmann)	Drube et al. (2021)
pcDNA3	GRK6	Julia Drube (AG Hoffmann)	Drube et al. (2021)
pcDNA3	GRK2-YFP	self-made	Isothermal assembly
pcDNA3	GRK3-YFP	self-made	Isothermal assembly
pcDNA3	GRK5-YFP	self-made	Isothermal assembly
pcDNA3	GRK6-YFP	self-made	Isothermal assembly
pFN21K	β2ADR-Nluc	self-made	Isothermal assembly
pcDNA3	β2ADR	Ulrike Zabel (AG Hoffmann)	–
pFN21K	PTH1R-HaloTag	self-made	Isothermal assembly
pcDNA3	PTH1R	Ulrike Zabel (AG Hoffmann)	–
pcDNA3	PTH1R-CFP	Ulrike Zabel (AG Hoffmann)	–
pcDNA3	Rab5-mCherry	Tom Kirchhausen	–
pcDNA3	M5R-CFP	Ulrike Zabel (AG Hoffmann)	–
pFN21K	β2V2-Nluc	self-made	Isothermal assembly
pFC32K	M1R-Nluc	Ulrike Zabel (AG Hoffmann)	–
pFC32K	M2R-Nluc	Ulrike Zabel (AG Hoffmann)	–
pFC32K	M3R-Nluc	Ulrike Zabel (AG Hoffmann)	–
pFC32K	M4R-Nluc	Ulrike Zabel (AG Hoffmann)	–
pFC32K	M5R-Nluc	Ulrike Zabel (AG Hoffmann)	–
pFN21K	MOP-Nluc	self-made	Isothermal assembly
pFN21K	C5aR1-Nluc	self-made	Isothermal assembly
pcDNA3	PTH1R-PD1	Cornelius Krasel	Zindel et al. (2016)
pFN21K	PTH1R-PD1-HaloTag	self-made	Isothermal assembly
pcDNA3	PTH1R-PD1-CFP	self-made	Isothermal assembly
pcDNA3	PTH1R-PD2	Cornelius Krasel	Zindel et al. (2016)
pFN21K	PTH1R-PD2-HaloTag	self-made	Isothermal assembly
pcDNA3	PTH1R-PD2-CFP	self-made	Isothermal assembly

β-arrestin-dFLR constructs were designed according to Cahill et al. (2017) by site-directed mutagenesis using KOD polymerase. Amino acids from Y63 to K77 were

deleted for β-arrestin1 and a homologous deletion was conducted for β-arrestin2 at amino acid positions ranging from Y64 to K78. The used primers are shown in **Table 3.4**.

Table 3.4 Site-directed mutagenesis primers

Primer	DNA Sequence
βArr1-dFLR_fwd	CTG ACC TGC GCC TTC CGC GAC CTG TTT GTG GCC AAC G
βArr1-dFLR_rev	GTT GGC CAC AAA CAG GTC GCG GAA GGC GCA GGT CAG CG
βArr2-dFLR_fwd	CTC ACC TGC GCC TTT CGC GAC CTG TTC ATC GCC AAC TAC C
βArr2-dFLR_rev	GTT GGC GAT GAA CAG GTC GCG AAA GGC GCA GGT GAG GG

The Rab5-mCherry construct was kindly provided by Tom Kirchhausen (Harvard Medical School, Boston, USA).

3.3 Intermolecular bioluminescence resonance energy transfer (BRET)

To assess β-arrestin recruitment via intermolecular BRET, either 1,2 (HEK293, Control, β-arrestin1/2 KO) or 1,6 (various ΔGRK cell lines) million cells were seeded into 600 mm tissue culture-treated plates. After 24 hours of incubation, cells were transfected with 2.5 µg DNA according to the Effectene transfection reagent manual by Qiagen. This step was common to all conducted experiments in this study, unless otherwise noted. Different transfection schemes were optimized depending on the localization of utilized BRET donor and acceptor molecules, summarized in **Table 3.5**.

Table 3.5 Transfection schemes for intermolecular BRET

	β-arrestin BRET donor		GPCR BRET donor	
Construct	**basic scheme**	**GRK-specific**	**basic scheme**	**GRK-specific**
GPCR-NanoLuc	–	–	0.5 µg	0.5 µg
HaloTag-β-arrestin	–	–	1 µg	1 µg
GPCR-HaloTag	1.5 µg	1.5 µg	–	–
β-arrestin-NanoLuc	0.375	0.375	–	–
GRK	–	0.25 µg	–	0.25 µg
pcDNA3	0.625 µg	0.375	1 µg	0.75 µg

After 24 hours, 40,000 cells were seeded per well into poly-D-lysine coated 96-well plates (Brand, #781965). For labelling of the Halo-tag used as a BRET donor, Halo-ligand(618) was added in a ratio of 1:2,000 to the cell suspension. For each transfection, triplicates and a condition lacking the Halo-ligand(618) were seeded. Another 24 hours later, the cells were washed twice with measuring buffer (140 mM NaCl, 10 mM HEPES, 5.4 mM KCl, 2 mM CaCl2, 1mM MgCl2; pH7.3) and 90 µL of NanoLuc substrate furimazine was added (used at a ratio of 1:35,000 in measuring buffer). The concentration-dependent BRET change was measured using a Synergy Neo2 plate reader (Biotek), utilizing a custom-made filter (donor emission registered at 555 nm wavelength and below, with an additional fluorescence filter to detect Halo-ligand(618) or FlAsH emission at 620/15 nm). The baseline measurements were conducted for three minutes. After stimulation with the respective PTH(1-34) concentrations, the measurements were continued for five minutes and subsequently averaged. Initial BRET changes were calculated by the division of the stimulated values by baseline values. The initial BRET change was then corrected for labelling efficiency via subtraction of values generated by mock labelling. To achieve the final Δ net BRET change, the corrected BRET change was divided by the vehicle control. The recruitment of the different β-arrestin-FlAsH conformational change sensors and of the β-arrestin-dFLR constructs to the PTH1R was measured accordingly.

3.4 Intramolecular BRET

For the assessment of β-arrestin conformational changes, 1,2 million cells were seeded into 600 mm tissue culture-treated plates. After 24 h of incubation, the cells were transfected with 1.2 µg untagged receptor, 0.12 µg of the respective β-arrestin FlAsH-tagged biosensor C-terminally coupled to NanoLuc and empty vector to adjust the total amount of DNA to 2 µg, following the Effectene transfection reagent protocol by Qiagen. 24 hours after transfection, 40,000 were seeded cells per well into poly-D-lysine coated 96-well plates and incubated overnight at 37°C. For this study, the FlAsH-labelling procedure previously described by Hoffmann et al. (2010) was adjusted for 96-well plates. Before the FlAsH-labelling procedure, the cells were washed twice with PBS, then incubated with 250 nM FlAsH in labelling buffer (150 mM NaCl, 10 mM HEPES, 25 mM KCl, 4 mM CaCl2, 2mM MgCl2, 10 mM glucose; pH7.3), complemented with 12.5 µM EDT for 60 minutes at 37°C. Eight wells per transfection

did not receive FlAsH labeling solution, but were instead incubated with a mock-labeling solution, which contained an additional 250 nM DMSO instead of FlAsH. After aspiration of the FlAsH labelling or mock labelling solutions, the cells were incubated for 10 min at 37°C with 100 µl 250 µM EDT in labelling buffer per well. Subsequent to this washing step, the cells were washed twice with labeling buffer. Addition of the NanoLuc substrate, measurement and analysis of the BRET change was performed as described above (see intermolecular BRET).

3.5 Evaluation of *Z*-factor

Z-factors for β-arrestin1/2-F5 conformational change biosensors was assessed by utilizing data of time-dependent signal following stimulation of the PTH1R with 3 µM PTH(1-34). Calculations were conducted following the original publication of Zhang et al. (1999). To assess means (µ) and standard deviations (σ), individual data points recorded after 200 seconds of stimulation with either vehicle (c) or 3 µM PTH(1-34) (s) were used and applied in the following equation:

$$Z = 1 - \frac{(3\sigma_s + 3\sigma_c)}{|\mu_s - \mu_c|}$$

3.6 Confocal microscopy

In case of fixed samples, HEK293 cells were transfected with 1 µg of GPCR-CFP, 0.5 µg of Rab5-mCherry and pcDNA3, adjusting the final DNA content to 2 µg, according to the Effectene transfection reagent manual by Qiagen. 24 h subsequent to transfection, 700,000 cells were seeded onto poly-D-lysine coated cover slips in 6-well plates. After receptor stimulation with 100 nm PTH(1-34) for 15 minutes, the cover slips were removed from the 6-well plates and fixed in PBS containing 4% formaldehyde for 15 minutes, then washed three times with PBS. To finalize sample preparation, the cover slips were transferred onto microscopic slides, cells facing down, using Fluoromount as a mounting medium. As soon as the mounting medium dried, the samples were ready for analysis via confocal microscopy or storage in the dark.

In case of conducted live cell microscopy experiments, the cells were transfected with 1 µg of GPCR-CFP, 0.5 µg of β-arrestin-YFP and 0.5 µg of Rab5-mCherry, according to the Effectene transfection reagent manual by Qiagen. After 24 hours, 700,000 cells

were seeded onto poly-D-lysine coated cover slips in 6-well plates and were ready for microscopy the following day.

Before microscopy, the cells were washed twice with measuring buffer. The confocal microscopy images were acquired before and 15 minutes after stimulation with the appropriate agonist at the Leica SP8 laser scanning microscope in a 1024x1024 pixel format, using a 63x water immersion objective, zoom factor 3, line average 3 and 400 Hz. CFP was excited at 442 nm, mCherry at 561 nm and YFP at 514 nm. The features of the acquired confocal images were segmented and quantified using an ImageJ based software called segmentation and quantification of subcellular shapes (Squassh) (Rizk et al. 2014). After Squassh's deconvolution, denoising and segmentation of the two or three fluorescence channels of each image, the raw data readout was eligible for analysis using the R based software SquasshAnalyst as described by Rizk et al. (2015). All image derived data in this study was processed and analyzed with this method.

3.7 Westernblot

For analysis of ERK phosphorylation, 600,000 HEK293 cells or β-arrestin1/2 KO cells were seeded in 6-well plates 24 h before transfection. The cells were transfected with 4 µg of indicated expression plasmids using PEI (diluted to 10 µg/ml, pH 7.2 adjusted with HCl). After 24 h, the cells were starved from FCS for 4 h and cells were then treated with 100 nM PTH(1-34) for 20 minutes or left untreated. Cells were then washed with ice-cold PBS and lysed with RIPA lysis buffer (1 % NP-40 (alternative), 1 mM EDTA, 50 mM Tris pH 7.4, 150 mM NaCl, 0.25 % sodium deoxycholate), supplemented with protease and phosphatase inhibitor cocktails. Samples were run on polyacrylamide gels and analyzed for vinculin, pERK or total ERK as indicated. Quantification was done using Fujifilm Multi Gauge software.

4. Results

This thesis is comprised of two closely linked projects that will be presented in the following chapters, sequentially. Both projects focus on the functionality of arrestins, yet the first set of presented results will address the GRK-specificity of GPCR–β-arrestin interactions. These experiments rely on the recently generated GRK knockout cell lines described in **chapter 1.3.2**. The used figures, tables, and descriptions are part of the manuscript by Drube et al. (2021).

4.1 GRK-specific β-arrestin recruitment

The currently accepted “barcode” hypothesis (Xiao und Liu 2016) of C-terminal GPCR phosphorylation entrails several reports about GRK- and site-specific phosphorylation of the β2ADR (Nobles et al. 2011, Yang et al. 2015). The presented findings suggest that the β2ADR is differentially phosphorylated by specific GRK isoforms (namely, GRK2 and GRK6). The resulting GRK-specific phosphorylation patterns have then been shown to induce different active arrestin conformations *in vitro*. Yet, these studies rely on the use of siRNA knockdown of GRKs or the use of synthesized C-terminal receptor peptides. Hence, they do not necessarily reflect on the cellular reactions that follow agonist-promoted β2ADR phosphorylation.

To elucidate the direct contribution of individual GRKs to β2ADR-induced β-arrestin recruitment, different assays were established during this thesis to utilize the full potential of the novel GRK knockout cell lines. Furthermore, the availability of tools for the direct analysis of site-specific receptor phosphorylation is limited across the GPCR superfamily. Phosphorylation-specific antibodies are often-times not available and comprehensive mass spectrometry analyses require specialized facilities. Thus, we utilized the universal GPCR adaptor proteins β-arrestin1 and 2 not only to assess GRK-dependent recruitment, but also to analyze the impact of individual GRKs on receptor regulation in general.

4.1.1 β-arrestin recruitment is strictly dependent on GRK expression levels

The schematic in **Figure 4.1 A** depicts the established BRET-based *in cellulo* β-arrestin recruitment assay, allowing us to reveal functional, GRK-specific GPCR phosphorylation. In order to incorporate the novel GRK knockout cell lines, two different

approaches have been devised, as presented in **Figure 4.1 B**. The recruitment assay enabled the investigation of endogenous GRK expression levels when performed in triple GRK knockout cell lines (ΔGRK3/5/6, ΔGRK2/5/6, ΔGRK2/3/6, ΔGRK2/3/5), featuring the remaining expression of only one specific GRK isoform (endogenous "kinase-screen"). In contrast, the overexpression of GRK isoforms in ΔQ-GRK was employed to assess the full potential of a specific GRK to enable β-arrestin recruitment ("kinase-screen"). Both strategies additionally utilize Control and/or ΔQ-GRK cells without the overexpression of GRKs as control conditions.

First, we studied the GRK-specific interactions between the β2ADR and β-arrestin2 utilizing the endogenous expression of GRKs in various ΔGRK cells. At endogenous expression levels of all four GRKs (Control), β-arrestin2 showed a clear isoproterenol-(Iso) induced recruitment to the β2ADR (**Figure 4.1 C**). In comparison, β-arrestin2 recruitment was substantially reduced when recorded in triple GRK KO cell lines, showing that neither of the analyzed GRKs can compensate for the loss of other GRK isoforms at endogenous expression levels.

While the individual endogenous expression of either GRK2, 3, or 5 induced only minimal BRET changes, these were, nevertheless, sufficient to detect a ligand-dependent increase in β-arrestin recruitment. In this study, data which could be described by a curve-fit will be further interpreted as functional recruitment. The highest amount of β-arrestin2 recruitment was found in ΔGRK2/3/5 cells, specifically induced by the endogenous expression of GRK6. This finding correlates with the relative abundance of GRKs in HEK293 cells (Thul et al. 2017), as compiled by the human protein atlas (http://proteinatlas.org/humanproteome/cell) (**Figure 4.1 D**), with GRK6 being approximately 5-fold more expressed than the other assessed isoforms. Thus, we identified GRK6 as the main mediator of Iso-promoted β-arrestin recruitment to the β2ADR, when measured under endogenous expression of GRKs in HEK293 cells. Still, the endogenous expression of GRK 6 is not sufficient to induce a full β-arrestin2 recruitment as seen in Control cells, suggesting that endogenous GRK expression levels are fine-tuned to collaboratively direct β-arrestin functions.

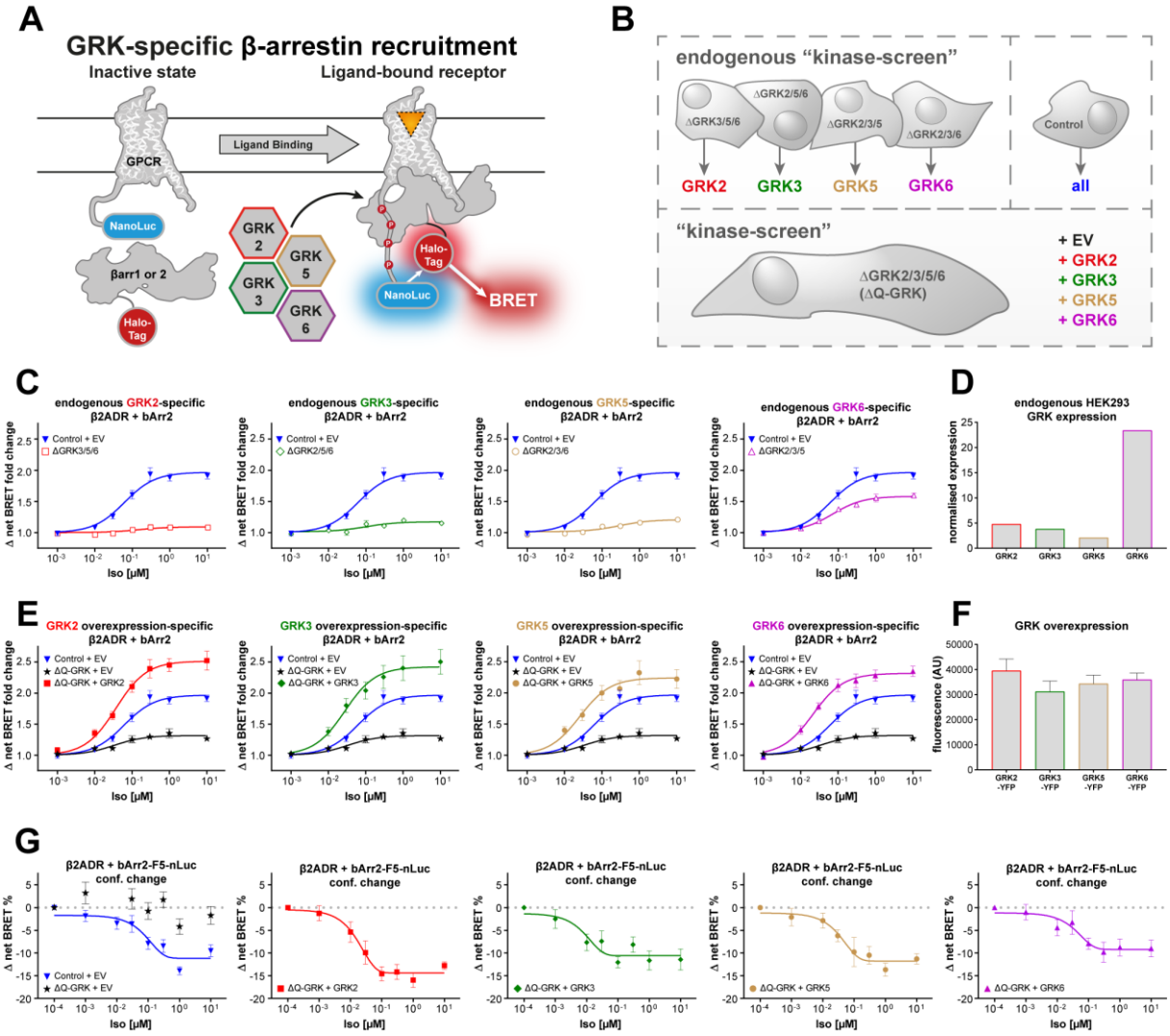

Figure 4.1 GRK2, 3, 5, and 6 are individually able to facilitate high-affinity β-arrestin 2 binding to the β2ADR

A Schematic depiction of the performed NanoBRET β-arrestin (βArr) recruitment assay and color-coding for GRK-specific conditions used throughout the thesis. The Halo-Tag-β-arrestin fusion protein is recruited to a NanoLuc-tagged GPCR upon agonist activation and subsequent receptor phosphorylation. Measured BRET ratios enable the agonist concentration-dependent analysis of β-arrestin recruitment. **B** Schematic depiction of the two different possibilities to measure GRK-specific β-arrestin recruitment. The Control cell line is always used to confirm the effect of all endogenously expressed GRKs. For application of the endogenous "kinase-screen", triple GRK KO cell lines are used, which only feature the remaining endogenous expression of one GRK isoform (ΔGRK3/5/6, ΔGRK2/5/6, ΔGRK2/3/6, ΔGRK2/3/5). To assess the capabilities of a single GRK isoform at a presumably saturated expression level ("kinase-screen"), the respective GRK isoform is overexpressed in ΔQ-GRK. **C** GRK-specific Halo-Tag-β-arrestin2 recruitment to the β2ADR-NanoLuc upon stimulation with isoproterenol (Iso) using triple GRK KO cell lines (endogenous "kinase-screen") **D** The normalized endogenous expression levels of all four GRKs in HEK293 cells (Thul et al. 2017), as compiled by the human protein atlas (http://proteinatlas.org/humanproteome/cell). **E** βArr2 recruitment to the β2ADR in ΔQ-GRK, overexpressing a single GRK. BRET data in (**C**) and (**E**) are presented as Δ net BRET fold change, mean of three independent experiments ± SEM. For better comparison, the Control and ΔQ-GRK curves are shown multiple times. **F** GRK-YFP fusion proteins were transfected in ΔQ-GRK and YFP fluorescence was measured to confirm similar expression levels of all transfected GRKs. Measured fluorescence is depicted as mean + SD of four independent transfections as arbitrary units (AU). **G** Analysis of β-arrestin2 conformational changes. ΔQ-GRK or Control cells were transfected with an untagged β2ADR expression construct and the β-arrestin2-F5-NanoLuc conformational change biosensor, in absence or presence of GRKs as noted and stimulated with Iso. Conformational change data are shown as Δ net BRET change in percent, mean of three independent repetitions ± SEM.

Since these findings specifically reflected on the expression levels of GRKs, we analyzed the molecular capability of each individual GRK to induce β2ADR–β-arrestin2 interactions via overexpression in ΔQ-GRK (**Figure 4.1 E**). The relative expression of transfected GRKs was assessed fluorometrically (**Figure 4.1 F**). Via introduction of a C-terminal YFP fusion into the identical vector backbone and subsequent equimolar transfection of GRK-YFP constructs, we confirmed similar expression levels of the transfected kinases. To allow for this comparison, the GRK-YFP fusion proteins were characterized with at least the same capability to mediate GPCR–β-arrestin interactions as their untagged counterparts, used in all other experiments (**Figure 4.2 A**). Using this controlled overexpression of individual GRKs in ΔQ-GRK, all four kinases showed a similar effect on β2ADR regulation: each individual GRK isoform enhanced the β2ADR–β-arrestin recruitment to higher levels than induced by the combined endogenous expression of GRKs in Control cells (**Figure 4.1 E**). Interestingly, we still encountered measurable β-arrestin2 recruitment in the absence of GRKs (ΔQ-GRK + EV). This could be explained by the inherent affinity of β-arrestin2 towards ligand-activated, yet unphosphorylated GPCRs, or the action of other kinases.

These findings clarify that all four tested GRKs are able to individually mediate high-affinity β-arrestin2 binding to the β2ADR and that their relative tissue expression ultimately defines GRK-specific contributions to this process.

Since all GRKs have been shown to induce similar levels of β-arrestin recruitment, we investigated whether isoform-specific phosphorylation of the β2ADR might still have a pronounced effect on the conformational changes that occur during arrestin activation. To address this, we overexpressed each individual GRK isoform alongside the untagged β2ADR and the novel intramolecular β-arrestin2-FlAsH5-NanoLuc BRET biosensor. This first application of a FlAsH-NanoLuc conformational change sensor showed that all four analyzed GRK isoforms are able to induce comparable conformational changes at the F5 position of β-arrestin2 when coupling with the β2ADR (**Figure 4.1 G**).

We further utilized the β2ADR, as a model receptor regulated by GRK2, 3, 5, and 6, to test the effect of endogenous ligands and pharmacological inhibition on GRK-specific β-arrestin-coupling processes. The application of the endogenous ligands epinephrine and norepinephrine resulted in overall lower GRK-specific β-arrestin2 recruitment to the β2ADR as compared to Iso (**Figure 4.2 B, C** compare with **Figure 4.1 E**).

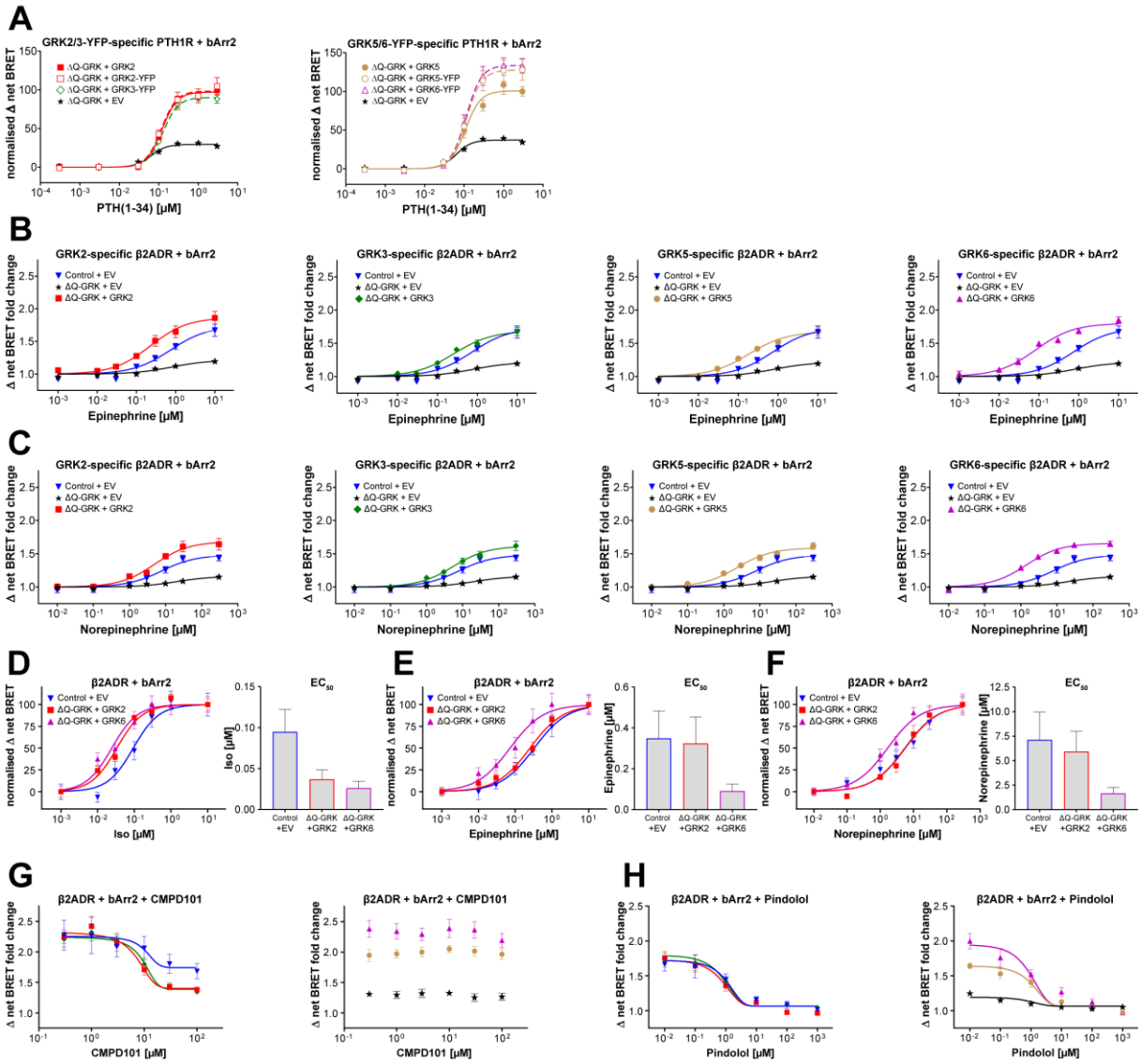

Figure 4.2 Assessment of GRK-specific effects for endogenous Ligands, antagonists, and GRK inhibitors

A ΔQ-GRK cells were transfected with either YFP-tagged or untagged GRKs as indicated and β-arrestin2 recruitment to the PTH1R was measured using the established NanoBRET. Data points are presented as the mean ± SEM of the calculated Δ net BRET fold change from three independent measurements. The utilization of the GRK-YFP constructs resulted in comparable β-arrestin2 recruitment as in presence of the untagged GRKs (corresponds to **Figure 4.1 F**). **B, C** GRK-specific β-arrestin2 recruitment to the β2ADR was measured in presence of the endogenous ligands epinephrine (**B**) or norepinephrine (**C**). Data for the Control + empty vector (EV) and ΔQ-GRK + EV conditions are depicted in each panel. The mean ± SEM of the Δ net BRET fold change from three independent experiments are shown. **D-F** The recruitment of β-arrestin2 to the β2ADR following stimulation with Iso (**D**), Epinephrine (**E**), or Norepinephrine (**F**) in Control cells or in presence of individually overexpressed GRK2 or GRK6 in ΔQ-GRK as indicated. Data are depicted as mean of three independent experiments ± SEM and normalized to individual maxima. The bar graphs represent the EC_{50} + SEM of the corresponding concentration-response curves. **G, H** Utilization of the β-arrestin recruitment assay for specificity determination of the GRK inhibitor cmpd101 in living cells. ΔQ-GRK or Control cells were transfected with β2ADR-NanoLuc, Halo-Tag-β-arrestin2, and either GRK2, 3, 5, 6, or EV as noted. The cells were incubated with different concentrations of cmpd101 (**G**) or the β2ADR antagonist pindolol (**H**) for 10 minutes prior to stimulation with 1 µM Iso. The recruitment-induced BRET changes are presented as Δ net BRET change in percent, as the mean ± SEM of four independent experiments.

Although the relative efficacies of individual GRKs to mediate epinephrine- and norepinephrine-induced β-arrestin2 binding were unchanged in comparison to Iso (ΔQ-GRK + GRK > Control + EV > ΔQ-GRK + EV), we observed a left shift of the measured

concentration-response curves specifically for GRK6 (**Figure 4.2 D, E, F**). This apparent increase in potency was observed for both endogenous ligands, although it was previously shown that epinephrine acts as a full agonist, whereas norepinephrine only partially activates the β2ADR (Reiner et al. 2010). This might have implications for the tissue-specific regulation of the β2ADR, as lower ligand concentrations might be sufficient to desensitize the receptor in tissues with relatively higher GRK6 expression.

Since we were able to measure GRK-specific β-arrestin recruitment, we hypothesized that this assay is also suitable to characterize the specificity of GRK inhibitors in a cellular system. Indeed, we were able to record the concentration-dependent inhibition of β-arrestin2 recruitment to the receptor by cmpd101 (a known GRK2 family inhibitor) only in cells expressing GRK2 or 3 **(Figure 4.2 G)**. This demonstrates cmpd101 selectivity in living cells by the lack of inhibition when overexpressing GRK5 or 6. When performing the analogous experiment using pindolol as a potent antagonist of the β2ADR, we recorded an inhibition of β-arrestin2 recruitment regardless of GRK (over-) expression **(Figure 4.2 H)**. Thus, we present the first cell-based GRK-inhibitor screening platform utilizing ΔQ-GRK.

4.1.3 GPCRs are regulated by either GRK2/3 or GRK2/3/5/6

To investigate the GRK-specificity of GPCR regulation, we compared the impact of GRK2, 3, 5 and 6 on β-arrestin recruitment across ten different GPCRs: β2ADR, β2ADR with an exchanged C-terminus of the V2R (β2V2), complement 5a receptor 1 (C5aR1), muscarinic acetylcholine receptors 1-5 (M1R, M2R, M3R, M4R, M5R), μ-opioid receptor (MOP), and PTH1R. This panel was deliberately selected to feature receptors with divergent lengths of intracellular loop 3 (ranging from 5 to 211 amino acids) and C-termini (ranging from 10 to 105 amino acids). **Table 4.1** shows a comprehensive overview about the analyzed receptors. Additionally to the lengths of important intracellular domains, also the number of putative phosphorylation sites as well as predominant G protein-coupling of the receptors were compiled.

Table 4.1 Overview of analyzed receptors

Depicted are the length (number of amino acids) of intracellular loop 3 (IL3) and C-termius for each analyzed GPCR with respective numbers of putative serine and threonine (S/T) phosphorylation sites. Information compiled from GPCRdb.org and Inoue et al. (2019)

receptor	length IL3	number S/T in IL3	length C-term	number S/T in C-term	G protein-coupling	used agonist
β2ADR	24	3	72	13	$G\alpha_s$	isoproterenol
β2V2	24	3	27	11	$G\alpha_s$	isoproterenol
C5aR1	5	2	37	11	$G\alpha_i$	C5a
MOP	5	1	46	11	$G\alpha_i$	DAMGO
PTH1R	8	1	105	21	$G\alpha_s$	PTH(1-34)
M1R	128	22	26	3	$G\alpha_q$	acetylcholine
M2R	152	31	10	1	$G\alpha_i$	acetylcholine
M3R	211	51	29	1	$G\alpha_q$	acetylcholine
M4R	156	24	10	1	$G\alpha_i$	acetylcholine
M5R	200	40	20	1	$G\alpha_q$	acetylcholine

As representative examples of our findings, the GRK-selective β-arrestin1 and 2 recruitment to the M5R and PTH1R are depicted in **Figure 4.3 A, B** and **Figure 4.3 C, D**, respectively (data for all receptors are shown in **Figure 4.5**). Both receptors were able to induce robust, agonist-dependent β-arrestin1 and 2 recruitment in Control cells, which was significantly reduced in ΔQ-GRK. In case of the M5R, β-arrestin1 recruitment was completely abolished in ΔQ-GRK. Still, a major difference in GRK-selectivity of the two receptors was found using this approach: the individual overexpression of GRK2, 3, 5, and 6 significantly increased β-arrestin recruitment to the PTH1R in ΔQ-GRK, whereas GRK5 and 6 were unable to facilitate M5R–β-arrestin complex formation.

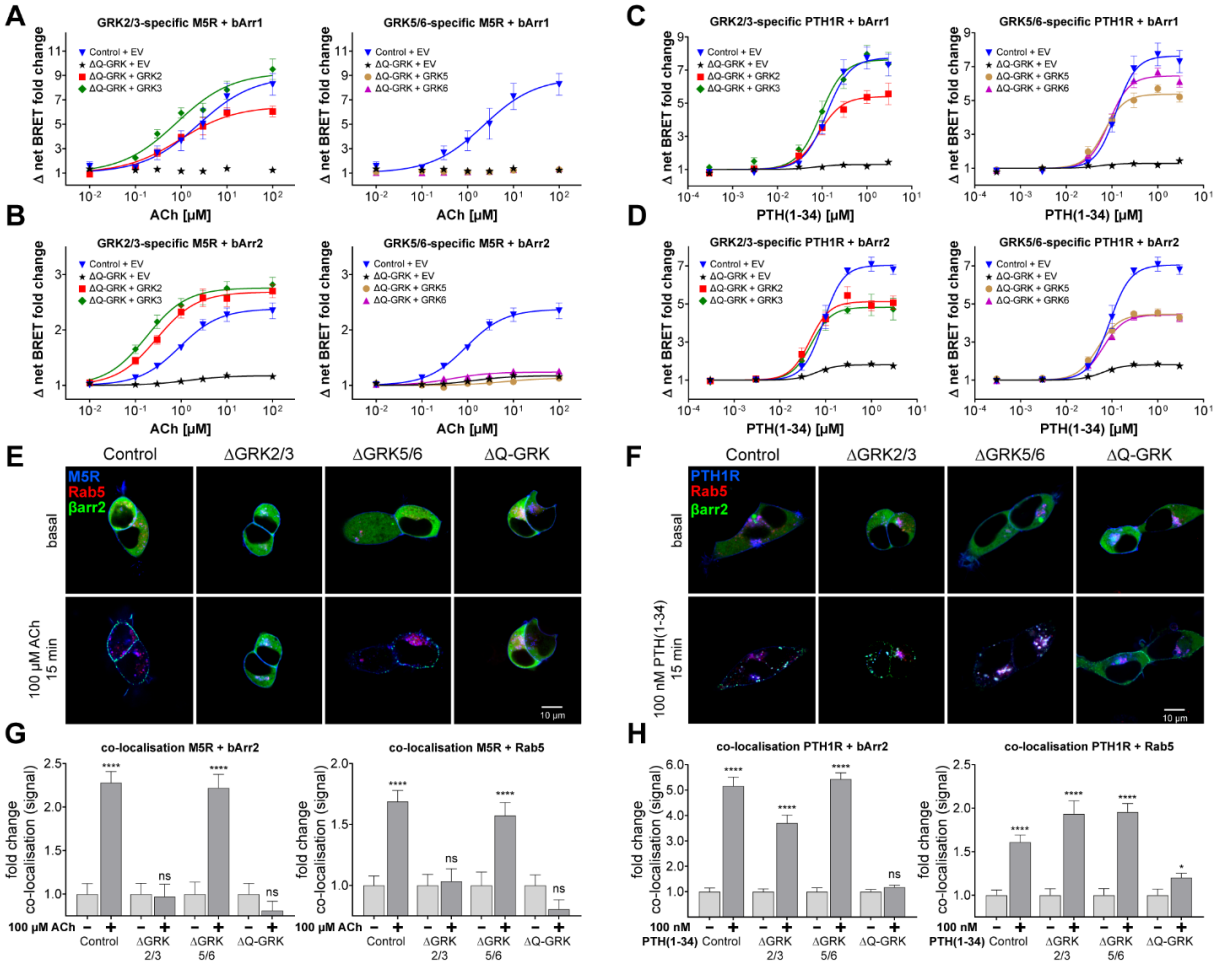

Figure 4.3 GRK-specificity of β-arrestin1 and 2 recruitment to PTH1R and M5R and assessment of GRK-dependent GPCR internalization and β-arrestin2 translocation

A-D GRK-specific β-arrestin1 (**A, C**) or β-arrestin2 (**B, D**) recruitment to the M5R upon acetylcholine (ACh) stimulation (**A, B**) or the PTH1R upon parathyroid-hormone 1-34 (PTH(1-34)) stimulation (**C, D**). Shown are concentration-response curves depicted as Δ net BRET fold change. The panels display the recruitment in presence of either GRK2 or 3, or GRK5 or 6. For better comparison, the Control and ΔQ-GRK curves are shown multiple times. **E, F** Control, ΔGRK2/3, ΔGRK5/6, and ΔQ-GRK cells were transfected with either M5R-CFP or PTH1R-CFP (blue), the early endosome marker Rab5-mCherry (red), and β-arrestin2-YFP (green) expression constructs. The cells were grown on cover slips and subjected to confocal live-cell microscopy. Shown are representative images, taken before and after 15 minutes of stimulation with either 100 μM ACh or 100 nM PTH(1-34), respectively. The normalized co-localization of M5R (**G**) or PTH1R (**H**) with β-arrestin2 or Rab5 was quantified using Squassh and SquasshAnalyst, with at least 30 images per condition, representing at least three independent transfections and experimental days. Data are presented as mean fold change in co-localization signal + SEM. Statistical analysis was performed using a two-way mixed model ANOVA followed by a paired t-test (*p < 0.05; ** p < 0.01; *** p < 0.001; **** p < 0.0001; ns (not significant)). BRET data for the M5R were kindly provided by Dr. Julia Drube.

Further, we employed confocal live-cell microscopy to assess the dependency of PTH1R and M5R internalization on endogenous GRK levels in Control, ΔGRK2/3, and ΔGRK5/6 as well as in ΔQ-GRK. Under basal conditions, β-arrestin2 is located in the cytosol, M5R and PTH1R in the cell membrane, and Rab5 (early endosome marker) in endosomes (**Figure 4.3 E, F, basal**).

As expected, the M5R was not able to induce β-arrestin2 translocation in the absence of GRK2 and 3 (ΔGRK2/3 and ΔQ-GRK) (**Figure 4.3 E**).The quantification of co-

localization between the M5R and β-arrestin2 (**Figure 4.3 G**) confirms our findings of **Figure 4.3 A, B**. Analysis of M5R co-localization with Rab5 (as a surrogate measurement for receptor internalization and initial trafficking) reveals that this interaction translates to functional receptor internalization only in the presence of GRK2 and 3 (**Figure 4.3 E, G**). For the PTH1R, we were able to detect ligand-induced co-localization with β-arrestin2 or Rab5 in all conditions expressing GRKs (**Figure 4.3 F, H**). Interestingly, the agonist-stimulated PTH1R was still able to induce a slight membrane translocation of β-arrestin2 in ΔQ-GRK, confirming the GRK-independent affinity of β-arrestin2 towards the ligand-activated receptor (**Figure 4.3 D**).

The BRET results for these two exemplary GPCRs were additionally confirmed in triple GRK KO cell lines and ΔGRK2/3 and ΔGRK5/6 family KOs (**Figure 4.4 A, B**). Interestingly, the endogenous expression of GRK2 and 3 in ΔGRK3/5/6 and ΔGRK2/5/6 was sufficient to increase the measured β-arrestin2 recruitment in comparison to ΔQ-GRK for both receptors. This finding essentially confirms the functionality of these two triple GRK KO cell lines and suggests that the M5R and PTH1R require lower amounts of GRK2 or 3 to be efficiently regulated in comparison to the β2ADR (**Figure 4.1 C**). As indicated by the experiments shown in **Figure 4.3 B**, ΔGRK cell lines only featuring the expression of GRK5 and/or 6 did not increase the β-arrestin2 recruitment to the M5R as in comparison to ΔQ-GRK.

Additionally, we also verified the confocal microscopy results, obtained for the PTH1R using endogenous GRK expression (**Figure 4.3 F, H**), in a reciprocal experiment for β-arrestin1 and 2. For this, we analyzed the co-localization of the PTH1R with either β-arrestin1 or 2 or Rab5 in ΔQ-GRK overexpressing individual GRKs (**Figure 4.4 C-F**). As suggested by the BRET results, all individually transfected GRK isoforms mediate a significant increase in co-localization of the PTH1R with both β-arrestins and Rab5 upon ligand stimulation.

With these experiments we confirm the PTH1R as being regulated by all four analyzed GRKs using BRET, confocal microscopy and seven specifically engineered GRK knockout cell lines, whereas the M5R only shows to be functionally phosphorylated by GRK2 and 3.

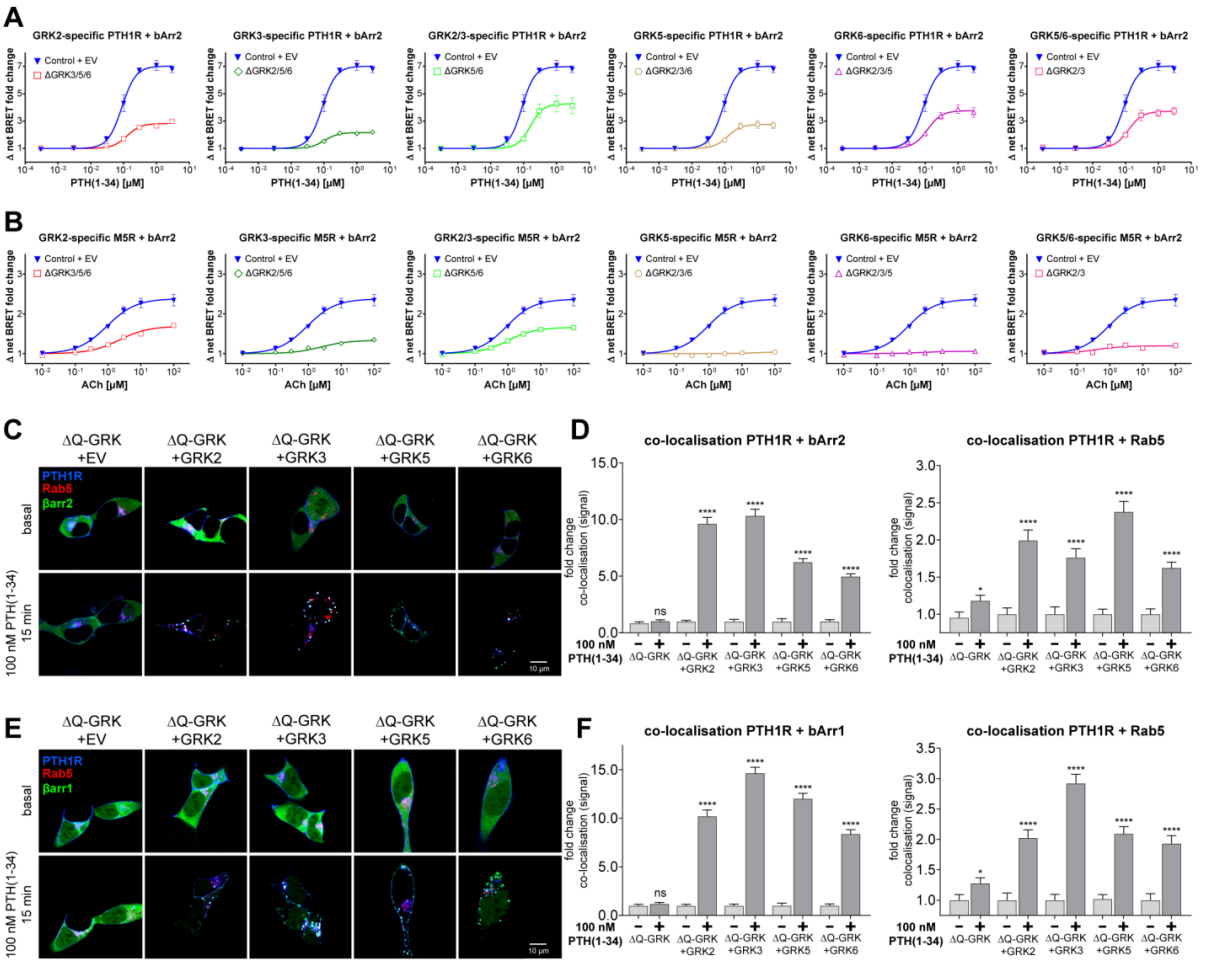

Figure 4.4 Endogenous "kinase-screens" for PTH1R and M5R and rescue of GRK knockout shown via confocal microscopy

A, B β-arrestin2 recruitment to the M5R (**A**) or PTH1R (**B**) in Control cells, only one remaining endogenous GRK (ΔGRK3/5/6, 2/5/6, 2/3/6, 2/3/5), or two remaining endogenous GRKs (ΔGRK5/6, 2/3) as indicated is shown as Δ net BRET fold change (mean ± SEM of three independent experiments). For easier comparison, Control curves are depicted in every panel. **C-F** Confocal live-cell microscopy was performed using ΔQ-GRK cells transfected with PTH1R-CFP (blue), Rab5-mCherry (red), β-arrestin2-YFP (**C**) or β-arrestin1-YFP (**E**) expression constructs (green) and individual untagged GRK2, 3, 5, or 6. Shown are representative images, taken before (basal) and after 15 minutes of stimulation with 100 nM parathyroid hormone (1-34) (PTH(1-34)). The normalized co-localization of PTH1R and β-arrestin2 or Rab5 (**D**) and β-arrestin1 or Rab5 (**F**) was quantified using Squassh and SquasshAnalyst, with at least 30 images per condition. Data are presented as mean fold change in co-localization signal + SEM. Statistical analysis was performed using a two-way mixed-model ANOVA followed by a paired t-test (* $p < 0.05$; ** $p < 0.01$; *** $p < 0.001$; **** $p < 0.0001$; ns (not significant)). The data in images for β-arrestin2-YFP in ΔQ-GRK + EV are depicted again (**Figure 4.3**) to enable the comparison with the corresponding GRK overexpressing conditions.

These apparent differences in GRK-specific β-arrestin recruitment, as exemplified by the M5R and the PTH1R, were encountered multiple times during our analysis across ten different GPCRs (**Figure 4.5**).

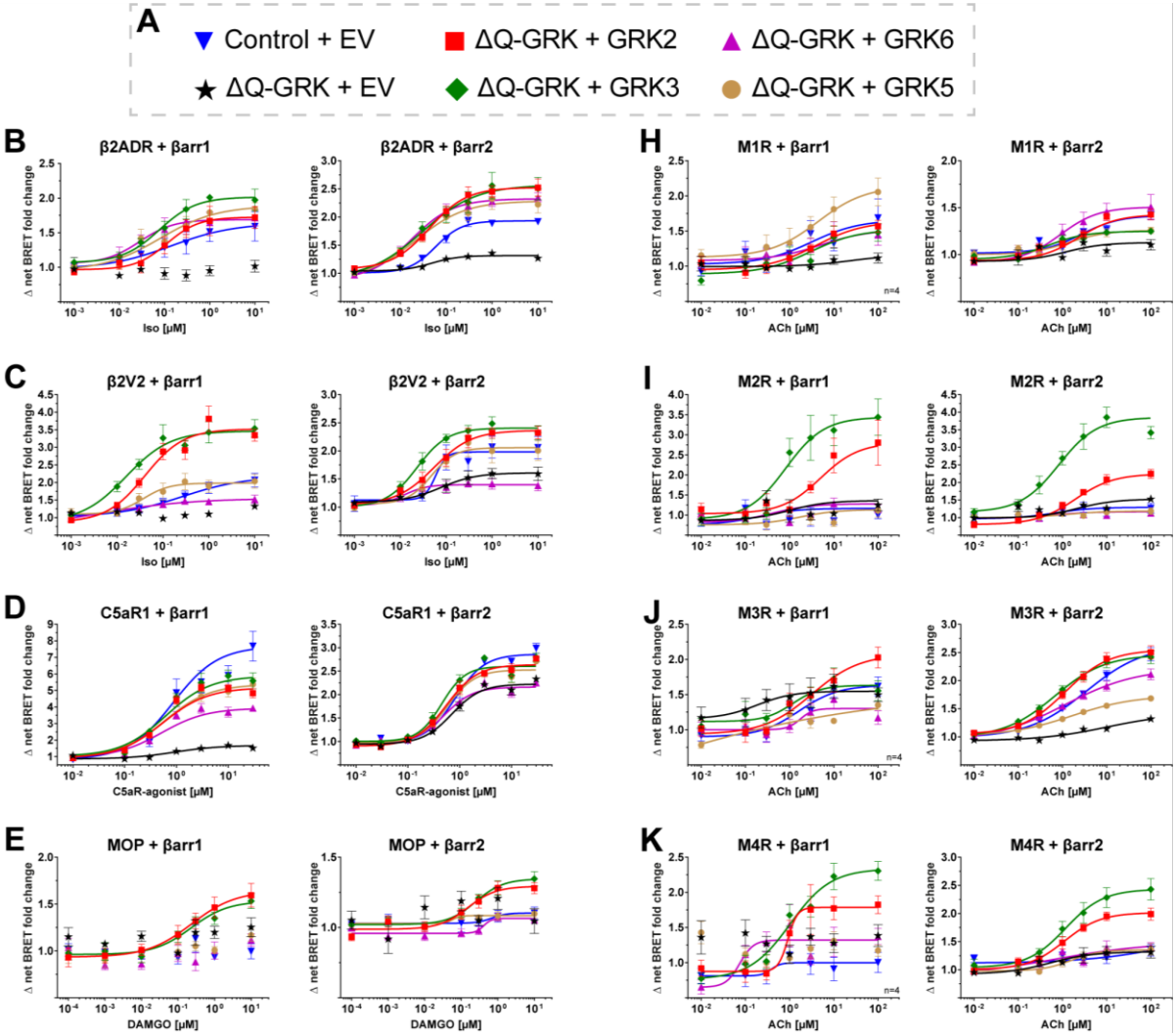

Figure 4.5 Kinase screen data

A Legend for concentration-response curves shown in (**B-K**). **B-K** The Halo-Tag-β-arrestin fusion protein is recruited to a NanoLuc-tagged GPCR upon agonist activation and subsequent receptor phosphorylation. Overexpression of single GRKs in ΔQ-GRK cells allows the assessment of the impact of individual GRKs on this process. ΔQ-GRK or Control cells were transfected with the respective tagged GPCR and β-arrestin1 or 2 fusion constructs. Additionally, either GRK2, 3, 5, 6, or empty vector (EV) were co-transfected as indicated. The dynamic BRET changes are shown as ligand concentration-response curves normalized to baseline values and vehicle control. All data points are calculated as Δ net BRET fold change as the mean of at least three independent measurements ± SEM. Results of the statistical analysis are listed in the appendix of this thesis (**Appendix Table 1** and **Appendix Table 2**). Experiments for the C5aR1, M3R, and M4R were conducted by Dr. Julia Drube, Edda Matthees, and Saskia Barz.

Via statistical multiple comparison of BRET fold changes at saturating ligand concentrations for each of the tested conditions (Control + EV, ΔQ-GRK + EV, ΔQ-GRK + GRK2, ΔQ-GRK + GRK3, ΔQ-GRK + GRK5, ΔQ-GRK + GRK6), we were able to cluster the respective GPCR–β-arrestin pairs into groups, depending on the observed GRK-selectivity (**Figure 4.6 A, B; Appendix Table 1** and **Appendix Table 2**).

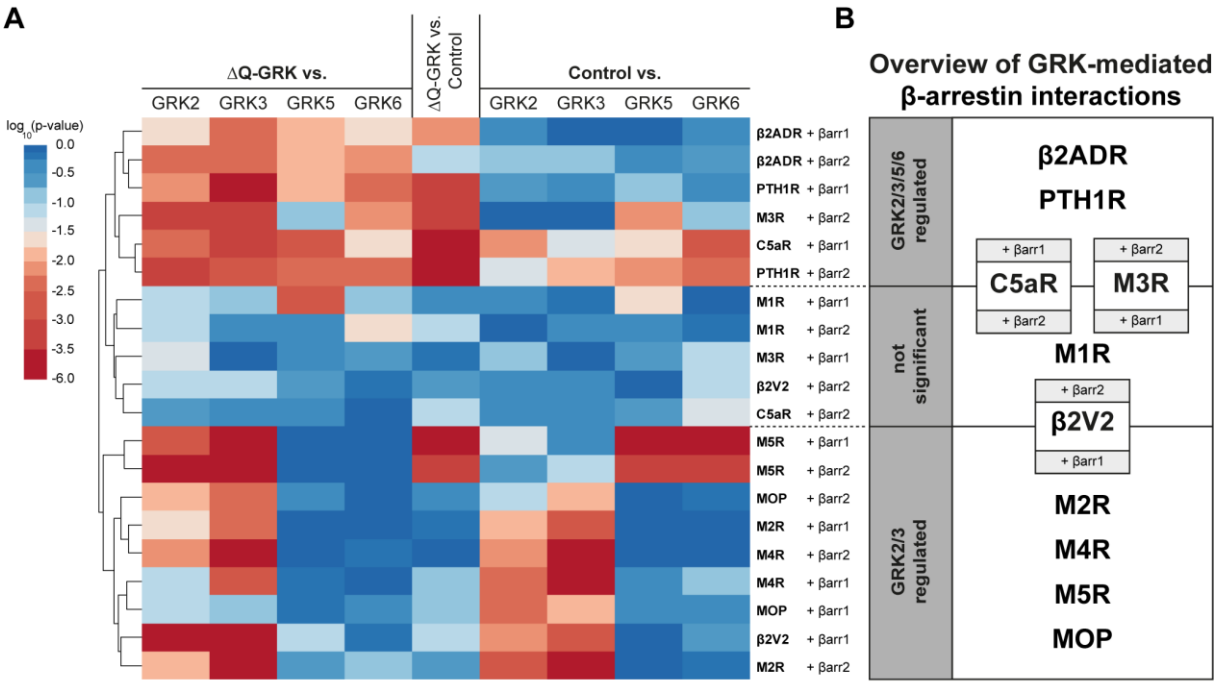

Figure 4.6 Clustering heatmap

A Clustering heatmap representing the statistical multiple comparison of β-arrestin recruitment data for ten different GPCRs. Conditions with overexpressed GRKs were tested against ΔQ-GRK + empty vector (EV) or Control + EV, as indicated. Additionally ΔQ-GRK + EV was compared to Control + EV. BRET fold changes at saturating ligand concentrations of at least three independent experiments were compared using ANOVA and Bonferroni's test (**Appendix Table 1** and **Appendix Table 2,** data derived from Figure 4.5). Transformed unadjusted p values are plotted. GPCR–β-arrestin pairs are clustered according to Canberra distance. **B** Schematic overview of the statistical clustering. GPCR–β-arrestin pairs group into the following categories: Those which are regulated by any tested GRK (GRK2/3/5/6 regulated), by GRK2 or 3 only (GRK2/3 regulated) and a third group, which is comprised of GPCR–β-arrestin pairs that do not consistently show significant differences between the tested conditions. The clustering heatmap was prepared and kindly provided by Mona Reichel.

Here we identified two main subsets of GPCRs: receptors for which β-arrestin interactions are mediated by overexpression of i) any GRK (β2ADR, PTH1R, C5aR1+β-arrestin1 and M3R+β-arrestin2) or ii) GRK2 or 3 only (M2R, M4R, M5R, MOP, and β2V2+β-arrestin1). Within our tested GPCRs, we did not observe β-arrestin interactions mediated exclusively by GRK5 or 6. Interestingly, some receptor–β-arrestin pairs did not consistently show significant differences between the tested conditions and hence could not be definitively assigned to one of the two groups (M1R, C5aR1+β-arrestin2, M3R+β-arrestin1, and β2V2+β-arrestin2). In case of C5aR1 + β-arrestin2 (**Figure 4.5**) this behavior is explained by exceptionally high β-arrestin2 recruitment in the absence of GRKs.

To our surprise, all receptors but the MOP recruited β-arrestin2 in the absence of GRKs (**Figure 4.3** and **Figure 4.5**). Only four of the analyzed receptors (C5aR1, M1R, M3R, and PTH1R) were able to induce GRK-independent β-arrestin1 recruitment. This

finding suggests that β-arrestin2 is better suited to form GRK-independent interactions with active GPCRs.

4.2 β-arrestin1 and 2 prefer distinct complex configurations and undergo different conformational changes when bound to the same GPCR

After disclosing the GRK-specificity of β-arrestin recruitment for ten different GPCRs, we further focused on the PTH1R. Specifically because of the robust recruitment of both β-arrestin isoforms (**Figure 4.3 C, D**), this receptor poses as an excellent model system to investigate differences between β-arrestin1 and 2. Accordingly, this second part of the thesis aims to decipher differences in complex configuration, conformational change and phosphorylation-dependency of PTH1R interactions with either β-arrestin1 or 2. The presented results, figures, and descriptions are part of the manuscript Haider et al. (in preparation).

4.2.1 The configuration of a GPCR–β-arrestin complex determines its functionality

To elucidate the differences between β-arrestin1 and 2 for binding of the PTH1R, we first examined whether they utilize different interaction interfaces. In addition to the already presented “kinase-screen” experiments, we performed intermolecular NanoBRET recruitment assays for β-arrestin1 and 2 in HEK293, ΔQ-GRK and for β-arrestin constructs lacking the FLR (dFLR; **Figure 4.7 A**). Since the β-arrestin-dFLR mutants miss essential amino acids for the binding of the intracellular receptor cavity, we interpret recruitment of those constructs as the formation of a “hanging” GPCR–β-arrestin complex (P-R complex, **Figure 4.7 B**), in line with previous studies (Thomsen et al. 2016). In contrast, the recruitment measured in ΔQ-GRK cells reflects the affinity of the respective β-arrestin towards the receptor, independent of GRK phosphorylation (R* complex, **Figure 4.7 B**).

Indeed, we found differences between β-arrestin1 and 2, as the deletion of the FLR differentially decreased recruitment for both β-arrestin isoforms (**Figure 4.7 A**). The β-arrestin2-dFLR (19 % of WT) mutant produced only half of the signal compared to the β-arrestin1-dFLR (37 % of WT), leading us to the conclusion that β-arrestin1 is better suited to form a “hanging” complex. In contrast to these results, the recruitment

measured for both β-arrestin isoforms in absence of GRKs, using ΔQ-GRK cells, shows considerably higher values for β-arrestin2.

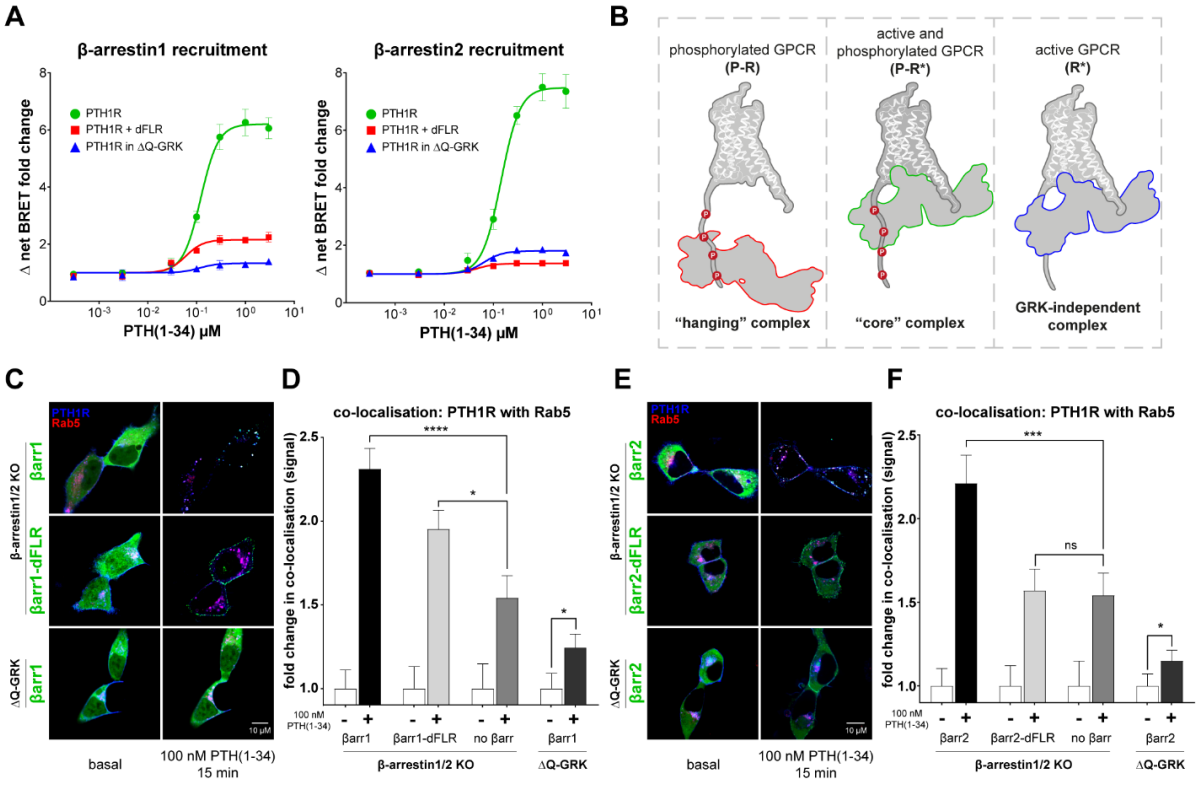

Figure 4.7 Assessment of different configurations of formed PTH1R–β-arrestin complexes

A NanoBRET measured recruitment of β-arrestin1 and 2 to the PTH1R upon stimulation with PTH(1-34). Recruitment measured for β-arrestin WT constructs in HEK293 cells is shown in green, the results of analogous experiments performed in ΔQ-GRK cells are depicted in blue. The red curves were generated by recruitment measurements of the respective β-arrestin-dFLR mutants in HEK293 cells. Results are shown as mean of three independent repetitions (n=3) ± SEM. **B** Schematic depiction of the "hanging", "core" and GRK-independent GPCR-β-arrestin complex configurations. **C** and **E** Representative live-cell confocal microscopy images of β-arrestin1/2 double knockout and ΔQ-GRK cells transfected with PTH1R-CFP (blue), the early endosome marker Rab5-mCherry (red) and the respective β-arrestin-YFP WT or dFLR constructs (green). At least 30 images were acquired before and after stimulation with 100 nM PTH(1-34) for 15 minutes from at least three independent transfections (n≥3). **D** and **F** The quantification of co-localization of PTH1R-CFP with Rab5-mCherry in β-arrestin1/2 knockout and ΔQ-GRK cells was calculated from at least 30 images per condition of at least three independent transfections (n≥3) using Squassh and SquasshAnalyst and is represented as mean fold change in co-localization signal + SEM. The statistical significance was calculated by two-way ANOVA, followed by a post-hoc pairwise comparison with Bonferroni correction (comparison between stimulated conditions) or paired t-test (comparison between basal and stimulated) (*, p<0.05; **, p<0.001; ***, p<0.0001; ****, p<0.00001).

To probe for functionality of these possible β-arrestin–PTH1R complexes we employed confocal life-cell microscopy, using β-arrestin1/2 knockout (O'Hayre et al. 2017) or ΔQ-GRK cells (Drube et al. 2021). Cells were transfected with PTH1R-CFP, β-arrestin-YFP and the early endosome marker Rab5-mCherry and stimulated with 100 nM PTH(1-34) for 15 minutes. Both β-arrestin isoforms, as well as the dFLR variants showed translocation upon agonist stimulation of the receptor (**Figure 4.7 C, E**).

The co-localization between the PTH1R and Rab5, as a surrogate measurement for receptor internalization and early trafficking, was significantly decreased in the absence of β-arrestins (**Figure 4.7 D, 2F**, data for "no β-arr" condition shown twice to enable comparability) when compared to re-expression of either β-arrestin1 or 2. The use of ΔQ-GRK cells showed substantially lower internalization (**Figure 4.7 D, 2F**), highlighting that there are other phosphorylation-dependent but β-arrestin-independent ways to internalize the receptor (Delom und Fessart 2011).

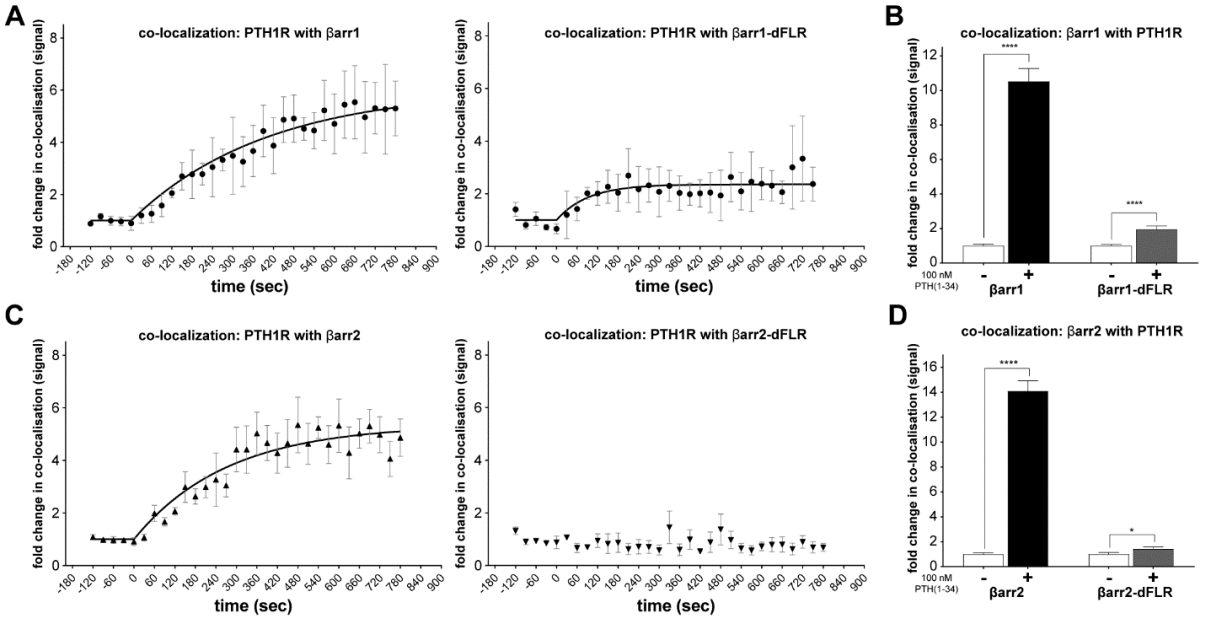

Figure 4.8 Time-dependent co-localization of PTH1R and β-arrestin1 and 2

A, C Live-cell confocal microscopy of β-arrestin1/2 double knockout cells transfected with PTH1R-CFP, the early endosome marker Rab5-mCherry and β-arrestin1-YFP WT or dFLR constructs (**A**) or β-arrestin2-YFP WT or dFLR constructs (**C**). For each condition, four representative movies of stimulation with 100 nM PTH(1-34) for 15 minutes were used to quantify the co-localization between PTH1R-CFP and the respective β-arrestin1, and 2-YFP constructs. This time-dependent quantification was calculated using Squassh and SquasshAnalyst, represented as mean fold change in co-localization signal ± SEM. **B, D** Analogous quantification calculated from at least 30 images per condition from at least three independent transfections (n≥3), acquired before and after stimulation with 100 nM PTH(1-34) for 15 minutes. Representative images are shown in **Figure 4.7 C, E.** The statistical significance was calculated by unpaired t test (*, p<0.05; **, p<0.001; ***, p<0.0001; ****, p<0.00001)

Interestingly, the overexpression of the β-arrestin1-dFLR mutant in β-arrestin1/2 knockout cells significantly increased the co-localization between the PTH1R and Rab5, whereas the β-arrestin2-dFLR variant was unable to support receptor internalization (**Figure 4.7 D, F**). This analysis discloses a second difference between the two β-arrestin isoforms, as we conclude that the "hanging" complex between β-arrestin1 and the PTH1R is still functional, in contrast to β-arrestin2. This is in line with

the findings of Cahill *et al.* Cahill et al. (2017), although the functionality of the β-arrestin2-dFLR mutant was not assessed to this date.

WT β-arrestin1 and 2 exhibit stable co-localization with the receptor (quantification shown in **Figure 4.8 B, D**) and can be found in intracellular compartments alongside Rab5 (**Figure 4.7 C, E**) after ligand stimulation. In contrast, the β-arrestin-dFLR mutants translocate to the membrane (**Figure 4.7 C**, **E**) but show reduced co-localization with the receptor (**Figure 4.8 B, D**). Via the quantification of four representative movies per condition, we were able to compare the time-dependent co-localization between the PTH1R and β-arrestin 1, 2, or the corresponding dFLR mutants (**Figure 4.8 A, B**). This analysis shows a clear one-step association with the receptor after ligand application for both WT β-arrestin proteins. A similar, albeit lower increase in co-localization can also be observed for the β-arrestin1-dFLR mutant. Yet, the β-arrestin2-dFLR mutant did not show a time-dependent co-localization with the PTH1R (**Figure 4.8 B**). The quantification of 30 images before and after ligand stimulation showed a small increase (**Figure 4.8 D**), which is in line with the low recruitment values of β-arrestin2-dFLR measured via the NanoBRET assay (**Figure 4.7 A**).

4.2.2 Differences in conformational change between β-arrestin1 and 2

Previous studies clarified that β-arrestin2 adopts different conformations upon binding to specific GPCRs or phosphopeptides (Nuber et al. 2016, Mayer et al. 2019, Yang et al. 2015, Lee et al. 2016). However, whether the same GPCR would induce different conformational changes for β-arrestin1 and 2 was not assessed to this point. Notably, Teixeira et al. (2017) previously presented comparative conformational change measurements for β-arrestin1 and 2 using biosensors that relied on the original design by Charest et al. (2005). Since this strategy enables the assessment of β-arrestin conformational changes from just a single point of view (intramolecular BRET between N- and C-terminal chromophores), the authors were not able to draw conclusions about differential conformational rearrangements of the two β-arrestin isoforms. Nonetheless, Teixeira et al. (2017) appropriately made use of these biosensors to show that stimulation of the angiotensin II type 1 receptor leads to the activation of β-arrestin1 and 2.

For the comprehensive assessment of GPCR-induced β-arrestin conformational states via intramolecular BRET, it is necessary to employ multiple sensors, which report from different points of interest of the respective β-arrestin (Nuber et al. 2016, Lee et al. 2016). Hence we designed novel NanoLuc/FlAsH-based biosensors for β-arrestin1 and 2 (**Figure 4.9 A**). Building on the FlAsH-binding site insertion positions published in Nuber et al. (2016), we exchanged the C-terminal CFP tag (FRET donor) with a NanoLuc to enable high-throughput BRET measurements. Accordingly, the FlAsH labelling procedure, previously described in Hoffmann et al. (2010), was optimized for adherent cells in 96-well plates.

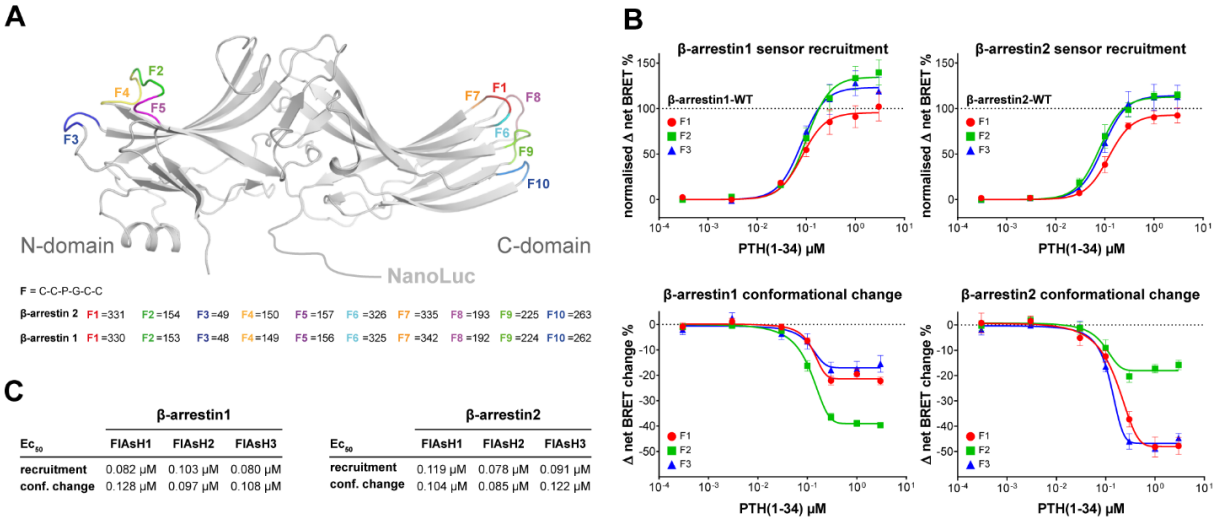

Figure 4.9 Sensor design and initial results of β-arrestin1 and 2 conformational change measurements

A Cartoon depiction of the used NanoLuc/FlAsH conformational change biosensors. The localization of the inserted FlAsH-sites is shown as colored loops (PDB: 3P2D) and specific insertion sites for FlAsH-binding (CCPGCC) are depicted below for β-arrestin1 and 2. **B** Concentration-dependent recruitment and conformational change of β-arrestin1 and 2, labelled in position F1, F2 or F3 upon activation of the PTH1R-WT with PTH(1-34) are shown as examples. Recruitment of the individual conformational change biosensors was assessed by co-transfection of a PTH1R-HaloTag expression construct and the measurement of intermolecular BRET upon stimulation with PTH(1-34). Recruitment data is depicted as Δ net BRET %, normalized to the maximum recruitment of the respective β-arrestin WT construct. For the generation of β-arrestin conformational change data HEK293 cells were transfected with an untagged PTH1R-WT expression construct and one β-arrestin conformational change biosensor, FlAsH-labelled and stimulated with PTH(1-34). Conformational change data are shown as Δ net BRET change in percent. All results are shown as mean of three independent repetitions (n=3) ± SEM. All recorded recruitment and conformational change data can be comprehensively assessed in **Figure 4.14**, **Figure 4.15**, and **Figure 4.16**. (C) Corresponding EC_{50} values of β-arrestin-F1, 2, 3 sensors found for the interaction with the PTH1R.

Utilizing these novel intramolecular conformational change biosensors, we first recorded the conformational change signatures of β-arrestin1 and 2 upon ligand stimulation of the co-expressed PTH1R. As an example, the concentration-dependent recruitment and conformational changes of the β-arrestin1 and 2 F1, F2, and F3 constructs are shown in **Figure 4.9 B**. These biosensors show robust WT-like

recruitment to the PTH1R. Yet, as expected, the respective intramolecular BRET values generated with the F1, F2, and F3 constructs are vastly different. As these biosensors register different signal amplitudes, but similar functional recruitment and effective ligand concentrations (EC_{50} values) (**Figure 4.9 C**), we can indeed conclude that they report on conformational changes that are specific for the respective labeling position. Interestingly, these F1-, F2-, and F3-derived conformational change signatures are also substantially different between the two β-arrestin isoforms (**Figure 4.9 B**). The comprehensive conformational fingerprints of both β-arrestin isoforms coupling to the PTH1R can be accessed in **Figure 4.10**.

All conformational change biosensors were measured, but since FlAsH constructs at the positions F6 and F8 did not produce concentration-dependent BRET signals, they were omitted from this study. To simplify the comparison of conformational change signatures, the mean Δ net BRET changes at ligand saturation are depicted as bar charts divided into FlAsH sensors located in the N- (**Figure 4.10 A**) and C-domain (**Figure 4.10 B**) of the β-arrestin isoforms. A surface projection of the obtained conformational change data is shown in **Figure 4.10 C**. Our data show major conformational differences for β-arrestin1 and 2 in the phosphate-sensing N-domains (**Figure 4.10 A**). Especially the F2 and F3 sensors responded diametrically, as F2 exhibited considerably lower BRET changes for β-arrestin2 and F3 showed reduced values for β-arrestin1. This suggests that β-arrestin1 and 2 interact with the PTH1R C-terminus in distinct complexes.

Of note, corresponding residues in the F3 loop of visual arrestin were reported to respond differently when binding to phosphorylated, light activated Rhodopsin (P-R*) (Ostermaier et al. 2014) or phosphorylated Opsin (P-R) (Peterhans et al. 2016). Since phosphorylated Opsin is in a predominantly inactive conformation one might assume that it is unable to form a “core” complex with arrestin, interacting mostly in a “hanging” complex configuration. Therefore, we hypothesize that the β-arrestin F3 position reports on the formation of distinct GPCR–arrestin complex configurations and might be able to differentiate between “hanging” and “core” complexes. These findings, taken together with the results shown in **Figure 4.7,** provide further evidence that β-arrestin1 and 2 form distinct complexes when coupling to the PTH1R.

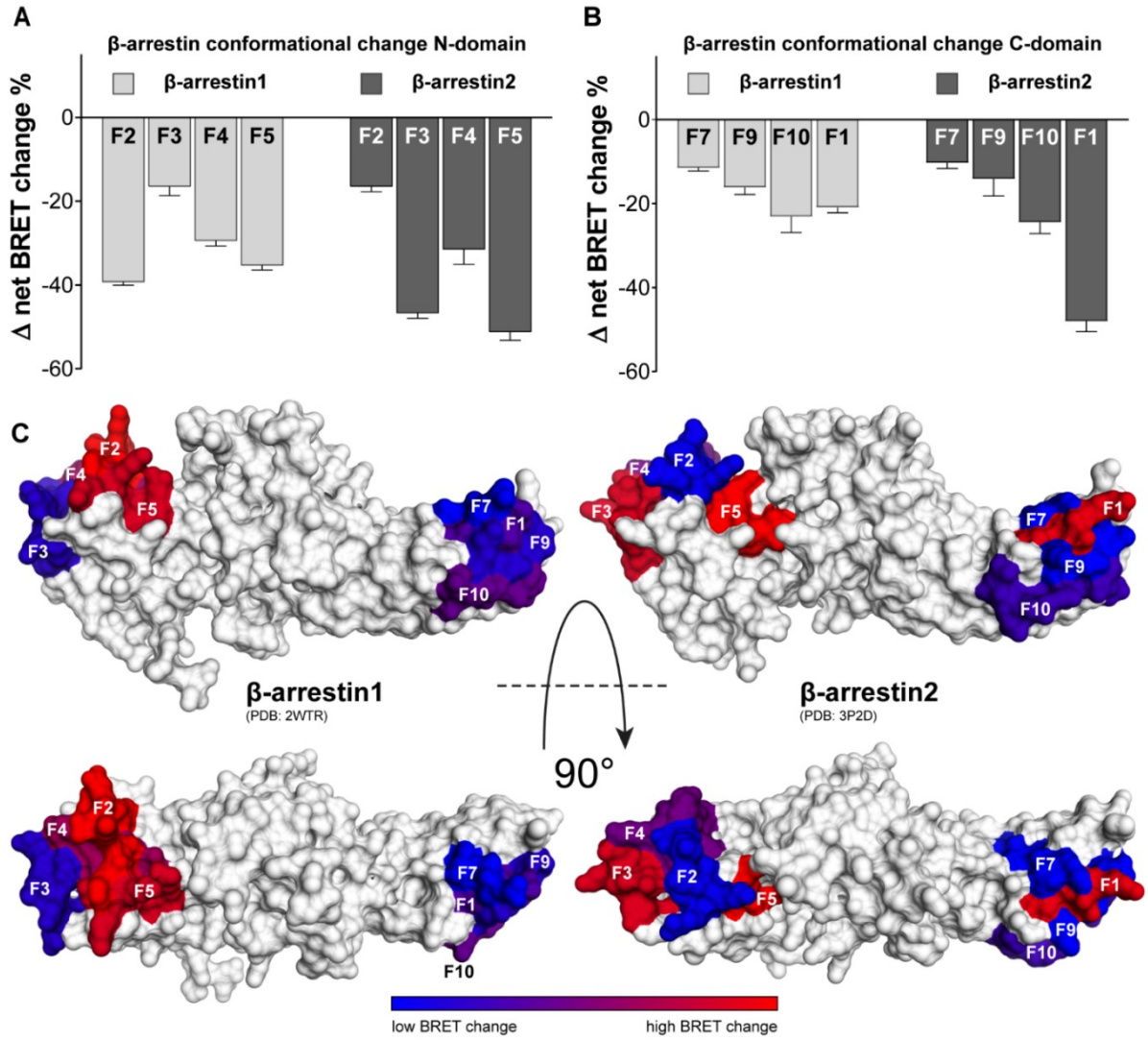

Figure 4.10 β-arrestin1 and 2 display different conformational change signatures upon recruitment to the PTH1R

A and **B** Conformational change of β-arrestin1 and 2 biosensors labelled in the N- or C-domain, respectively, for the interaction with PTH1R-WT at saturating PTH(1-34) concentrations. Results are depicted as Δ net BRET change in percent and shown as mean of three independent repetitions (n=3) ± SEM. **C** Surface projection of the measured conformational change data onto crystal structures of inactive β-arrestin1 (PDB: 2WTR) and β-arrestin2 (PDB: 3P2D). The Δ net BRET change in percent is plotted on loop (-fragments), harboring the respective FlAsH site as spectrum ranging from blue to red.

Within the C-domains of β-arrestin1 and 2 we were able to find a higher degree of similarities for conformational changes (**Figure 4.10 B**). Signals obtained from the F7, F9, and F10 sensors, located in the outward loops of the respective C-domains, yield a similar signature for both β-arrestin isoforms. Interestingly, conformational changes recorded for the F1 position resulted in vastly different signal amplitudes for β-arrestin1 and 2. The FlAsH site for these constructs is located in the so-called C-edge loop 2, a supposed membrane anchor for receptor-bound arrestin (Lally et al. 2017, Staus et al. 2020). As this loop has been shown to play different roles for different GPCR–arrestin

complex configurations (Staus et al. 2020, Kang et al. 2015), our results suggest that the two β-arrestin isoforms differentially engage the GPCR to form distinct complexes. Ghosh et al. (2019) approximated differences between β-arrestins to be located within the C-domain, we further localized this finding to the F1 position.

These findings, enabled by utilization of these homologous conformational change biosensors, clarify that β-arrestin1 and 2 indeed undergo different conformational changes when associating with the same GPCR.

4.2.3 Phosphorylation-dependency of β-arrestin1 and 2 conformational changes

As the two β-arrestin isoforms exhibited distinct conformational changes for the interaction with the PTH1R, we hypothesized that specific receptor phosphorylation patterns would affect β-arrestin1 and 2 differentially. Hence, we additionally investigated two phosphorylation-deficient mutants of the PTH1R and further analyzed the PTH1R independently of GRK-mediated phosphorylation. These previously published variants of the receptor (Zindel et al. 2016) were generated by alanine substitution of either a proximal (PD1) or distal (PD2) C-terminal phosphorylation cluster.

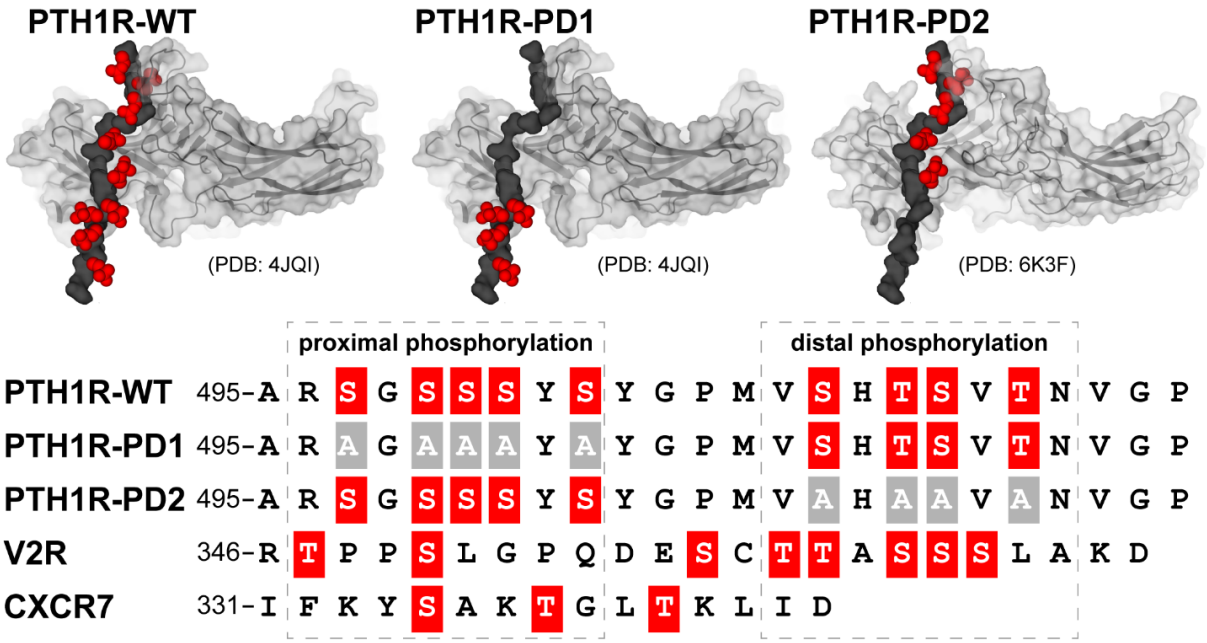

Figure 4.11 Mechanistic model of the PTH1R C-terminal binding interface

Mechanistic model of β-arrestin interactions with PTH1R-WT, -PD1 and -PD2, utilizing crystal structures of complexes with the V2R-pp (PDB: 4JQI) (Shukla et al., 2013) and the ACKR3-pp (PDB: 6K3F) (Min et al., 2020) as well as a C-terminal alignment.

A mechanistic model of β-arrestin interactions with PTH1R-WT, -PD1 and -PD2, utilizing crystal structures of complexes with the V2R-pp (PDB: 4JQI) (Shukla et al. 2013) and the ACKR3-pp (PDB: 6K3F) (Min et al. 2020b) as well as a C-terminal alignment is depicted in **Figure 4.11**.

A schematic depiction of our complete approach to assess the impact of C-terminal GPCR phosphorylation is shown in **Figure 4.12 A**. All three PTH1R variants recruit β-arrestin1 and 2 upon application of the ligand PTH(1-34) in a concentration-dependent manner (**Figure 4.12 B**, PTH1R-WT data from **Figure 4.7 A** was normalized and is shown again to enable comparability). The two receptor mutants exhibited a stepwise reduction of β-arrestin2 binding, with the recruitment being more prominently obstructed for PTH1R-PD2. Interestingly, β-arrestin1 recruitment was not significantly reduced for PTH1R-PD1, whereas PTH1R-PD2 showed an attenuation of recruitment analogous to β-arrestin2. This analysis reveals yet another difference between β-arrestin1 and 2 regarding their respective requirement for specific C-terminal receptor phosphorylation: both phosphorylation clusters affect high affinity β-arrestin2 binding, whereas β-arrestin1 interactions with the PTH1R do not require the proximal phosphorylation cluster.

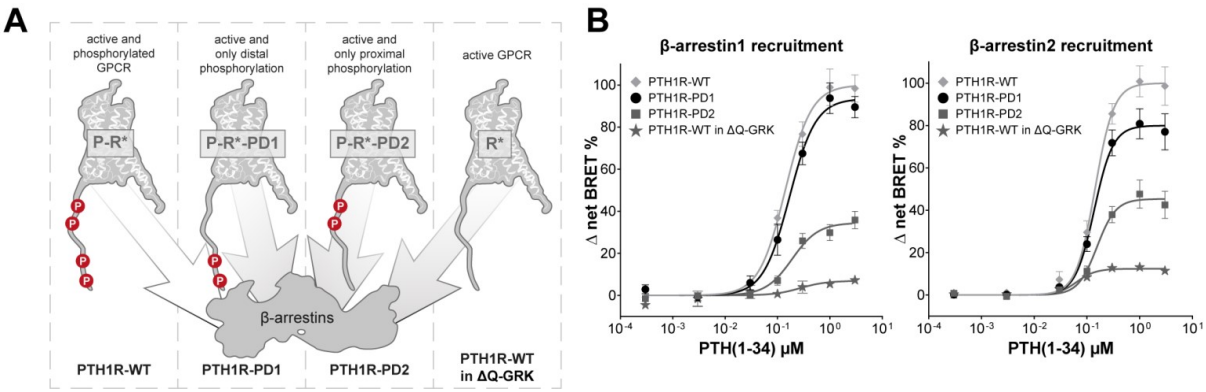

Figure 4.12 PTH1R phosphorylation states differentially affect the recruitment of β-arrestin1 and 2

A Schematic depiction of our approach to measure phosphorylation-specific conformational changes of β-arrestin1 and 2, induced either by the active and phosphorylated PTH1R (P-R*), two phosphorylation-deficient receptor mutants (P-R*-PD1/PD2) or the active receptor independent of GRK phosphorylation (R*). **B** NanoBRET assessed recruitment of β-arrestin1 and 2 to the three receptor variants. Briefly, HEK293 or ΔQ-GRK cells were transfected with either PTH1R-WT, PTH1R-PD1, or PTH1R-PD2 coupled to a C-terminal HaloTag and β-arrestin1 or 2-NanoLuc expression constructs. Upon stimulation with PTH(1-34), the concentration-dependent change in BRET signal was measured. Data is shown as Δ net BRET change in percent, and represented as the mean of at least three independent repetitions (n≥3) ± SEM, and normalized to PTH1R-WT recruitment in HEK293.

Analogous to the WT receptor, we investigated β-arrestin conformational changes for the PTH1R-PD1 and -PD2 mutants as well as for the PTH1R WT in ΔQ-GRK.

Therefore, we can analyze differences in molecular rearrangement between β-arrestin1 and 2 regarding specific C-terminal GPCR phosphorylation (**Figure 4.13**).

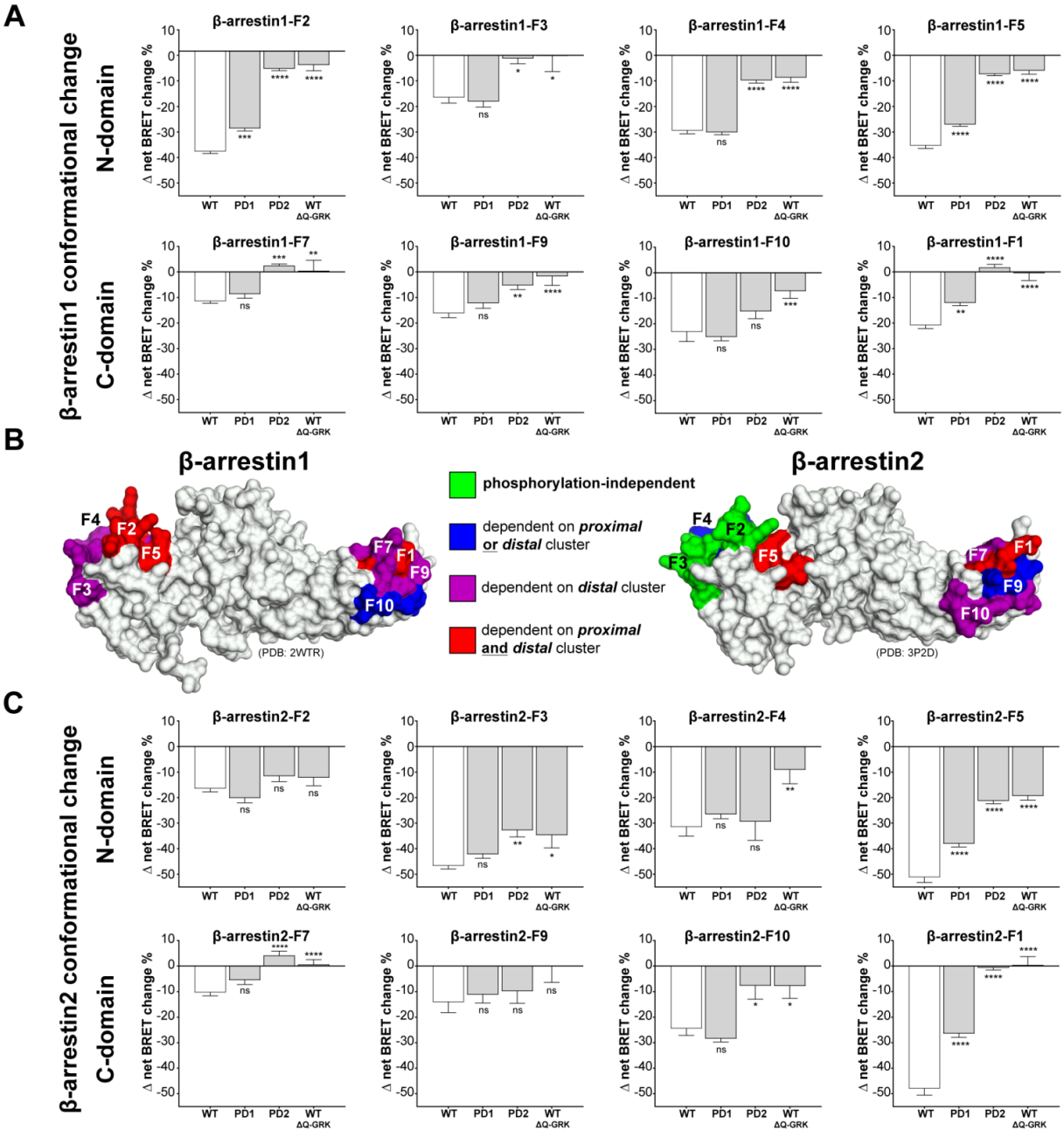

Figure 4.13 PTH1R phosphorylation states induce distinct conformational changes in β-arrestin1 and 2

A-C Conformational change of β-arrestin1 (**A**) and 2 (**C**) biosensors labelled in the N- or C-domain, respectively, interacting with PTH1R-PD1, PTH1R-PD2, or PTH1R-WT in ΔQ-GRK at saturating PTH(1-34) concentrations. In short, HEK293 cells were transfected with either an untagged PTH1R-PD1 or PTH1R-PD2 expression construct and one β-arrestin conformational change biosensor, FlAsH-labelled and stimulated with PTH(1-34). Conformational change data are shown as Δ net BRET change in percent, mean of three independent repetitions (n=3) + SEM. The statistical significance was calculated by one-way ANOVA (*, p<0.05; **, p<0.001; ***, p<0.0001; ****, p<0.00001). **B** The phosphorylation-dependency of conformational change was projected onto crystal surface structures of β-arrestin1 (PDB: 2WTR) and β-arrestin2 (PDB: 3P2D), with green indicating regions that undergo phosphorylation-independent conformational changes, blue for regions that are dependent on either the proximal or distal cluster to be phosphorylated, magenta indicating sites that are just dependent on the distal cluster, and red indicating positions that respond differentially upon any modification of C-terminal GPCR phosphorylation.

Our approach enabled us to differentiate between conformational changes that are induced by the active and phosphorylated (**P-R***) or just the active receptor (**R***), independent of GRK-mediated phosphorylation. Moreover, the use of both cluster mutants aided to further match phosphorylation-dependent effects with the availability of the proximal phosphorylation cluster (deleted in **P-R*-PD1**), or distal phosphorylation cluster (deleted in **P-R*-PD2**) (**Figure 4.13 A, C**).

For most sensors, any removal of receptor phosphorylation reduced the measured conformational change signals. Interestingly, the biosensors exhibited different phosphorylation-dependent behaviors, depending on the localization of the specific FlAsH labelling site (**Figure 4.13 B**). For β-arrestin1, this analysis revealed three distinct groups: sites that respond differently to any changes in receptor phosphorylation (dependent on proximal and distal cluster, F1, F2, F5), sites that are dependent on the distal cluster (F3, F4, F7, F9) and a site that requires at least one of the two assessed phosphorylation clusters to be available (dependent on proximal or distal cluster, F10) to undergo P-R*-like conformational changes.

Only three positions showed an identical pattern of phosphorylation-dependency for β-arrestin2, namely the F1, F5, and F7 sites. Accordingly, we found that the β-arrestin2 F1 and F5 sites are dependent on both, the proximal and distal phosphorylation clusters. The F7 and F10 site require only the distal cluster, whereas F4 and F9 need at least one of the two clusters to be present. Surprisingly, the β-arrestin2-F2 sensor reported similar conformational changes, independent of the receptor phosphorylation state. Strikingly, we were also able to record robust conformational changes of the β-arrestin2-F3 sensor for all conditions in the range of -35 to -45 % Δ net BRET change, maintaining most of the signal even in the absence of GRK-mediated receptor phosphorylation. Hence, the signals recorded for the β-arrestin2-F3 sensor resemble this phosphorylation-independent behavior, although this site exhibited a significant signal reduction for the interactions with P-R*-PD2 and R*.

Dependence of the F5 site on the proximal and distal receptor phosphorylation clusters was expected, as this labelling site is located in the respective phosphate-sensing N-domains of β-arrestin1 and 2. This finding reflects directly on the missing C-terminal GPCR phosphorylation, as the F5 loop has been shown to interact with phosphorylated GPCR C-termini (Kang et al. 2015, Kang et al. 2016, Shukla et al. 2013). Interestingly, a similar behavior was also found for the respective F1 sensors. Despite the higher

conformational change signals of the β-arrestin2-F1 sensor for the interaction with P-R* compared to β-arrestin1 (**Figure 4.10**), the interaction with P-R*-PD1 reduced the conformational changes at F1 for both β-arrestins by relative 50 %, while for P-R*-PD2 they are completely abolished (**Figure 4.13 A, C**). Furthermore, the loss of GRK activity in ΔQ-GRK induced identical effects as PTH1R-PD2 at these sites, confirming the distal phosphorylation cluster as a crucial binding interface for both β-arrestins. From these findings we conclude that the membrane-anchoring of the β-arrestin C-edge region is altered by differential receptor phosphorylation. One possible explanation could be differentially formed complex geometries of β-arrestins and PTH1R receptor variants, which may lead to an incomplete interaction with the plasma membrane or membranous components (White et al. 2020, Staus et al. 2020, Lally et al. 2017) .

As mentioned above, the F3 position might give additional insight into the assumed β-arrestin–GPCR complex configurations. The retained, phosphorylation-independent conformational changes for β-arrestin2-F3 possibly result from a virtually unaltered capability to form a “core” complex with the PTH1R, regardless of the receptor phosphorylation state. From our experiments shown in **Figure 4.7**, we concluded that β-arrestin1 is better suited to engage the receptor in a “hanging” complex. The F3 position for β-arrestin1 was found to be only dependent on the distal cluster, as it retained P-R*-like conformational changes for P-R*-PD1 but did not register conformational changes when coupling to the P-R*-PD2 or R* receptor states. This is in line with the hypothesis that proximal receptor phosphorylation is dispensable for the formation of a “hanging” complex and distal phosphorylation sites, still present in PTH1R-PD1, predominantly enable the formation of such complexes (Sente et al. 2018).

Additionally, the recruitment of all used β-arrestin conformational change biosensors to the PTH1R, PD1 and PD2 variants was assessed in order to confirm their functionality (**Figure 4.14**).

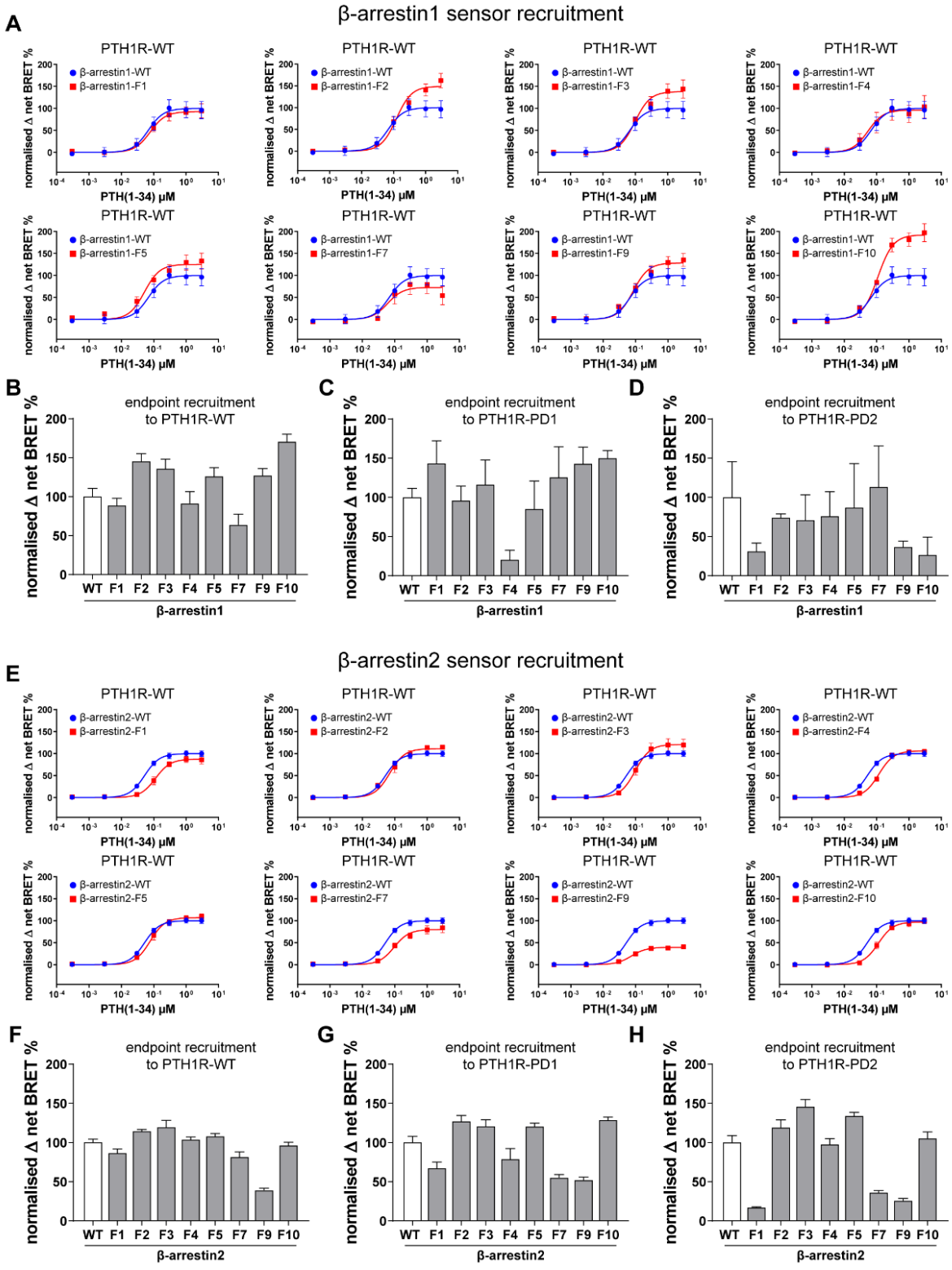

Figure 4.14 NanoBRET analysis of β-arrestin1 and 2 biosensor recruitment to PTH1R, -PD1, and -PD2

Assessment of β-arrestin1 (**A-D**) and 2 (**E-H**) biosensor (F1, 2, 3, 4, 5, 7, 9, 10) recruitment to the PTH1R-WT (**A, B** and **E, F**), and two phosphorylation-deficient receptor mutants, PTH1R-PD1 (**C** and **G**), and PTH1R-PD2 (**D** and **H**) via intermolecular NanoBRET and upon stimulation with PTH(1-34). Concentration-dependent recruitment is shown for the conditions featuring the PTH1R-WT, with data recorded for the β-arrestin-WT constructs shown multiple times to ensure comparability. Additionally, the BRET changes recorded at saturating ligand concentrations are depicted as bar charts for all three receptor variants, normalized to the respective β-arrestin-WT recruitment (**B-D** and **F-H**). Data are shown as Δ net BRET change in percent, mean of three independent repetitions (n=3) ± SEM.

All conformational change measurements in this study were performed in a concentration-dependent manner. The data for conformational changes induced by β-arrestin interactions with the PTH1R, -PD1, and -PD2 receptor variants can be comprehensively accessed in **Figure 4.15**.

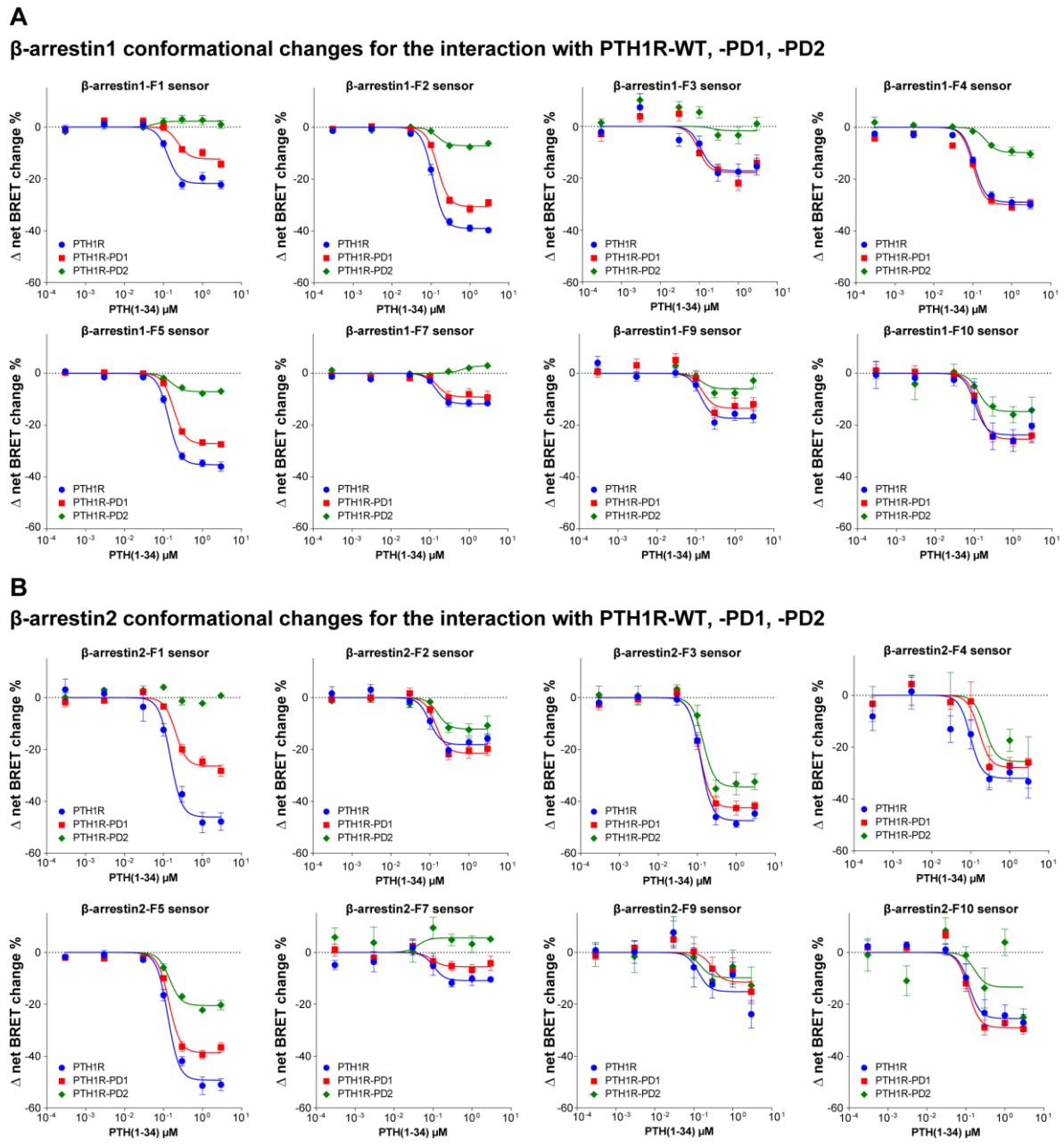

Figure 4.15 NanoBRET analysis of β-arrestin1 and 2 conformational change for PTH1R, -PD1, and -PD2

Data shown corresponds to bar graphs depicted in **Figure 4.10** and **Figure 4.13**. Concentration dependent conformational change data for β-arrestin1 (A) and 2 (B) biosensors interacting with untagged PTH1R-WT, -PD1, PD2 variants after FlAsH-labelling and stimulation with PTH(1-34). Data are shown as Δ net BRET change in percent, mean of three independent repetitions (n=3) ± SEM.

Additionally, we observed EC_{50} values for conformational changes to be similar for all biosensors of both β-arrestin isoforms (**Table 4.2** and **Table 4.3**).

Table 4.2 EC_{50} values for β-arrestin1 conformational changes

EC_{50} values and standard errors derived from conformational change measurements of individual β-arrestin1 FlAsH biosensors upon stimulation of the respective PTH1R variant with PTH(1-34) in µM. Measurements that did not allow for assessment of EC_{50} values are marked as "not/available" (N/A).

β-arrestin1	PTH1R-WT	PTH1R-PD1	PTH1R-PD2
F1	0,126 ± 0,015	0,217 ± 0,039	N/A
F2	0,115 ± 0,006	0,149 ± 0,010	0,159 ± 0,048
F3	0,107 ± 0,030	0,088 ± 0,018	0,146 ± 0,080
F4	0,120 ± 0,010	0,117 ± 0,010	0,184 ± 0,052
F5	0,140 ± 0,009	0,179 ± 0,011	0,188 ± 0,037
F7	0,157 ± 0,032	0,168 ± 0,074	0,473 ± 0,324
F9	0,123 ± 0,025	0,124 ± 0,030	0,125 ± 0,058
F10	0,110 ± 0,037	0,122 ± 0,017	0,141 ± 0,073

Table 4.3 EC_{50} values for β-arrestin2 conformational changes

EC_{50} values and standard errors derived from conformational change measurements of individual β-arrestin2 FlAsH biosensors upon stimulation of the respective PTH1R variant with PTH(1-34) in µM. Measurements that did not allow for assessment of EC_{50} values are marked as "not/available" (N/A).

β-arrestin2	PTH1R-WT	PTH1R-PD1	PTH1R-PD2
F1	0,160 ± 0,025	0,202 ± 0,024	N/A
F2	0,088 ± 0,019	0,140 ± 0,028	0,172 ± 0,061
F3	0,125 ± 0,010	0,119 ± 0,012	0,136 ± 0,025
F4	0,119 ± 0,042	0,162 ± 0,057	N/A
F5	0,144 ± 0,011	0,149 ± 0,011	0,175 ± 0,023
F7	0,126 ± 0,071	0,092 ± 0,066	N/A
F9	0,112 ± 0,057	0,266 ± 0,127	N/A
F10	0,112 ± 0,026	0,104 ± 0,011	N/A

All concentration-dependent conformational change signatures that were recorded in ΔQ-GRK are comprehensively shown in **Figure 4.16**.

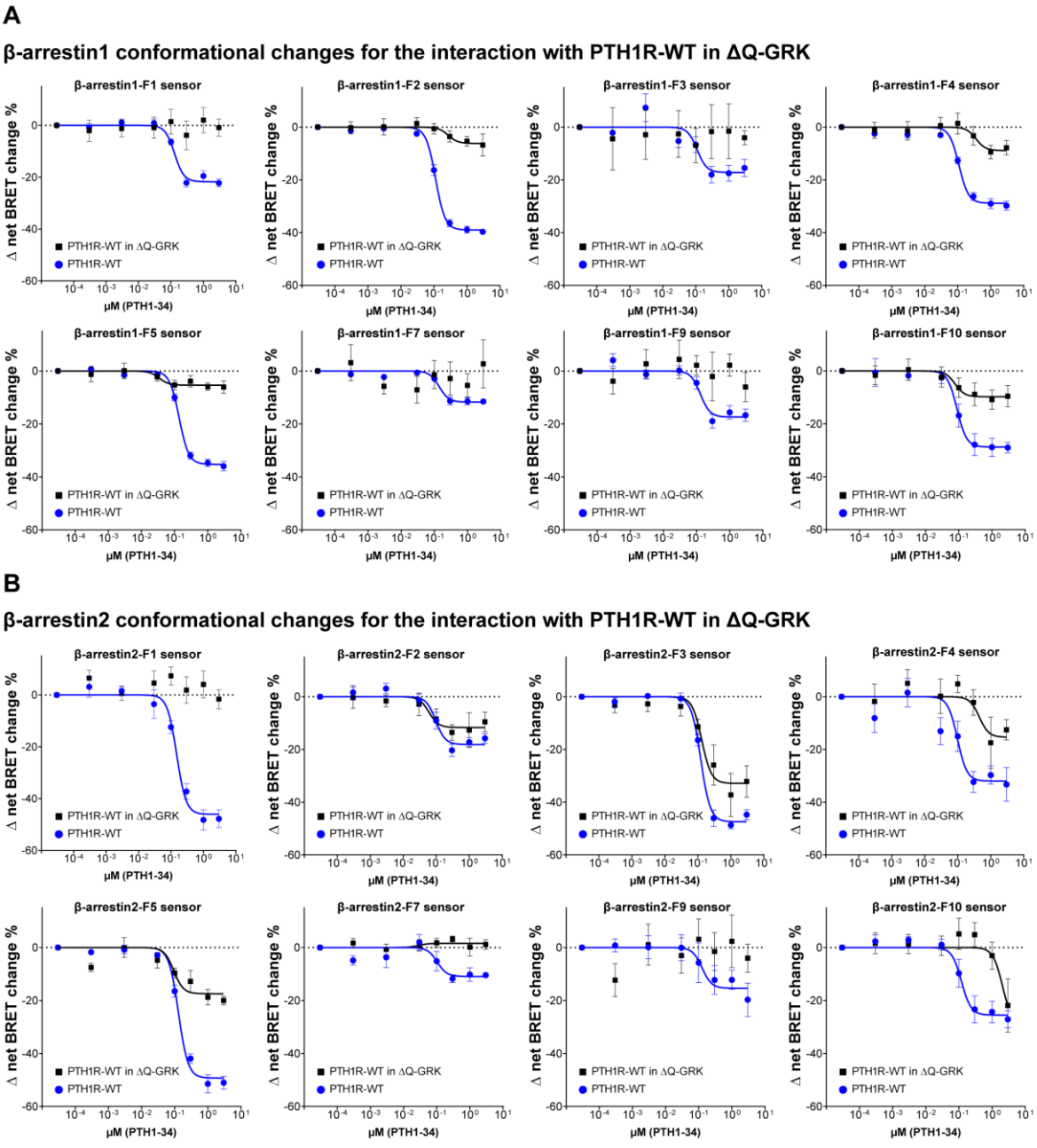

Figure 4.16 Concentration-dependent conformational changes of β-arrestin1 and 2 for the interaction with PTH1R in presence or absence of GRKs

Data shown corresponds to bar graphs depicted in **Figure 4.13**. Concentration dependent conformational change data for β-arrestin1 (**A**) and 2 (**B**) biosensors interacting with untagged PTH1R-WT in the absence of GRKs using ΔQ-GRK cells after FlAsH-labelling and stimulation with PTH(1-34). PTH1R-WT curves recorded in HEK293 (**Figure 4.15**) are depicted again to ensure comparability. Data are shown as Δ net BRET change in percent, mean of three independent repetitions (n=3) ± SEM.

4.2.4 Phosphorylation-dependency of β-arrestin complex configurations and downstream functions

As a further experiment to support our interpretation of “hanging” or “core” complex-dependent conformational changes, we deleted the FLR of β-arrestin1-F5. The WT version of this sensor showed conformational changes that are dependent on both assessed phosphorylation clusters (**Figure 4.13**), as our measurements register significant differences between the P-R*, P-R*-PD1, and P-R*-PD2 conditions. Assuming that the proximal phosphorylation cluster is not needed for the formation a “hanging” complex between the PTH1R and β-arrestin 1, the mutant β-arrestin1-dFLR-F5 sensor should register the same conformational changes for activation of PTH1R WT and -PD1 receptor variants. Indeed, the β-arrestin1 mutant biosensor changed its behavior and registered almost identical signals for the interaction with P-R* and P-R*-PD1 upon deletion of the FLR, as it cannot make use of the “core” complex binding interface (**Figure 4.17 A**). The PTH1R-PD2 mutant did not induce concentration-dependent conformational changes at the β-arrestin1-dFLR-F5 sensor, confirming the distal phosphorylation cluster as a crucial binding interface for the formation of a “hanging” PTH1R–β-arrestin complex.

Next, to assess whether differential PTH1R phosphorylation leads to the induction of specific β-arrestin-mediated downstream functions, we investigated the internalization and ERK-signaling capabilities of the PTH1R-WT, -PD1, and -PD2 variants.

Using confocal microscopy, our internalization analysis of all three receptor variants revealed robust co-localization with Rab5 after ligand stimulation (**Figure 4.17 B, C**). Despite identical β-arrestin1 recruitment to PTH1R-WT and -PD1 (**Figure 4.12 B**), internalization of PTH1R-PD1 is significantly reduced by 20 % (**Figure 4.17 B**). This indicates that the proximal phosphorylation cluster plays a more pronounced role for initial trafficking, and its lack leads to the formation of a trafficking-dysfunctional β-arrestin complex.

Additionally, receptor activation-dependent ERK1/2 phosphorylation was analyzed in HEK293 and β-arrestin1/2 knockout cells (O'Hayre et al. 2017). As previously shown (Gesty-Palmer et al. 2006, Gurevich und Gurevich 2018, Lee et al. 2016), agonist stimulation of the PTH1R-WT leads to increased ERK1/2 phosphorylation (**Figure 4.17 D**), which is decreased in the absence of β-arrestins.

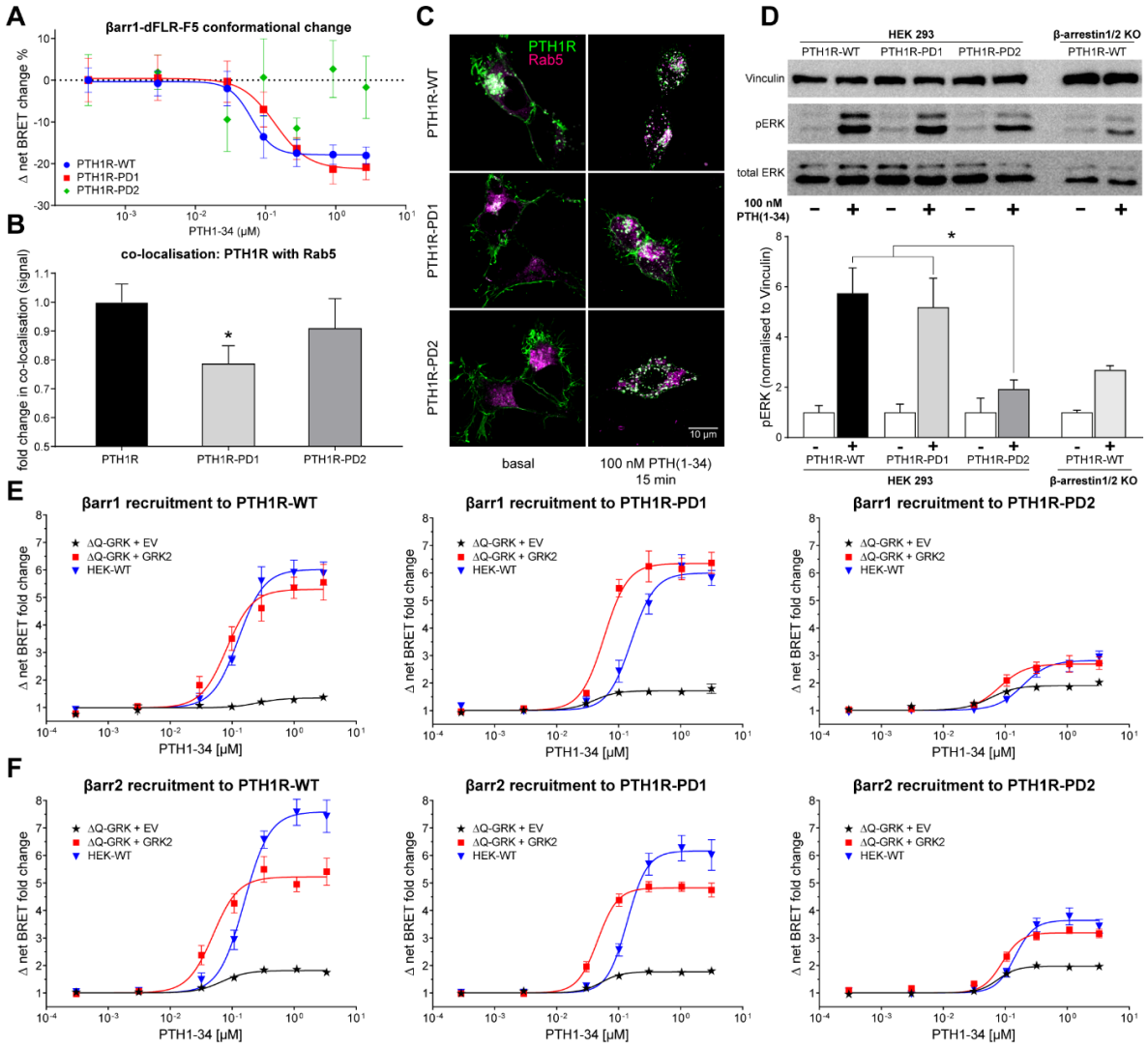

Figure 4.17 Phosphorylation states of the receptor determine β-arrestin recruitment, internalization, and ERK1/2 signaling

A Concentration-dependent conformational change of β-arrestin1-dFLR, labelled in position F5 upon activation of either the PTH1R-WT, -PD1 or PD2 variants with PTH(1-34). Results are shown as mean of three independent repetitions (n=3) ± SEM. **B** Internalization and early trafficking of the three receptor variants was analyzed via confocal microscopy. HEK293 cells were transfected with fluorescently labelled variants of the PTH1R-WT, -PD1 or -PD2 receptor mutants and Rab5-mCherry. The cells were grown on cover slips and either fixed before or after 15 minutes of stimulation with 100 nM PTH(1-34). Z-stacks of at least 25 cells of three independent experiments (n=3) were recorded using a confocal microscope. Co-localization of PTH1R and Rab5 in all images and all focal planes was calculated using Squassh and SquasshAnalyst and is presented as mean co-localization signal + SEM, normalized to WT basal levels. Statistical significance was calculated with a one-way ANOVA (*, p<0.05). **C** Shown are representative images of cells in the basal state (single confocal plane) and after ligand stimulation (maximum intensity projection). **D** Western blot analysis of the PTH1R-dependent induction of ERK1/2. HEK293 and β-arrestin1/2 double knockout cells were transfected with the respective PTH1R receptor variants and lysed before or after 15 minutes of stimulation with 100 nM PTH(1-34). A representative blot as well as the mean quantification of four independent experiments (n=4) + SEM is shown. The statistical significance was calculated by unpaired t test (*, p<0.05). **E, F** NanoBRET measured concentration-dependent recruitment of β-arrestin1 and 2 to PTH1R-WT, -PD1, -PD2 upon stimulation with PTH(1-34) in ΔQ-GRK cells. PTH1R recruitment in WT HEK cells (**Figure 4.12 B**) was shown again to ensure comparability.

Interestingly, PTH1R-PD2 induced ERK1/2 phosphorylation is diminished to similar levels despite the presence of β-arrestins. The PTH1R-PD1 displayed no significant reduction compared to PTH1R-WT. This is in line with the results of Lee *et al.*, as they

proposed that the receptor-dependent ERK1/2 phosphorylation is reflected by conformational changes measured for β-arrestin2-F10 (Lee et al. 2016) (the β-arrestin2-F10 position used in this thesis is homologous to the Lee *et al.* β-arrestin2-F5 position). Consistent with this observation, our β-arrestin2 conformational change signatures for PTH1R-WT and PTH1R-PD1 showed similar values for the F10 position, while PTH1R-PD2 showed a significantly reduced signal (**Figure 4.13 C**). Thus, we conclude that the phosphorylation of the distal cluster is essential for β-arrestin-supported ERK1/2 signaling.

Additionally, to the recruitment measured for PTH1R-WT, -PD1, and -PD2 in absence (ΔQ-GRK) and in presence of endogenously expressed GRKs (Control), we analyzed the impact of single GRK overexpression in ΔQ-GRK (combined in **Figure 4.18**). All tested GRK isoforms are able to mediate β-arrestin1 recruitment to PTH1R-WT, -PD1, and -PD2 at least to the same extend as in HEK293 (**Figure 4.17 E, Figure 4.18 B**). On the other hand, the overexpression of a single GRK could not fully rescue the ΔQ-GRK phenotype for β-arrestin2 recruitment to PTH1R-WT and -PD1 (**Figure 4.17 F, Figure 4.18 D**). In ΔQ-GRK cells, the three receptor variants induced almost identical respective recruitment of β-arrestin1 and 2, confirming that the difference in β-arrestin recruitment between these receptor variants is dependent on GRK phosphorylation (**Figure 4.17 E, F; Figure 4.18 B, D**).

For GRK6 overexpression in ΔQ-GRK we noticed an increased recruitment of β-arrestins for PTH1R-PD2 compared to the other GRK subtypes (**Figure 4.18 B, D**). It is tempting to speculate that the proximal phosphorylation cluster exhibits a preference for GRK6. However, our current cluster approach does not allow an individual assignment to phosphorylation sites, especially since we have no information of k_{cat}-values of individual GRKs. Taken together, we speculate that more than one GRK is needed to phosphorylate multiple receptor sites. In line with this, β-arrestin2 was found to need both phosphorylation sites, whereas β-arrestin1 can be recruited to full extent with distal phosphorylation only.

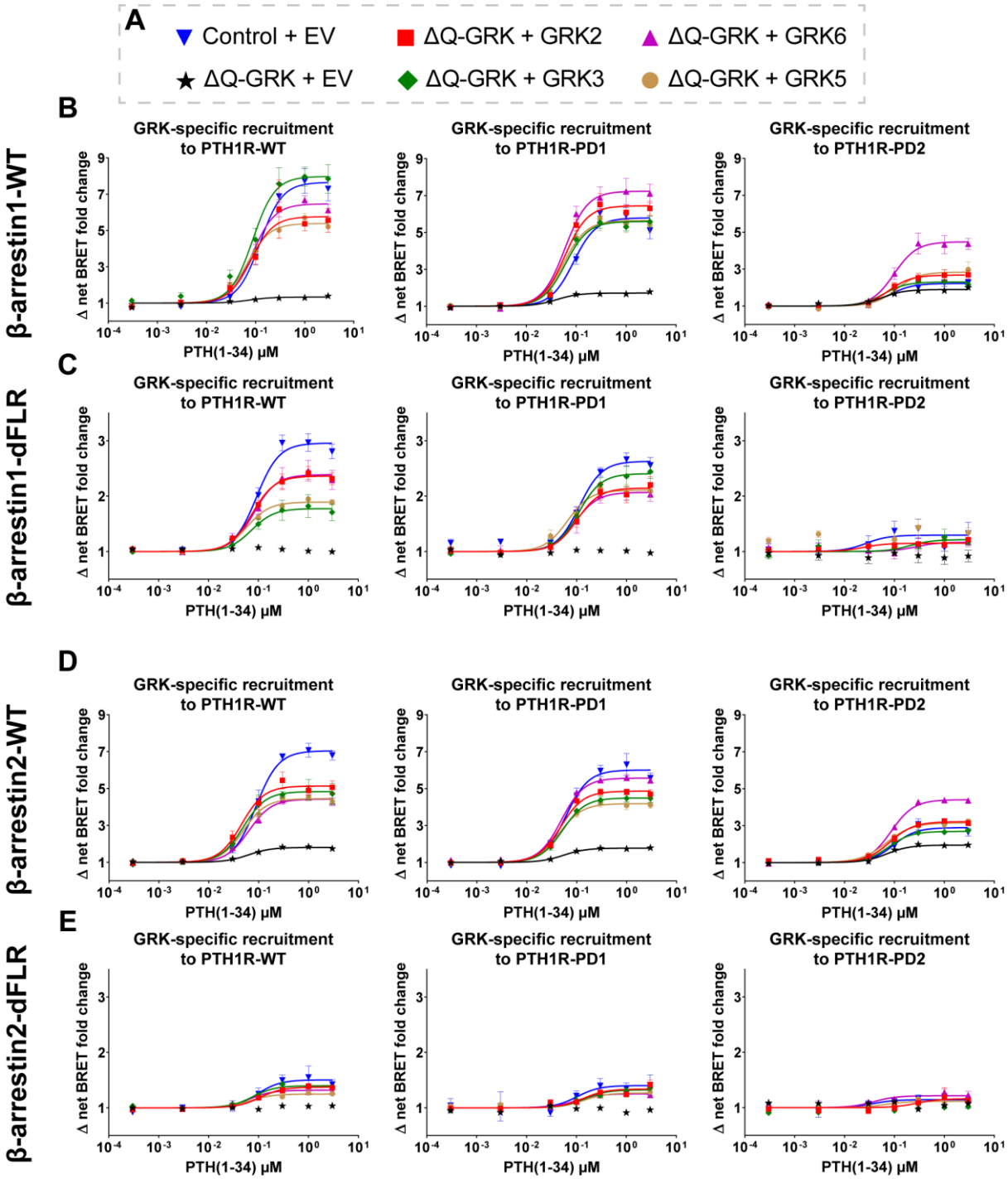

Figure 4.18 GRK-specific recruitment of β-arrestin-WT and -dFLR constructs to PTH1R-WT, -PD1, -PD2

A Color-coding for GRK-specific conditions. ΔQ-GRK or Control cells were transfected with C-terminally Halo-tagged PTH1R-WT, -PD1, -PD2 variants and β-arrestin1 (**B**), β-arrestin1-dFLR (**C**), β-arrestin2 (**D**), or β-arrestin2-dFLR (**E**) -NanoLuc fusion constructs. Additionally, either GRK2, 3, 5, 6, or the empty vector (EV) were co-transfected. The BRET changes are shown as ligand concentration-response curves. All data points are calculated as Δ net BRET fold change as the mean of at least three independent measurements (n≥3) ± SEM.

Furthermore, we conducted analogous “kinase-screen” experiments also for the β-arrestin1 and 2 dFLR constructs (**Figure 4.18 C, E**). In the absence of GRKs (ΔQ-GRK), none of the analyzed receptor variants (PTH1R-WT, -PD1, and -PD2) were able

to induce concentration-dependent recruitment β-arrestin-dFLR recruitment. Hence, we can conclude that the formation of “hanging” complexes between the PTH1R and β-arrestins are strictly dependent on GRK-mediated receptor phosphorylation.

In general, the PTH1R-WT and -PD1 variants induced a very similar pattern of GRK-specific β-arrestin-dFLR recruitment. Both receptor variants showed a robust interaction with β-arrestin1-dFLR, albeit individual GRKs mediate slightly lower levels of recruitment as measured in the control cell line. In contrast, the β-arrestin2-dFLR construct exhibited drastically reduced recruitment values for all three receptor variants (**Figure 4.18 E**). Interestingly, the PTH1R-PD2 receptor variant was not able to form concentration-dependent complexes with either β-arrestin-dFLR mutant. These experiments provide more evidence for β-arrestin1 being better suited to form a “hanging” complex with the PTH1R. Additionally, we can confirm the hypothesis of Sente et al. (2018), as proximal receptor phosphorylation alone (PTH1R-PD2) was not able to induce the formation of a “hanging” complex. In contrast, phosphorylation of the distal cluster (PTH1R-PD1) was sufficient to induce WT-like levels of β-arrestin-dFLR recruitment.

5. Discussion

In the following section, the most prominent results presented in this thesis are discussed in the context of recent literature and the underlying aims described in **chapter 2**. This discussion also follows the general structure of the results section, as the GRK-specific β-arrestin recruitment and phosphorylation-dependent β-arrestin conformational change data are addressed consecutively.

5.1 Analysis of GRK-specific β-arrestin recruitment and implications on the "barcode" hypothesis

The establishment of a comprehensive panel of GRK KO cell lines enabled us to identify biological patterns of GRK-specific β-arrestin-mediated GPCR regulation. Our comprehensive analysis revealed clustering of GPCRs into two different groups: GRK2/3-regulated and GRK2/3/5/6-regulated receptors. This finding adds to the "barcode" hypothesis and reveals that certain GPCRs exhibit a coupling preference towards specific GRK isoforms, as depicted in **Figure 5.1**.

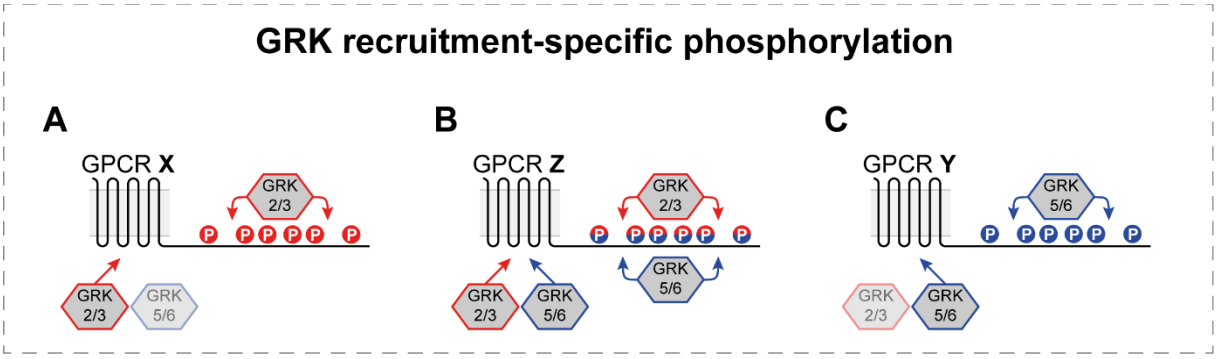

Figure 5.1 Implications on the "barcode" hypothesis

Certain GPCRs have been shown to be functionally phosphorylated by (**A**) GRK2/3 only, or (**B**) GRK2/3/5/6 (**Figure 4.6**). This might constitute another layer of coupling preference at the foundation of the "barcode" hypothesis. Although we did not encounter receptors for which β-arrestin recruitment was mediated exclusively by GRK5/6 (**C**), we cannot exclude their existence as our analysis just comprised 20 out of ~1600 possible human GPCR–β-arrestin pairs. (Figure was similarly published in Matthees et al. (2021) and reproduced with permission according to the Elsevier copy right agreement)

Using our triple GRK KO cell lines, it became evident that different GPCRs require certain levels of GRK expression in order to recruit arrestins. This circumstance lead to initially puzzling results, especially for the interpretation of GRK2- and GRK3-specific β-arrestin recruitment. These two kinases were able to facilitate stable recruitment to all tested receptors when overexpressed. In contrast to this finding, the β2ADR did not

exhibit substantial recruitment of β-arrestin2 when measured in either ΔGRK3/5/6 or ΔGRK2/5/6 cells (**Figure 4.1 C**), revealing that the residual endogenous expression of GRK2 or 3 is not sufficient to induce a stable β2ADR–β-arrestin2 complex. On the other hand, the PTH1R and M5R showed robust β-arrestin2 recruitment in ΔGRK3/5/6 and ΔGRK2/5/6 cells (**Figure 4.4**). This does not reflect on the ability of GRK2 to regulate the β2ADR, which has been shown multiple times in literature and our presented overexpression experiments (**Figure 4.1 E**). These results rather demonstrate that the affinities of GRK isoforms to GPCRs differ depending on the individual receptor. Thus, the tissue-specific expression levels (Matthees et al. 2021) of individual GRKs might have divergent effects for different GPCRs, even if phosphorylation is theoretically possible. These apparent differences between certain GPCR–GRK interactions could be explained by different affinities of GRKs to specific GPCRs, or different complex configurations (Cato et al. 2021) that GRKs form with specific receptors. Here, more experiments are needed and the presented results have to be supplemented with time-resolved GRK-recruitment data and possibly also specific GRK mutants to determine the key domains, or residues, which mediate the differences between the two GRK families and their individual members.

Several studies demonstrated that GRK2 and GRK6 preferably phosphorylate the β2ADR at different C-terminal serine and/or threonine residues (Krasel et al. 2008, Tran et al. 2004). Additionally, phosphorylation by GRK2 or 6 was shown to serve different functions (Nobles et al. 2011, Yang et al. 2015). In our study, we observed that all GRKs can mediate receptor–β-arrestin interactions to the same extent and by using a single β-arrestin2 conformational change sensor (FlAsH5 according to Nuber et al. (2016)), we could demonstrate that the N-domain of β-arrestin2, which recognizes the phosphorylated receptor C-terminus, showed similar conformational changes for the interaction with the β2ADR, even when facilitated by different kinases (**Figure 4.1 G**). However, more experiments have to be performed to rule out that differential β2ADR phosphorylation by GRK2 or 6 might lead to distinct β-arrestin2 conformational changes. While different GRK isoforms might preferably phosphorylate distinct sites of the β2ADR, resulting in different C-terminal phosphorylation patterns, our experiments clarify that the phosphorylation by each GRK isoform is sufficient to induce high-affinity β-arrestin recruitment (**Figure 4.1 E**).

For each receptor case with unclear GRK assignment by statistical analysis (**Figure 4.6**), alternative kinases were previously reported to be involved in receptor phosphorylation. In case of the M1R and M3R, casein kinase 1 alpha and casein kinase 2 were shown to be involved in receptor phosphorylation, respectively (Mou et al. 2006, Torrecilla et al. 2007). For the C5aR1, PKCβ was shown to contribute to receptor phosphorylation (Pollok-Kopp et al. 2007). Therefore, our cellular platform enables the rapid differentiation between receptors with purely GRK-dependent arrestin recruitment and receptors that rely on the action of other intracellular kinases for efficient arrestin-binding, desensitization, and internalization.

With the help of our novel ΔQ-GRK cell line, we were able to show that high expression levels of GRK2 and 3 are able to mediate β-arrestin interactions with all tested GPCRs. GRK5 and 6 seem to fulfill divergent roles depending on the analyzed GPCR, as they were not able to induce β-arrestin-coupling of the M2R, M4R, M5R and MOP (**Figure 4.5 and Figure 4.6**). Interestingly, this is not necessarily due to a lack of receptor phosphorylation, as it was shown that GRK5 and 6 phosphorylate the MOP upon agonist activation, but fail to mediate β-arrestin recruitment and receptor internalization (Drube et al. 2021). Nevertheless, we found receptors for which the GRK5- and 6-facilitated receptor regulation is indistinguishable from that mediated by GRK2 and 3 (namely the PTH1R and β2ADR, **Figure 4.1 and Figure 4.3**).

While GRK5 and 6 are membrane-localized (Komolov und Benovic 2018), GRK2 and 3 are primarily cytosolic and translocate to the plasma membrane supported by interactions with βγ-subunits of activated G proteins (Tesmer et al. 2005). It is still conceivable that GRK5 and 6 interactions with certain GPCRs might be obstructed due to their distinct cellular localization. The plasma membrane features a rather heterogeneous distribution of proteins and it has been shown that certain GPCRs tend to reside in specific membrane confinements (Calebiro et al. 2020). Some receptors might localize in membranous compartments that are inaccessible for GRK5 and 6. Following this hypothesis, these GPCRs would be accessible to GRK2 and 3 since they emerge from the cytosol and would not be limited to two dimensional diffusion and hindered by possible confinements. This still does not exclude the existence of GPCRs which do not serve as substrates for GRK2 or 3, due to e.g. low affinity.

In conclusion, we were able to elucidate the GRK-specificity of receptor regulation for 10 different GPCRs. Our analysis demonstrates that different GRK isoforms may have

identical, overlapping or divergent functions, depending on the targeted GPCR. This adds another layer of complexity to the regulation of GPCR signalling and trafficking and a possible explanation of how different β-arrestin functions are mediated across various tissues and cell types, especially considering often dysregulated, pathophysiological GRK expression levels.

5.1.1 The cellular context of GRK-specific GPCR regulation

The common regulation machinery of GPCRs is comprised of a surprisingly small number of intracellular proteins. Merely four ubiquitously expressed GRKs and two β-arrestin isoforms are responsible for the coordination of receptor desensitization, internalization and trafficking for most of the 800 GPCRs that are encoded in the human genome. Considering that individual receptors undergo vastly different regulatory processes to achieve peak functionality at an organism scale, it becomes evident that GRKs and β-arrestins have to sense receptor-specific information in order to fulfill targeted functions for different GPCRs.

The different primary and secondary structures of GPCRs have to be considered as main determinants for this molecular “decision-making”, as they are immediately enabling or preventing the association of different GRK and β-arrestin isoforms by providing appropriate binding interfaces. Yet, consensus sequences for the interaction of specific GPCRs with different GRK and β-arrestin isoforms are still elusive and even the well-established “barcode” hypothesis is not necessarily able to explain why the same GPCR might be differently regulated in various cell types and tissues.

One of the most striking conclusions that can be drawn from the presented results is that even though different GPCRs might pose as suitable substrates for the same GRK isoform, they still require specific GRK expression levels for functional phosphorylation to occur. This is illustrated by comparison of the data recorded in the newly established triple GRK knockout cell lines and the results that were generated using GRK overexpression. These experiments show, that β-arrestin recruitment to the β2ADR and PTH1R can be theoretically facilitated by GRK2, but the endogenous “leftover” expression of GRK2 fails to mediate this interaction for the β2ADR. Thus, cells have the possibility to control the level of GPCR downregulation by varying GRK expression levels, and these changes will have different effects for different GPCRs.

A given cell might express tens or hundreds of different GPCRs to fulfill its physiological functions. The results presented in this thesis suggest that subsets of these receptors can be specifically targeted by two different approaches: First, the expression of certain GRK isoforms of different families. This possibility is conceivable, as even high expression levels of GRK5 or 6 will not lead to the downregulation of muscarinic acetylcholine receptors, whereas the same kinases are very well suited to facilitate β-arrestin recruitment to the β2ADR. According to our data, high expression levels of GRK2/3 family kinases, on the other hand, would generally mediate downregulation processes for all expressed GPCRs. Second, cells are specifically able to target certain GPCRs, even if they are regulated by the same GRK isoform, by variation of expression levels, fine-tuned to still act on e.g. the PTH1R, but not the β2ADR.

These conclusions point out that every GPCR has to be seen as a specific gene, detached from general classification systems. In fact, cells of a certain tissue might express different GPCRs from various sub-classes of the GRAFS system and these receptors have to signal in concert to enable biological functionality. Tightly controlled GRK expression levels have to mediate targeted downregulation processes for these functional groups of GPCRs, hence consensus sequences for GRK-mediated receptor regulation might not necessarily align with the established GPCR classes. Patterns might rather be found in physiology, suggesting that more research has to be done on correlating expression levels of different GPCRs, GRKs and arrestins, as these proteins have to be present in a certain equilibrium to mediate the essential processes of life.

5.2 Differential analysis of β-arrestin conformational changes and implications on functional diversity of arrestins

As universal adaptor proteins modulating distinct signaling outcomes of GPCRs, β-arrestins have been shown to undergo different conformational changes when binding specific receptors or phosphopeptides (Lee et al. 2016, Nuber et al. 2016, Mayer et al. 2019, Yang et al. 2015, Latorraca et al. 2020). Notably, Nobles et al. (2007) already provided some evidence, that the V2Rpp-bound conformations of β-arrestin1 and 2 are different. The authors came to this conclusion by comparing tryptic digest patterns of purified and phosphopeptide-bound arrestins, thus they were not able to pinpoint regions that, in fact, undergo different conformational changes. Most of these studies

also link these GPCR-specific conformational changes to distinct downstream signaling functions, making it clear that β-arrestins adjust their functionality according to the geometry of the resulting GPCR–β-arrestin complex. Until now, these assessments of β-arrestin conformational changes mostly focus on one of the two β-arrestin isoforms, making it impossible to judge whether β-arrestin1 and 2 perform redundant, overlapping or divergent functions when binding to same GPCR. Additionally, studies working with phosphopeptides (Latorraca et al. 2020, Yang et al. 2015, Mayer et al. 2019) only register one binding interface between β-arrestins and GPCRs, which is constituted by charge-charge interactions between the arrestin N-domain and phosphorylated peptide stretches. These experiments negate the definitive impact of the GPCR transmembrane helix bundle, which is crucial for the formation of tight “core” complexes. Hence, the conveyed insights do not necessarily reflect the whole picture and rather characterize arrestin conformational states that correspond to “hanging” complex configurations.

With the comprehensive approach presented in this thesis, we were able to reveal major differences between the two β-arrestin isoforms, as we show that they do not only undergo different conformational changes (**Figure 4.10**), but also prefer distinct, functional complex configurations (**Figure 4.7**) when binding to the same receptor. Moreover, the two β-arrestins respond differentially to the C-terminal phosphorylation state of a GPCR (**Figure 4.13**), revealing that they interpret the same phosphorylation pattern in different ways.

With the help of specific knockout cells and β-arrestin mutants, we present evidence that β-arrestin1 is better suited to form a “hanging” complex, whereas β-arrestin2 relies more on the interaction with the intracellular GPCR cavity (**Figure 4.7**). This constitutes a major difference between the two isoforms, especially since β-arrestin1 can still drive receptor internalization without the FLR, whereas β-arrestin2 fails to form a functional “hanging” complex (**Figure 4.7**). Moreover, this finding might be directly reflected by multiple reports of β-arrestin1 engaging phosphorylated peptide stretches of non-GPCR signaling molecules, like e.g. receptor tyrosine kinases (Dalle et al. 2001, Girnita et al. 2007).

Interestingly, β-arrestin2 does not only show a higher preference to form “core” complexes, but also seems to form them more readily than β-arrestin1, even in the absence of GRKs. This is another conclusion that can be drawn from the presented

GRK-specific recruitment screen (**Figure 4.5**), as β-arrestin2 always exhibited a higher recruitment in ΔQ-GRK, when compared to β-arrestin1, regardless of which GPCR was tested. This behavior of β-arrestin2 has already been hypothesized in the publication of Zhan et al. (2011). The authors provide a crystal structure of β-arrestin2 and show that the protein displays a higher flexibility than other arrestin isoforms. Because of this, β-arrestin2 is more likely to "probe" different inactive and active conformations, even in the absence of phosphorylated and/or active GPCRs. This property of β-arrestin2 is attributed to a more disordered C-domain, as compared to other arrestins. Specifically, β-sheet XI (located in the C-domain β-sandwich) appears to be shortened, in comparison to β-arrestin1, and continues as an unstructured loop. As this structural component also takes part in interactions of the arrestin hinge region, close to the polar core, structural instability could lead to the spontaneous activation of β-arrestin2, without the need to engage phosphorylated GPCR C-termini. Thus, the authors of Zhan et al. (2011) provide an adequate explanation why β-arrestin2 is better suited to form phosphorylation-independent GPCR-complexes.

5.2.1 Novel β-arrestin1 and 2 FlAsH/NanoLuc conformational change biosensors

Utilizing our novel NanoLuc/FlAsH-based biosensors for β-arrestin1 and 2, we were able to show that the two isoforms indeed undergo different conformational changes when binding to the same GPCR. Furthermore, we located the hotspots of differential conformational changes in the phosphate-sensing N-domains and C-edge regions of the two proteins (**Figure 4.10**), suggesting that they interact differently with the phosphorylated C-terminus of a GPCR and the cell membrane. The possibility to measure arrestin conformational changes at such a resolution and in living cells originates from the change of biosensor design described in this thesis.

The preceding sensor design used in Nuber et al. (2016) employed a CFP/FlAsH FRET version of these biosensors, which made them suitable for single-cell measurements conducted with FRET microscopes. With this measurement system it was possible to assess kinetics of β-arrestin2 conformational changes with high temporal precision. Yet, this technique showed two clear disadvantages, when compared to measurements conducted with the novel sensors presented here. While providing excellent kinetic information about the biological system, the single-cell measurements made it tedious to assess effective ligand concentrations or differential conformational

changes that are induced by specific GPCRs or mutant receptors. Furthermore, the measured FRET responses yielded comparably low signal amplitudes, possibly masking smaller conformational changes in certain regions of β-arrestin2. The change to a NanoBRET system addressed these shortcomings in multiple ways. The new sensor design enabled the ensemble measurement of thousands of transfected cells in a 96-well format. Hence, it is now very feasible to measure a complete concentration-response curve with a single transfection of these biosensors in just 15 minutes of using the appropriate plate-reader setup. The same applies also to the screening of multiple GPCR constructs, as illustrated in the thesis at hand. Moreover, the employment of a NanoLuc as the designated BRET donor of the system lead to an increase of measured BRET responses due to its significantly increased brightness (as compared to other luciferases (Hall et al. 2012)) and the possibility to assess these conformational changes without the application of an external light source, radically reducing the background noise of the measurement system. Nevertheless, these benefits come at the cost of losing precise kinetic information, as the measurement intervals in 96-well plate readers cannot compete with the rapid signal quantification achieved by using the aforementioned FRET microscope setup.

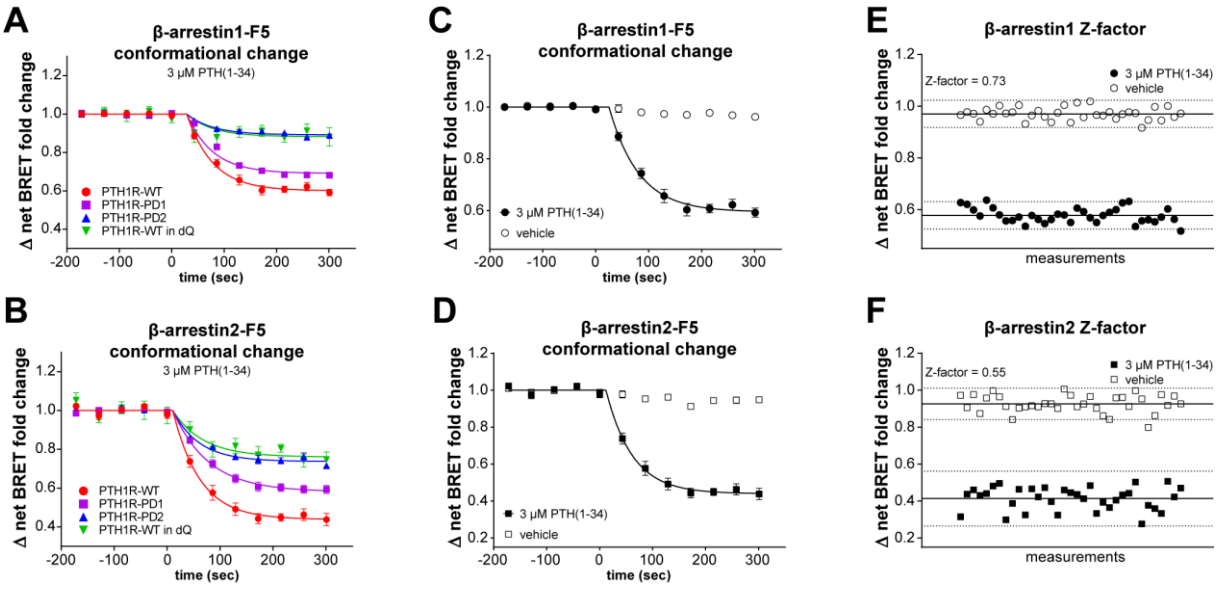

Figure 5.2 Time-dependent conformational changes and characterization of FlAsH/NanoLuc biosensors

A and **B** depicted are time-dependent conformational changes registered for the β-arrestin1/2-F5 conformational change biosensors upon interaction with PTH1R-WT, -PD1, -PD2, stimulated with 3 µM PTH(1-34) at second zero. **C** and **D** shows time-dependent conformational change of β-arrestin1/2-F5 upon coupling to the PTH1R-WT induced by application of 3 µM PTH(1-34) or vehicle at second zero. Data are shown as Δ net BRET change in percent, mean of three independent repetitions (n=3, three wells per independent transfection) ± SEM. To assess the inherent Z-factor of the applied assay, data points for β-arrestin1 and 2 recorded after reaching the plateau signal are plotted individually in **B** and **D**, respectively. Additionally, lines indicating the mean and three times the standard deviation are depicted to evaluate separation band between vehicle and 3 µM PTH(1-34) induced samples. The calculated Z-factors resulting from those measurements are depicted accordingly.

Z-factor analysis of the newly designed NanoLuc/FlAsH β-arrestin1 and 2-F5 conformational change biosensors confirmed that this measuring system is suitable for high-throughput screening (**Figure 5.2**), as both sensors feature a Z-factor > 0.5 (Zhang et al. 1999). This might prove especially useful, as measurements featuring these sensors require no modification of the tested GPCR and could potentially constitute a screening platform for e.g. the de-orphanization of receptors or the development of biased agonists.

5.2.2 The measurement of phosphorylation pattern-specific β-arrestin conformational changes

As one of the primary interaction interfaces between GPCRs and arrestins, C-terminal receptor phosphorylation patterns constitute an ideal system, in which receptor-specific information is encoded to be later translated by arrestins into specific functions. Especially, since GPCR phosphorylation is transient and modulated by several intracellular kinases and phosphatases, this type of coordination offers multiple ways for the cellular implementation of feedback loops and “fail-safe” mechanisms. The main function of these differential phosphorylation patterns during arrestin binding and activation, appears to be the controlled modulation of arrestin conformational changes.

As our measurements comprise not only conformational changes induced by the PTH1R-WT but also utilize two cluster mutants, missing key C-terminal phosphorylation sites, we provide *in cellulo* experimental proof of the computational and biochemical results of Latorraca *et al*. and Mayer *et al.* (Latorraca et al. 2020, Mayer et al. 2019), confirming that β-arrestin conformational changes are, in fact, dependent on the specific C-terminal phosphorylation of a GPCR. Furthermore, we recorded the complete conformational fingerprint of both β-arrestins when coupling to the PTH1R in the absence of GRKs, using quadruple GRK knockout cells (**Figure 4.13**). As all three tested receptor variants induced identical β-arrestin recruitment in ΔQ-GRK (**Figure 4.17 and Figure 4.18**), we assume that no other intracellular kinases play a decisive role in this process, suggesting that the assessed receptor variants are unphosphorylated in this condition. This constitutes a major advancement over previous studies (Latorraca et al. 2020, Lee et al. 2016, Yang et al. 2015, Nuber et al. 2016), as we are able to differentiate phosphorylation-dependent β-arrestin

conformational changes from the ones that are induced by the intracellular cavity of a GPCR in living cells.

Strikingly, we found positions in β-arrestin2 that undergo similar conformational changes independent of receptor phosphorylation (**Figure 4.13**). This is again in line with the finding, that β-arrestin2 functions are more reliant on the formation of a “core” complex, especially since all tested sites for β-arrestin1 are sensitive towards differential GPCR phosphorylation. That being said, the presented results show that both β-arrestin isoforms assume significantly different conformational states for the binding of PTH1R-WT, -PD1, -PD2, and the unphosphorylated PTH1R. The P-R* receptor state induced the highest conformational change signals for all tested biosensors. Individual deletions of C-terminal receptor phosphorylation sites progressively reduced the measured signals, albeit differently for the two β-arrestin isoforms and not for all assessed positions. These data demonstrate that β-arrestins are able to accommodate a multitude of different phosphorylation- and conformational states of a GPCR while translating this information into specific β-arrestin conformational changes that govern the functionality of the resulting GPCR–β-arrestin complex.

5.2.3 C-terminal phosphorylation patterns dictate GPCR complex configurations and downstream functions for β-arrestin1 and 2

With the set of experiments conducted in the course of this thesis, it becomes evident that these phosphorylation-dependent conformational changes define the nature and functionality of resulting GPCR–arrestin complexes. The differential impact of proximal and distal receptor phosphorylation clusters, as concluded from the presented results, is schematically depicted in **Figure 5.3**.

The general downstream effects of proximal and distal GPCR phosphorylation clusters (**Figure 4.17**) can be summarized as follows: Proximal receptor phosphorylation is crucial for arrestin-facilitated receptor internalization and trafficking. Distal phosphorylation, on the other hand, appears to be important for arrestin activation in general, and the arrestin-facilitated amplification of MAPK signaling. Interestingly, the data comprised in this thesis does not only show that β-arrestin1 and 2 undergo different conformational changes upon interaction with the same GPCR, but also suggests that the two β-arrestin isoforms are differently affected by proximal and distal

receptor phosphorylation. Multiple experiments of this thesis show that β-arrestin1 is better suited to form a phosphorylation-dependent “hanging” complex with different GPCRs, whereas β-arrestin2 seems to preferably form tight complexes with GPCRs by engaging their seven transmembrane cores. In line with this, proximal phosphorylation of the PTH1R C-terminus only has a small effect on β-arrestin1 binding, as these phosphates proposedly associate with arrestins close to the FLR. This interaction will break the FLR-lock and specifically stabilize “core” complexes. An analogous behavior can also be seen for β-arrestin2, as the dFLR mutants for both isoforms show similar recruitment for PTH1R-WT and -PD1 (**Figure 4.18**).

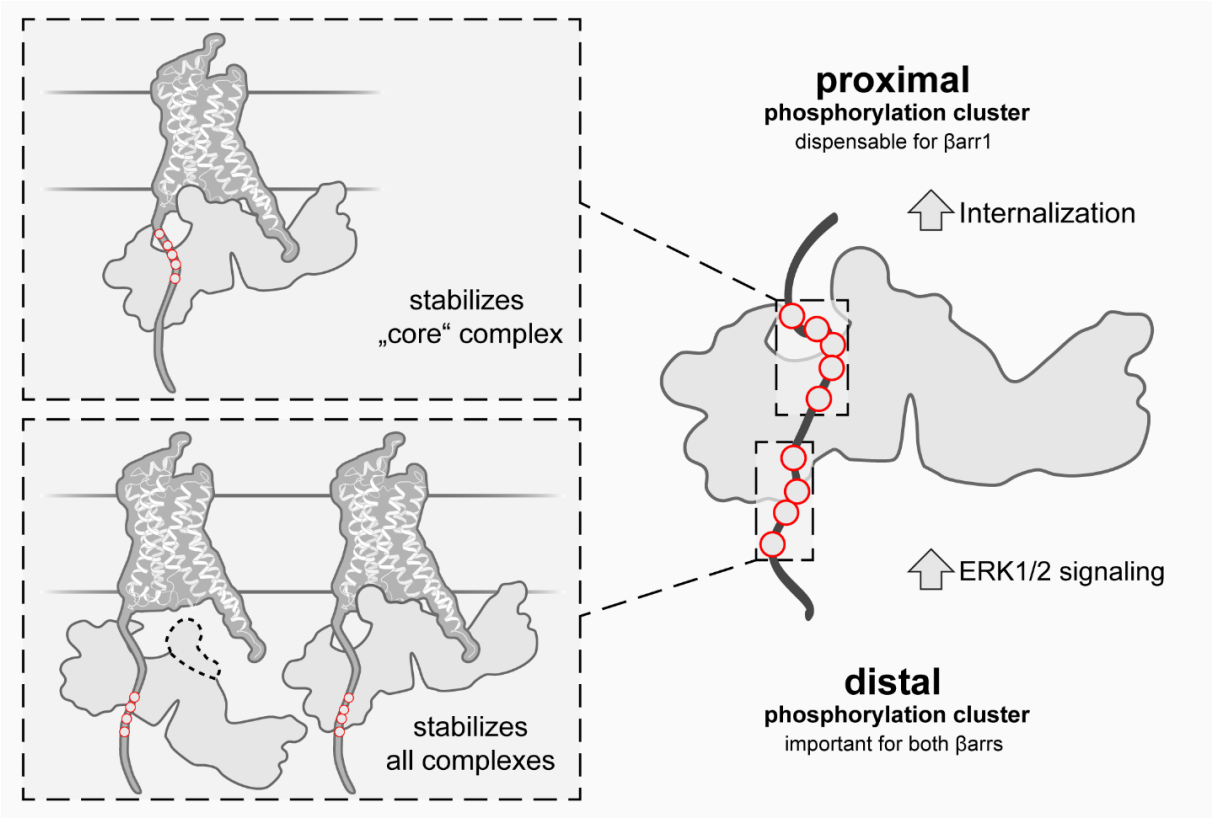

Figure 5.3 The differential impact of C-terminal receptor phosphorylation on β-arrestin binding and functionality

A schematic depiction of the influences of proximal and distal receptor phosphorylation on arrestin functions. Proximal receptor phosphorylation was found to be dispensable for β-arrestin1 binding but crucial for arrestin-mediated receptor internalization and the formation of “core” complexes. Distal receptor phosphorylation appears to be important for both β-arrestin isoforms and essential for the formation of “hanging” complexes and the arrestin-facilitated amplification of ERK1/2 signaling.

Removal of the distal phosphorylation cluster showed severe effects for the binding of both β-arrestin isoforms. This data suggests that the polar core and three-element site

are more important for general arrestin activation, as the distal phosphorylated residues most likely bind arrestins close to those intramolecular interactions.

In summary, our findings demonstrate inherent differences between the two homologous arrestin isoforms for the interaction with the same GPCR. Furthermore, we show that the phosphorylation state of a given receptor induces specific conformational rearrangements that determine the functional diversity between the two β-arrestin isoforms.

6. Conclusions

The novel tools developed and employed in this thesis helped to design experiments that shed light on the complex system of GPCR regulation. The first part of the project was focused on the GRK-specificity of GPCR–β-arrestin interactions and provides a characterization for ten different GPCRs. From the results that were generated via the utilization of various GRK knockout cell lines, different BRET assays, and confocal microscopy, the following conclusions can be drawn:

- *Specific GPCRs exhibit a previously undescribed coupling preference towards different GRK isoforms. According to the presented data, receptors are either functionally phosphorylated by GRK2 and 3 or GRK2, 3, 5, and 6.*
- *Certain receptors require different GRK expression levels for efficient regulation to occur, suggesting that small changes in GRK expression levels will have different effects for different GPCRs.*
- *GPCR Internalization, early trafficking, and β-arrestin co-localization is mediated by the same kinases as β-arrestin recruitment.*
- *β-arrestin2 is better suited to form GRK-independent GPCR complexes as compared to β-arrestin1.*

In the second part of this thesis, differences between β-arrestin1 and 2 for the interaction with the PTH1R were investigated in detail. The design and employment of novel intramolecular conformational change sensors for both β-arrestin isoforms and specific β-arrestin mutants, enabled experiments that revealed the following biological insights:

- *β-arrestin1 and 2 undergo different conformational changes for coupling to the same GPCR.*
- *β-arrestin1 is able to form a functional "hanging" complex with the PTH1R, in contrast to β-arrestin2, which prefers the formation of tight "core" complexes.*
- *β-arrestin1 and 2 respond differently to changes in C-terminal GPCR phosphorylation patterns. All measured β-arrestin1 conformational changes were dependent on the receptor phosphorylation state. In contrast to this, certain positions in β-arrestin2 are able to undergo phosphorylation-independent conformational changes.*
- *Proximal receptor phosphorylation stabilizes GPCR–β-arrestin "core" complexes and coordinates arrestin-mediated receptor internalization.*
- *Distal receptor phosphorylation is crucial for efficient arrestin activation and subsequent MAPK signal amplification.*

Taken together, this thesis demonstrates that substantial differences between specific GRK and β-arrestin isoforms enable the targeted regulation of 800 different GPCRs. The presented data suggest that cells of specific tissues adjust the expression levels of these individual genes to specifically regulate the expressed subset of GPCRs, which is required for biological functionality.

Appendix

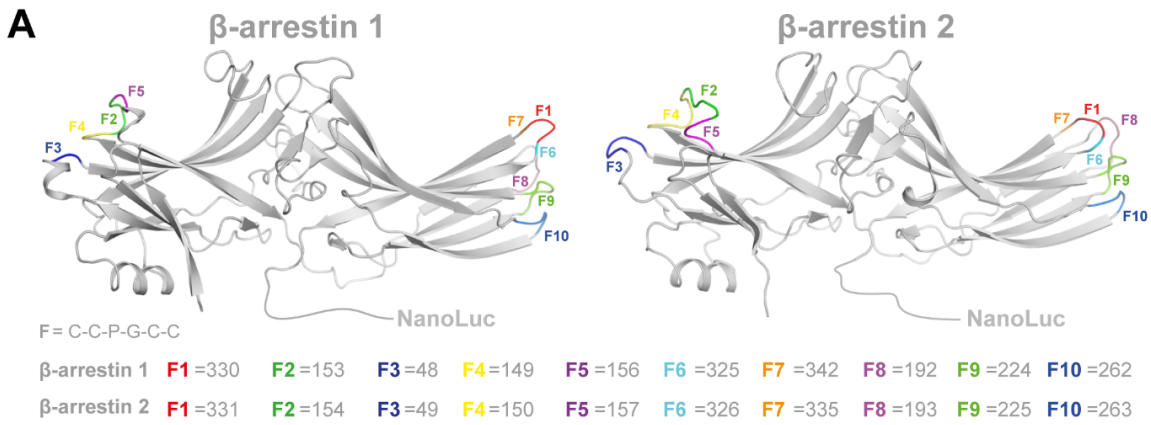

B

Alignment

```
                                                                                F3
bArr1    1 MGDK-GTRVFKKASPNGKLTVYLGKRDFVDHIDLVEPVDGVVLVDPEYL|KERRVYVTLTC    59
bArr2    1 MGEKPGTRVFKKSSPNCKLTVYLGKRDFVDHLDKVDPVDGVVLVDPDYL|KDRKVFVTLTC    60

bArr1   60 AFRYGREDLDVLGLTFRKDLFVANVQSFPPAPEDKKPLTRLQERLIKKLGEHAYPFTFEI    119
bArr2   61 AFRYGREDLDVLGLSFRKDLFIANYQAFPPTPNPPRPPTRLQERLLRKLGQHAHPFFFTI    120

                                                F4   F2   F5
bArr1  120 PPNLPCSVTLQPGPEDTGKACGVDYEVKAF|CAEN|LEE|KIHKRNSVRLVIRKVQYAPERPG 179
bArr2  121 PQNLPCSVTLQPGPEDTGKACGVDFEIRAF|CAKS|LEE|KSHKRNSVRLVIRKVQFAPEKPG 180

                        F8                                          F9
bArr1  180 PQPTAETTRQFLM|SDKPLHLEASLDKEIYYHGEPISVNVHVTNNT|NKTVKKIKISVRQYA  239
bArr2  181 PQPSAETTRHFLM|SDRSLHLEASLDKELYYHGEPLNVNVHVTNNS|TKTVKKIKVSVRQYA  240

                                    F10
bArr1  240 DICLFNTAQYKCPVAMEEADDTV|APSSTFCKVYTLTPFLANNREKRGLALDGKLKHEDTN   299
bArr2  241 DICLFSTAQYKCPVAQVEQDDQV|SPSSTFCKVYTITPLLSNNREKRGLALDGKLKHEDTN   300

                                        F6       F1          F7
bArr1  300 LASSTLLREGANREILGIIVSYKVKV|KLVVSR|GGLLGDLASSDV|AVELPFTLMHPKPKEE 359
bArr2  301 LASSTIVKEGANKEVLGILVSYRVKV|KLVVSR|GG--------DV|SVELPFVLMHPKPHDH 352

bArr1  360 ----PPHREVPEHETPVDTNLIELDTN---DDDIVFEDFARQRLKGMKDDKEEEEDGTGS    412
bArr2  353 IALPRPQSAVPETDAPVDTNLIEFETNYATDDDIVFEDFARLRLKGLKDEDYDDQFC---

bArr1  413 PRLNDR
bArr2      ------
```

Appendix Figure 1 Alignment of utilized β-arrestin1 and 2 conformational change biosensors

A Cartoon depiction of the used NanoLuc/FlAsH conformational change biosensors. The inserted FlAsH-sites are indicated as colored loops using crystal structures for β-arrestin1 (PDB: 2WTR) and 2 (PDB: 3P2D). The location specific insertion sites for FlAsH-binding (CCPGCC) is depicted below. **B** Shown is an alignment between bovine β-arrestin1 (NCBI reference sequence: NP_776668.1) and 2 (NCBI reference sequence: NP_001192206.1), again highlighting the positions of homologously inserted FlAsH binding sites. The alignment was created using the Clustal Omega alignment tool (https://www.ebi.ac.uk/Tools/msa/clustalo/).

Appendix Table 1 Statistical analysis of GRK-specific β-arrestin recruitment (ΔQ vs all)

BRET fold changes at saturating ligand concentrations of at least three independent experiments were compared using ANOVA and Bonferroni's test (* p < 0.05; ** p < 0.01; *** p < 0.001; **** p < 0.0001).

GPCR	βarr	ΔQ-GRK vs. GRK2			ΔQ-GRK vs. GRK3			ΔQ-GRK vs. GRK5			ΔQ-GRK vs. GRK6			ΔQ-GRK vs. Control		
		non adj.	adj.		non adj.	adj.		non adj.	adj.		non adj.	adj.		non adj.	adj.	
β2ADR	βarr1	0,024	0,220		0,005	0,042	*	0,011	0,098		0,026	0,230		0,010	0,088	
β2ADR	βarr2	0,003	0,031	*	0,004	0,034	*	0,017	0,155		0,009	0,079		0,086	0,770	
β2V2R	βarr1	0,000	0,002	**	0,000	0,001	***	0,089	0,801		0,619	1,000		0,078	0,704	
β2V2R	βarr2	0,064	0,573		0,064	0,572		0,271	1,000		0,570	1,000		0,216	1,000	
C5aR1	βarr1	0,000	0,001	**	0,000	0,000	***	0,000	0,002	**	0,007	0,064		0,000	0,000	***
C5aR1	βarr2	0,180	1,000		0,318	1,000		0,367	1,000		0,870	1,000		0,063	0,566	
M1R	βarr1	0,079	0,713		0,149	1,000		0,001	0,013	*	0,175	1,000		0,360	1,000	
M1R	βarr2	0,073	0,658		0,399	1,000		0,368	1,000		0,030	0,273		0,081	0,731	
M2R	βarr1	0,030	0,274		0,005	0,043	*	0,827	1,000		0,882	1,000		0,700	1,000	
M2R	βarr2	0,018	0,158		0,003	0,029	*	0,553	1,000		0,492	1,000		0,649	1,000	
M3R	βarr1	0,050	0,447		0,825	1,000		0,561	1,000		0,209	1,000		0,641	1,000	
M3R	βarr2	0,000	0,004	**	0,001	0,007	**	0,167	1,000		0,008	0,068		0,001	0,005	**
M4R	βarr1	0,092	0,828		0,002	0,014	*	0,653	1,000		0,958	1,000		0,138	1,000	
M4R	βarr2	0,007	0,066		0,000	0,002	**	0,818	1,000		0,650	1,000		0,873	1,000	
M5R	βarr1	0,001	0,009	**	0,000	0,000	***	0,977	1,000		0,929	1,000		0,000	0,000	***
M5R	βarr2	0,000	0,000	***	0,000	0,000	***	0,903	1,000		0,710	1,000		0,000	0,004	**
MOP	βarr1	0,079	0,707		0,141	1,000		0,633	1,000		0,456	1,000		0,169	1,000	
MOP	βarr2	0,017	0,152		0,004	0,035	*	0,540	1,000		0,922	1,000		0,510	1,000	
PTHR	βarr1	0,009	0,082		0,000	0,002	**	0,015	0,134		0,004	0,039	*	0,001	0,008	**
PTHR	βarr2	0,001	0,007	**	0,002	0,016	*	0,005	0,046	*	0,005	0,048	*	0,000	0,000	***

Appendix Table 2 Statistical analysis of GRK-specific β-arrestin recruitment (Control vs all)

BRET fold changes at saturating ligand concentrations of at least three independent experiments were compared using ANOVA and Bonferroni's test (* p < 0.05; ** p < 0.01; *** p < 0.001; **** p < 0.0001).

GPCR	βarr	Control vs. GRK2			Control vs. GRK3			Control vs. GRK5			Control vs. GRK6		
		non adj.	adj.		non adj.	adj.		non adj.	adj.		non adj.	adj.	
β2ADR	βarr1	0,448	1,000		0,966	1,000		0,709	1,000		0,435	1,000	
β2ADR	βarr2	0,105	0,948		0,115	1,000		0,392	1,000		0,235	1,000	
β2V2R	βarr1	0,006	0,053		0,002	0,022	*	0,941	1,000		0,183	1,000	
β2V2R	βarr2	0,476	1,000		0,475	1,000		0,881	1,000		0,083	0,747	
C5aR1	βarr1	0,243	1,000		0,963	1,000		0,145	1,000		0,004	0,035	*
C5aR1	βarr2	0,543	1,000		0,333	1,000		0,288	1,000		0,047	0,420	
M1R	βarr1	0,442	1,000		0,652	1,000		0,020	0,179		0,717	1,000	
M1R	βarr2	0,953	1,000		0,324	1,000		0,352	1,000		0,591	1,000	
M2R	βarr1	0,015	0,132		0,002	0,021	*	0,867	1,000		0,812	1,000	
M2R	βarr2	0,007	0,062		0,001	0,010	**	0,889	1,000		0,813	1,000	
M3R	βarr1	0,120	1,000		0,806	1,000		0,301	1,000		0,092	0,832	
M3R	βarr2	0,899	1,000		0,829	1,000		0,008	0,071		0,172	1,000	
M4R	βarr1	0,004	0,035	*	0,000	0,001	***	0,338	1,000		0,151	1,000	
M4R	βarr2	0,010	0,089		0,000	0,002	**	0,943	1,000		0,768	1,000	
M5R	βarr1	0,041	0,366		0,349	1,000		0,000	0,000	***	0,000	0,000	***
M5R	βarr2	0,187	1,000		0,086	0,772		0,000	0,004	**	0,001	0,009	**
MOP	βarr1	0,005	0,049	*	0,010	0,093		0,350	1,000		0,502	1,000	
MOP	βarr2	0,058	0,525		0,014	0,122		0,962	1,000		0,573	1,000	
PTHR	βarr1	0,222	1,000		0,472	1,000		0,147	1,000		0,396	1,000	
PTHR	βarr2	0,039	0,351		0,017	0,149		0,006	0,052		0,006	0,050	*

List of tables

List of figures

Ehrenwörtliche Erklärung

Hiermit erkläre ich, dass mir die Promotionsordnung der Medizinischen Fakultät der FriedrichSchiller-Universität bekannt ist,

ich die Dissertation selbst angefertigt habe und alle von mir benutzten Hilfsmittel, persönlichen Mitteilungen und Quellen in meiner Arbeit angegeben sind,

mich folgende Personen bei der Auswahl und Auswertung des Materials sowie bei der Herstellung des Manuskripts unterstützt haben: Prof. Dr. Carsten Hoffmann, Edda Matthees M.Sc., Dr. Julia Drube, Mona Reichel M.Sc.,

die Hilfe eines Promotionsberaters nicht in Anspruch genommen wurde und dass Dritte weder unmittelbar noch mittelbar geldwerte Leistungen von mir für Arbeiten erhalten haben, die im Zusammenhang mit dem Inhalt der vorgelegten Dissertation stehen,

dass ich die Dissertation noch nicht als Prüfungsarbeit für eine staatliche oder andere wissenschaftliche Prüfung eingereicht habe und

dass ich die gleiche, eine in wesentlichen Teilen ähnliche oder eine andere Abhandlung nicht bei einer anderen Hochschule als Dissertation eingereicht habe.

Jena, 24.09.2021

Acknowledgements

With the completion of this thesis, another stage of my life is concluded. I am in love with molecular biology and the chemistry that keeps the wheels of evolution on this planet turning at a steady rate. This feeling of mine is only surpassed by my appreciation for all these caring individuals who accompanied and aided me in finishing my doctoral studies.

First and foremost, I want to express my gratitude towards my primary supervisor, Professor Carsten Hoffmann. From the moment we first talked, it was clear to me that we did not only agree in our view of science but also connected on a personal level. With his supervision, I felt appreciated as a member of the scientific community and was handed all the tools, resources, knowledge, and advice that I needed to conduct the thesis at hand. His guidance was also crucial to assemble a strong team during my time in Jena. With Edda Sofie Fabienne Matthees, Julia Drube, and Mona Reichel, (together we would call ourselves the “ArresTeam” and felt not the slightest amount of embarrassment by doing so) on my side, there was no challenge that felt out of reach. Again, I want to express my deepest gratitude towards these three amazing scientists – only with their help it was possible for me to thrive.

Additionally, I want to show my gratefulness towards my second supervisor, Professor Stefan Schulz. With his willingness to share his expertise and tools, he was a strong ally for our working group as we established ourselves in Jena.

I want to thank Amod Godbole, who was not only a secure anchor for my personal life and best friend in Jena but was also always available for me to talk science. His critical comments grounded my work and allowed me to experience another point of view. Furthermore, I am genuinely grateful for Dorith Schmidt and all the help she offered me during my doctoral studies. She is passionately talented in entangling the complex web of German bureaucracy and the kind soul that keeps our lab functional and such a pleasant place to work in.

Moreover, I want to thank my parents. Their unending love towards each other is not only the reason why I am here today but also the life goal I am striving to achieve. They taught me that kindness is a good that does not deplete and showed me that politeness and fraternity are far superior to elbows. The same is true for my brother, who I love dearly. Through all the hardship my family had to endure during my seemingly endless studies, he taught me that hope and optimism is never out of place.

With these final lines, I want to thank my love, Sophie, from the absolute bottom of my heart. She is the most brilliant scientist but also the most empathetic and loyal person I ever had the pleasure to meet. She always stood by me and chose me again and again, day after day, and through all these thousands of kilometers we journeyed just to catch a glimpse of each other. Her appearance and love are my first thought every new morning and I wish for nothing more than her being the final thought at the end of my journey through this life. She is and always will be the moon of my life.

Curriculum vitae

Der Lebenslauf wurde aufgrund datenschutzrechtlicher Gründe aus der online Version der vorliegenden Dissertation entfernt.

References

Alhadeff R, Vorobyov I, Yoon HW, Warshel A. 2018. Exploring the free-energy landscape of GPCR activation. Proc Natl Acad Sci U S A, 115 (41):10327-10332.

Beautrait A, Michalski KR, Lopez TS, Mannix KM, McDonald DJ, Cutter AR, Medina CB, Hebert AM, Francis CJ, Bouvier M, Tesmer JJ, Sterne-Marr R. 2014. Mapping the putative G protein-coupled receptor (GPCR) docking site on GPCR kinase 2: insights from intact cell phosphorylation and recruitment assays. J Biol Chem, 289 (36):25262-25275.

Boguth CA, Singh P, Huang CC, Tesmer JJ. 2010. Molecular basis for activation of G protein-coupled receptor kinases. EMBO J, 29 (19):3249-3259.

Bohn LM, Lefkowitz RJ, Gainetdinov RR, Peppel K, Caron MG, Lin FT. 1999. Enhanced morphine analgesia in mice lacking beta-arrestin 2. Science, 286 (5449):2495-2498.

Budnik B, Levy E, Harmange G, Slavov N. 2018. SCoPE-MS: mass spectrometry of single mammalian cells quantifies proteome heterogeneity during cell differentiation. Genome Biol, 19 (1):161.

Cahill TJ, 3rd, Thomsen AR, Tarrasch JT, Plouffe B, Nguyen AH, Yang F, Huang LY, Kahsai AW, Bassoni DL, Gavino BJ, Lamerdin JE, Triest S, Shukla AK, Berger B, Little Jt, Antar A, Blanc A, Qu CX, Chen X, Kawakami K, Inoue A, Aoki J, Steyaert J, Sun JP, Bouvier M, Skiniotis G, Lefkowitz RJ. 2017. Distinct conformations of GPCR-beta-arrestin complexes mediate desensitization, signaling, and endocytosis. Proc Natl Acad Sci U S A, 114 (10):2562-2567.

Calebiro D, Koszegi Z, Lanoiselee Y, Miljus T, O'Brien SL. 2020. G protein-coupled receptor-G protein interactions: a single-molecule perspective. Physiol Rev.

Cassier E, Gallay N, Bourquard T, Claeysen S, Bockaert J, Crepieux P, Poupon A, Reiter E, Marin P, Vandermoere F. 2017. Phosphorylation of beta-arrestin2 at Thr(383) by MEK underlies beta-arrestin-dependent activation of Erk1/2 by GPCRs. Elife, 6.

Cato MC, Yen YC, Francis CJ, Elkins KE, Shareef A, Sterne-Marr R, Tesmer JJG. 2021. The Open Question of How GPCRs Interact with GPCR Kinases (GRKs). Biomolecules, 11 (3).

Charest PG, Terrillon S, Bouvier M. 2005. Monitoring agonist-promoted conformational changes of beta-arrestin in living cells by intramolecular BRET. EMBO Rep, 6 (4):334-340.

Cheloha RW, Gellman SH, Vilardaga JP, Gardella TJ. 2015. PTH receptor-1 signalling-mechanistic insights and therapeutic prospects. Nat Rev Endocrinol, 11 (12):712-724.

Chen Q, Plasencia M, Li Z, Mukherjee S, Patra D, Chen CL, Klose T, Yao XQ, Kossiakoff AA, Chang L, Andrews PC, Tesmer JJG. 2021. Structures of rhodopsin in complex with G-protein-coupled receptor kinase 1. Nature, 595 (7868):600-605.

Chen Q, Perry NA, Vishnivetskiy SA, Berndt S, Gilbert NC, Zhuo Y, Singh PK, Tholen J, Ohi MD, Gurevich EV, Brautigam CA, Klug CS, Gurevich VV, Iverson TM. 2017. Structural basis of arrestin-3 activation and signaling. Nat Commun, 8 (1):1427.

Cherezov V, Rosenbaum DM, Hanson MA, Rasmussen SG, Thian FS, Kobilka TS, Choi HJ, Kuhn P, Weis WI, Kobilka BK, Stevens RC. 2007. High-resolution crystal structure of an engineered human beta2-adrenergic G protein-coupled receptor. Science, 318 (5854):1258-1265.

Chuang TT, LeVine H, 3rd, De Blasi A. 1995. Phosphorylation and activation of beta-adrenergic receptor kinase by protein kinase C. J Biol Chem, 270 (31):18660-18665.

Claing A, Laporte SA, Caron MG, Lefkowitz RJ. 2002. Endocytosis of G protein-coupled receptors: roles of G protein-coupled receptor kinases and beta-arrestin proteins. Prog Neurobiol, 66 (2):61-79.

Clapham DE, Neer EJ. 1997. G protein beta gamma subunits. Annu Rev Pharmacol Toxicol, 37:167-203.

Conklin BR, Farfel Z, Lustig KD, Julius D, Bourne HR. 1993. Substitution of three amino acids switches receptor specificity of Gq alpha to that of Gi alpha. Nature, 363 (6426):274-276.

Conklin BR, Herzmark P, Ishida S, Voyno-Yasenetskaya TA, Sun Y, Farfel Z, Bourne HR. 1996. Carboxyl-terminal mutations of Gq alpha and Gs alpha that alter the fidelity of receptor activation. Mol Pharmacol, 50 (4):885-890.

Conner DA, Mathier MA, Mortensen RM, Christe M, Vatner SF, Seidman CE, Seidman JG. 1997. beta-Arrestin1 knockout mice appear normal but demonstrate altered cardiac responses to beta-adrenergic stimulation. Circ Res, 81 (6):1021-1026.

Dalle S, Ricketts W, Imamura T, Vollenweider P, Olefsky JM. 2001. Insulin and insulin-like growth factor I receptors utilize different G protein signaling components. J Biol Chem, 276 (19):15688-15695.

Delom F, Fessart D. 2011. Role of Phosphorylation in the Control of Clathrin-Mediated Internalization of GPCR. Int J Cell Biol, 2011:246954.

DeWire SM, Ahn S, Lefkowitz RJ, Shenoy SK. 2007. Beta-arrestins and cell signaling. Annu Rev Physiol, 69:483-510.

Doll C, Poll F, Peuker K, Loktev A, Gluck L, Schulz S. 2012. Deciphering micro-opioid receptor phosphorylation and dephosphorylation in HEK293 cells. Br J Pharmacol, 167 (6):1259-1270.

Downes GB, Gautam N. 1999. The G protein subunit gene families. Genomics, 62 (3):544-552.

Drube J, Haider RS, Matthees ESF, Reichel M, Zeiner J, Fritzwanker S, Ziegler C, Barz S, Klement L, Kliewer A, Miess E, Kostenis E, Schulz S, Hoffmann C. 2021. GRK2/3/5/6 knockout: The impact of individual GRKs on arrestin-binding and GPCR regulation. bioRxiv:2021.2002.2012.430971.

Eichel K, Jullie D, Barsi-Rhyne B, Latorraca NR, Masureel M, Sibarita JB, Dror RO, von Zastrow M. 2018. Catalytic activation of beta-arrestin by GPCRs. Nature, 557 (7705):381-386.

Ferrandon S, Feinstein TN, Castro M, Wang B, Bouley R, Potts JT, Gardella TJ, Vilardaga JP. 2009. Sustained cyclic AMP production by parathyroid hormone receptor endocytosis. Nat Chem Biol, 5 (10):734-742.

Förster t. 1948. Zwischenmolekulare Energiewanderung und Fluoreszenz. Annalen der Physik, 437:55-75.

Fredriksson R, Lagerstrom MC, Lundin LG, Schioth HB. 2003. The G-protein-coupled receptors in the human genome form five main families. Phylogenetic analysis, paralogon groups, and fingerprints. Mol Pharmacol, 63 (6):1256-1272.

Gesty-Palmer D, Chen M, Reiter E, Ahn S, Nelson CD, Wang S, Eckhardt AE, Cowan CL, Spurney RF, Luttrell LM, Lefkowitz RJ. 2006. Distinct beta-arrestin- and G protein-dependent pathways for parathyroid hormone receptor-stimulated ERK1/2 activation. J Biol Chem, 281 (16):10856-10864.

Ghosh E, Dwivedi H, Baidya M, Srivastava A, Kumari P, Stepniewski T, Kim HR, Lee MH, van Gastel J, Chaturvedi M, Roy D, Pandey S, Maharana J, Guixa-Gonzalez R, Luttrell LM, Chung KY, Dutta S, Selent J, Shukla AK. 2019. Conformational Sensors and Domain Swapping Reveal Structural and Functional Differences between beta-Arrestin Isoforms. Cell Rep, 28 (13):3287-3299 e3286.

Gibson DG, Young L, Chuang RY, Venter JC, Hutchison CA, 3rd, Smith HO. 2009. Enzymatic assembly of DNA molecules up to several hundred kilobases. Nat Methods, 6 (5):343-345.

Girnita L, Worrall C, Takahashi S, Seregard S, Girnita A. 2014. Something old, something new and something borrowed: emerging paradigm of insulin-like growth factor type 1 receptor (IGF-1R) signaling regulation. Cell Mol Life Sci, 71 (13):2403-2427.

Girnita L, Shenoy SK, Sehat B, Vasilcanu R, Vasilcanu D, Girnita A, Lefkowitz RJ, Larsson O. 2007. Beta-arrestin and Mdm2 mediate IGF-1 receptor-stimulated ERK activation and cell cycle progression. J Biol Chem, 282 (15):11329-11338.

Godbole A, Lyga S, Lohse MJ, Calebiro D. 2017. Internalized TSH receptors en route to the TGN induce local Gs-protein signaling and gene transcription. Nat Commun, 8 (1):443.

Goodman OB, Jr., Krupnick JG, Santini F, Gurevich VV, Penn RB, Gagnon AW, Keen JH, Benovic JL. 1996. Beta-arrestin acts as a clathrin adaptor in endocytosis of the beta2-adrenergic receptor. Nature, 383 (6599):447-450.

Graham FL, Smiley J, Russell WC, Nairn R. 1977. Characteristics of a human cell line transformed by DNA from human adenovirus type 5. J Gen Virol, 36 (1):59-74.

Gurevich EV, Tesmer JJ, Mushegian A, Gurevich VV. 2012. G protein-coupled receptor kinases: more than just kinases and not only for GPCRs. Pharmacol Ther, 133 (1):40-69.

Gurevich VV, Gurevich EV. 2017. Molecular Mechanisms of GPCR Signaling: A Structural Perspective. Int J Mol Sci, 18 (12).

Gurevich VV, Gurevich EV. 2018. Arrestin-mediated signaling: Is there a controversy? World J Biol Chem, 9 (3):25-35.

Haider RS, Godbole A, Hoffmann C. 2019a. To sense or not to sense-new insights from GPCR-based and arrestin-based biosensors. Curr Opin Cell Biol, 57:16-24.

Haider RS, Rizk A, Schertler GFX, Ostermaier MK. 2017. Comprehensive analysis of the role of arrestin residues in receptor binding. In: Gurevich VV, Hrsg. The structural basis of arrestin functions. Cham: Springer, 83-102.

Haider RS, Wilhelm F, Rizk A, Mutt E, Deupi X, Peterhans C, Muhle J, Berger P, Schertler GFX, Standfuss J, Ostermaier MK. 2019b. Arrestin-1 engineering facilitates complex stabilization with native rhodopsin. Sci Rep, 9 (1):439.

Hall MP, Unch J, Binkowski BF, Valley MP, Butler BL, Wood MG, Otto P, Zimmerman K, Vidugiris G, Machleidt T, Robers MB, Benink HA, Eggers CT, Slater MR, Meisenheimer PL, Klaubert DH, Fan F, Encell LP, Wood KV. 2012. Engineered luciferase reporter from a deep sea shrimp utilizing a novel imidazopyrazinone substrate. ACS Chem Biol, 7 (11):1848-1857.

Hauser AS, Attwood MM, Rask-Andersen M, Schioth HB, Gloriam DE. 2017. Trends in GPCR drug discovery: new agents, targets and indications. Nat Rev Drug Discov, 16 (12):829-842.

Hendy GN, Bennett HP, Gibbs BF, Lazure C, Day R, Seidah NG. 1995. Proparathyroid hormone is preferentially cleaved to parathyroid hormone by the prohormone convertase furin. A mass spectrometric study. J Biol Chem, 270 (16):9517-9525.

Hirsch JA, Schubert C, Gurevich VV, Sigler PB. 1999. The 2.8 A crystal structure of visual arrestin: a model for arrestin's regulation. Cell, 97 (2):257-269.

Ho B, Baryshnikova A, Brown GW. 2018. Unification of Protein Abundance Datasets Yields a Quantitative Saccharomyces cerevisiae Proteome. Cell Syst, 6 (2):192-205 e193.

Hoare SRJ, Tewson PH, Quinn AM, Hughes TE. 2020. A kinetic method for measuring agonist efficacy and ligand bias using high resolution biosensors and a kinetic data analysis framework. Sci Rep, 10 (1):1766.

Hoffmann C, Gaietta G, Zurn A, Adams SR, Terrillon S, Ellisman MH, Tsien RY, Lohse MJ. 2010. Fluorescent labeling of tetracysteine-tagged proteins in intact cells. Nat Protoc, 5 (10):1666-1677.

Homan KT, Tesmer JJ. 2014. Structural insights into G protein-coupled receptor kinase function. Curr Opin Cell Biol, 27:25-31.

Huang W, Masureel M, Qu Q, Janetzko J, Inoue A, Kato HE, Robertson MJ, Nguyen KC, Glenn JS, Skiniotis G, Kobilka BK. 2020. Structure of the neurotensin receptor 1 in complex with beta-arrestin 1. Nature, 579 (7798):303-308.

Inoue A, Raimondi F, Kadji FMN, Singh G, Kishi T, Uwamizu A, Ono Y, Shinjo Y, Ishida S, Arang N, Kawakami K, Gutkind JS, Aoki J, Russell RB. 2019. Illuminating G-Protein-Coupling Selectivity of GPCRs. Cell, 177 (7):1933-1947 e1925.

Kang Y, Gao X, Zhou XE, He Y, Melcher K, Xu HE. 2016. A structural snapshot of the rhodopsin-arrestin complex. FEBS J, 283 (5):816-821.

Kang Y, Zhou XE, Gao X, He Y, Liu W, Ishchenko A, Barty A, White TA, Yefanov O, Han GW, Xu Q, de Waal PW, Ke J, Tan MH, Zhang C, Moeller A, West GM, Pascal BD, Van Eps N, Caro LN, Vishnivetskiy SA, Lee RJ, Suino-Powell KM, Gu X, Pal K, Ma J, Zhi X, Boutet S, Williams GJ, Messerschmidt M, Gati C, Zatsepin NA, Wang D, James D, Basu S, Roy-Chowdhury S, Conrad CE, Coe J, Liu H, Lisova S, Kupitz C, Grotjohann I, Fromme R, Jiang Y, Tan M, Yang H, Li J, Wang M, Zheng Z, Li D, Howe N, Zhao Y, Standfuss J, Diederichs K, Dong Y, Potter CS, Carragher B, Caffrey M, Jiang H, Chapman HN, Spence JC, Fromme P, Weierstall U, Ernst OP, Katritch V, Gurevich VV, Griffin PR, Hubbell WL, Stevens RC, Cherezov V, Melcher K, Xu HE. 2015. Crystal structure of rhodopsin bound to arrestin by femtosecond X-ray laser. Nature, 523 (7562):561-567.

Katritch V, Cherezov V, Stevens RC. 2012. Diversity and modularity of G protein-coupled receptor structures. Trends Pharmacol Sci, 33 (1):17-27.

Katritch V, Cherezov V, Stevens RC. 2013. Structure-function of the G protein-coupled receptor superfamily. Annu Rev Pharmacol Toxicol, 53:531-556.

Kim J, Ahn S, Ren XR, Whalen EJ, Reiter E, Wei H, Lefkowitz RJ. 2005. Functional antagonism of different G protein-coupled receptor kinases for beta-arrestin-mediated angiotensin II receptor signaling. Proc Natl Acad Sci U S A, 102 (5):1442-1447.

Kim YJ, Hofmann KP, Ernst OP, Scheerer P, Choe HW, Sommer ME. 2013. Crystal structure of pre-activated arrestin p44. Nature, 497 (7447):142-146.

Kohout TA, Lin FS, Perry SJ, Conner DA, Lefkowitz RJ. 2001. beta-Arrestin 1 and 2 differentially regulate heptahelical receptor signaling and trafficking. Proc Natl Acad Sci U S A, 98 (4):1601-1606.

Komolov KE, Benovic JL. 2018. G protein-coupled receptor kinases: Past, present and future. Cell Signal, 41:17-24.

Krasel C, Bunemann M, Lorenz K, Lohse MJ. 2005. Beta-arrestin binding to the beta2-adrenergic receptor requires both receptor phosphorylation and receptor activation. J Biol Chem, 280 (10):9528-9535.

Krasel C, Zabel U, Lorenz K, Reiner S, Al-Sabah S, Lohse MJ. 2008. Dual role of the beta2-adrenergic receptor C terminus for the binding of beta-arrestin and receptor internalization. J Biol Chem, 283 (46):31840-31848.

Krupnick JG, Goodman OB, Jr., Keen JH, Benovic JL. 1997. Arrestin/clathrin interaction. Localization of the clathrin binding domain of nonvisual arrestins to the carboxy terminus. J Biol Chem, 272 (23):15011-15016.

Lagerstrom MC, Schioth HB. 2008. Structural diversity of G protein-coupled receptors and significance for drug discovery. Nat Rev Drug Discov, 7 (4):339-357.

Lally CC, Bauer B, Selent J, Sommer ME. 2017. C-edge loops of arrestin function as a membrane anchor. Nat Commun, 8:14258.

Laporte SA, Oakley RH, Holt JA, Barak LS, Caron MG. 2000. The interaction of beta-arrestin with the AP-2 adaptor is required for the clustering of beta 2-adrenergic receptor into clathrin-coated pits. J Biol Chem, 275 (30):23120-23126.

Latorraca NR, Masureel M, Hollingsworth SA, Heydenreich FM, Suomivuori CM, Brinton C, Townshend RJL, Bouvier M, Kobilka BK, Dror RO. 2020. How GPCR Phosphorylation Patterns Orchestrate Arrestin-Mediated Signaling. Cell, 183 (7):1813-1825 e1818.

Lee MH, Appleton KM, Strungs EG, Kwon JY, Morinelli TA, Peterson YK, Laporte SA, Luttrell LM. 2016. The conformational signature of beta-arrestin2 predicts its trafficking and signalling functions. Nature, 531 (7596):665-668.

Lee Y, Warne T, Nehme R, Pandey S, Dwivedi-Agnihotri H, Chaturvedi M, Edwards PC, Garcia-Nafria J, Leslie AGW, Shukla AK, Tate CG. 2020. Molecular basis of beta-arrestin coupling to formoterol-bound beta1-adrenoceptor. Nature, 583 (7818):862-866.

Lefkowitz RJ. 2000. The superfamily of heptahelical receptors. Nat Cell Biol, 2 (7):E133-136.

Lefkowitz RJ. 2013. A brief history of G-protein coupled receptors (Nobel Lecture). Angew Chem Int Ed Engl, 52 (25):6366-6378.

Lohse MJ, Nuber S, Hoffmann C. 2012. Fluorescence/bioluminescence resonance energy transfer techniques to study G-protein-coupled receptor activation and signaling. Pharmacol Rev, 64 (2):299-336.

Los GV, Encell LP, McDougall MG, Hartzell DD, Karassina N, Zimprich C, Wood MG, Learish R, Ohana RF, Urh M, Simpson D, Mendez J, Zimmerman K, Otto P, Vidugiris G, Zhu J, Darzins A, Klaubert DH, Bulleit RF, Wood KV. 2008. HaloTag: a novel protein labeling technology for cell imaging and protein analysis. ACS Chem Biol, 3 (6):373-382.

Manglik A, Kim TH, Masureel M, Altenbach C, Yang Z, Hilger D, Lerch MT, Kobilka TS, Thian FS, Hubbell WL, Prosser RS, Kobilka BK. 2015. Structural Insights into the Dynamic Process of beta2-Adrenergic Receptor Signaling. Cell, 161 (5):1101-1111.

Matthees ESF, Haider RS, Hoffmann C. 2020. β-arrestin–based biosensors: Tools to explore structural determinants of metabolic functions? Current Opinion in Endocrine and Metabolic Research, Volume 16 (2021):Pages 66-74.

Matthees ESF, Haider RS, Hoffmann C, Drube J. 2021. Differential Regulation of GPCRs-Are GRK Expression Levels the Key? Front Cell Dev Biol, 9:687489.

Mayer D, Damberger FF, Samarasimhareddy M, Feldmueller M, Vuckovic Z, Flock T, Bauer B, Mutt E, Zosel F, Allain FHT, Standfuss J, Schertler GFX, Deupi X, Sommer ME, Hurevich M, Friedler A, Veprintsev DB. 2019. Distinct G protein-coupled receptor phosphorylation motifs modulate arrestin affinity and activation and global conformation. Nat Commun, 10 (1):1261.

Miess E, Gondin AB, Yousuf A, Steinborn R, Mosslein N, Yang Y, Goldner M, Ruland JG, Bunemann M, Krasel C, Christie MJ, Halls ML, Schulz S, Canals M. 2018. Multisite phosphorylation is required for sustained interaction with GRKs and arrestins during rapid mu-opioid receptor desensitization. Sci Signal, 11 (539).

Min K, Yoon HJ, Park JY, Baidya M, Dwivedi-Agnihotri H, Maharana J, Chaturvedi M, Chung KY, Shukla AK, Lee HH. 2020a. Crystal Structure of beta-Arrestin 2 in Complex with CXCR7 Phosphopeptide. Structure, 28 (9):1014-1023 e1014.

Min K, Yoon HJ, Park JY, Baidya M, Dwivedi-Agnihotri H, Maharana J, Chaturvedi M, Chung KY, Shukla AK, Lee HH. 2020b. Crystal Structure of beta-Arrestin 2 in Complex with CXCR7 Phosphopeptide. Structure.

Moller TC, Pedersen MF, van Senten JR, Seiersen SD, Mathiesen JM, Bouvier M, Brauner-Osborne H. 2020. Dissecting the roles of GRK2 and GRK3 in mu-opioid receptor internalization and beta-arrestin2 recruitment using CRISPR/Cas9-edited HEK293 cells. Sci Rep, 10 (1):17395.

Moore CA, Milano SK, Benovic JL. 2007. Regulation of receptor trafficking by GRKs and arrestins. Annu Rev Physiol, 69:451-482.

Mou L, Gates A, Mosser VA, Tobin A, Jackson DA. 2006. Transient hypoxia induces sequestration of M1 and M2 muscarinic acetylcholine receptors. J Neurochem, 96 (2):510-519.

Mushegian A, Gurevich VV, Gurevich EV. 2012. The origin and evolution of G protein-coupled receptor kinases. PLoS One, 7 (3):e33806.

Nguyen AH, Thomsen ARB, Cahill TJ, 3rd, Huang R, Huang LY, Marcink T, Clarke OB, Heissel S, Masoudi A, Ben-Hail D, Samaan F, Dandey VP, Tan YZ, Hong C, Mahoney JP, Triest S, Little Jt, Chen X, Sunahara R, Steyaert J, Molina H, Yu Z, des Georges A, Lefkowitz RJ. 2019. Structure of an endosomal signaling GPCR-G protein-beta-arrestin megacomplex. Nat Struct Mol Biol, 26 (12):1123-1131.

Nobles KN, Guan Z, Xiao K, Oas TG, Lefkowitz RJ. 2007. The active conformation of beta-arrestin1: direct evidence for the phosphate sensor in the N-domain and conformational differences in the active states of beta-arrestins1 and -2. J Biol Chem, 282 (29):21370-21381.

Nobles KN, Xiao K, Ahn S, Shukla AK, Lam CM, Rajagopal S, Strachan RT, Huang TY, Bressler EA, Hara MR, Shenoy SK, Gygi SP, Lefkowitz RJ. 2011. Distinct phosphorylation sites on the beta(2)-adrenergic receptor establish a barcode that encodes differential functions of beta-arrestin. Sci Signal, 4 (185):ra51.

Nuber S, Zabel U, Lorenz K, Nuber A, Milligan G, Tobin AB, Lohse MJ, Hoffmann C. 2016. beta-Arrestin biosensors reveal a rapid, receptor-dependent activation/deactivation cycle. Nature, 531 (7596):661-664.

O'Hayre M, Eichel K, Avino S, Zhao X, Steffen DJ, Feng X, Kawakami K, Aoki J, Messer K, Sunahara R, Inoue A, von Zastrow M, Gutkind JS. 2017. Genetic evidence that beta-arrestins are dispensable for the initiation of beta2-adrenergic receptor signaling to ERK. Sci Signal, 10 (484).

Oakley RH, Laporte SA, Holt JA, Barak LS, Caron MG. 1999. Association of beta-arrestin with G protein-coupled receptors during clathrin-mediated endocytosis dictates the profile of receptor resensitization. J Biol Chem, 274 (45):32248-32257.

Oishi A, Dam J, Jockers R. 2020. beta-Arrestin-2 BRET Biosensors Detect Different beta-Arrestin-2 Conformations in Interaction with GPCRs. ACS Sens, 5 (1):57-64.

Oldham WM, Hamm HE. 2008. Heterotrimeric G protein activation by G-protein-coupled receptors. Nat Rev Mol Cell Biol, 9 (1):60-71.

Ostermaier MK, Peterhans C, Jaussi R, Deupi X, Standfuss J. 2014. Functional map of arrestin-1 at single amino acid resolution. Proc Natl Acad Sci U S A, 111 (5):1825-1830.

Palczewski K, Buczylko J, Lebioda L, Crabb JW, Polans AS. 1993. Identification of the N-terminal region in rhodopsin kinase involved in its interaction with rhodopsin. J Biol Chem, 268 (8):6004-6013.

Peterhans C, Lally CC, Ostermaier MK, Sommer ME, Standfuss J. 2016. Functional map of arrestin binding to phosphorylated opsin, with and without agonist. Sci Rep, 6:28686.

Pierce KL, Premont RT, Lefkowitz RJ. 2002. Seven-transmembrane receptors. Nat Rev Mol Cell Biol, 3 (9):639-650.

Pollok-Kopp B, Huttenrauch F, Rethorn S, Oppermann M. 2007. Dynamics of protein kinase C-mediated phosphorylation of the complement C5a receptor on serine 334. J Biol Chem, 282 (7):4345-4353.

Pronin AN, Benovic JL. 1997. Regulation of the G protein-coupled receptor kinase GRK5 by protein kinase C. J Biol Chem, 272 (6):3806-3812.

Rasmussen SG, DeVree BT, Zou Y, Kruse AC, Chung KY, Kobilka TS, Thian FS, Chae PS, Pardon E, Calinski D, Mathiesen JM, Shah ST, Lyons JA, Caffrey M, Gellman SH, Steyaert J, Skiniotis G, Weis WI, Sunahara RK, Kobilka BK. 2011. Crystal structure of the beta2 adrenergic receptor-Gs protein complex. Nature, 477 (7366):549-555.

Reiner S, Ambrosio M, Hoffmann C, Lohse MJ. 2010. Differential signaling of the endogenous agonists at the beta2-adrenergic receptor. J Biol Chem, 285 (46):36188-36198.

Ren XR, Reiter E, Ahn S, Kim J, Chen W, Lefkowitz RJ. 2005. Different G protein-coupled receptor kinases govern G protein and beta-arrestin-mediated signaling of V2 vasopressin receptor. Proc Natl Acad Sci U S A, 102 (5):1448-1453.

Reyes-Alcaraz A, Lee YN, Yun S, Hwang JI, Seong JY. 2018. Conformational signatures in beta-arrestin2 reveal natural biased agonism at a G-protein-coupled receptor. Commun Biol, 1:128.

Rizk A, Mansouri M, Ballmer-Hofer K, Berger P. 2015. Subcellular object quantification with Squassh3C and SquasshAnalyst. Biotechniques, 59 (5):309-312.

Rizk A, Paul G, Incardona P, Bugarski M, Mansouri M, Niemann A, Ziegler U, Berger P, Sbalzarini IF. 2014. Segmentation and quantification of subcellular structures in fluorescence microscopy images using Squassh. Nat Protoc, 9 (3):586-596.

Santos R, Ursu O, Gaulton A, Bento AP, Donadi RS, Bologa CG, Karlsson A, Al-Lazikani B, Hersey A, Oprea TI, Overington JP. 2017. A comprehensive map of molecular drug targets. Nat Rev Drug Discov, 16 (1):19-34.

Schihada H, Vandenabeele S, Zabel U, Frank M, Lohse MJ, Maiellaro I. 2018. A universal bioluminescence resonance energy transfer sensor design enables high-sensitivity screening of GPCR activation dynamics. Commun Biol, 1:105.

Schipani E, Langman CB, Parfitt AM, Jensen GS, Kikuchi S, Kooh SW, Cole WG, Juppner H. 1996. Constitutively activated receptors for parathyroid hormone and parathyroid hormone-related peptide in Jansen's metaphyseal chondrodysplasia. N Engl J Med, 335 (10):708-714.

Seibold A, Williams B, Huang ZF, Friedman J, Moore RH, Knoll BJ, Clark RB. 2000. Localization of the sites mediating desensitization of the beta(2)-adrenergic receptor by the GRK pathway. Mol Pharmacol, 58 (5):1162-1173.

Sente A, Peer R, Srivastava A, Baidya M, Lesk AM, Balaji S, Shukla AK, Babu MM, Flock T. 2018. Molecular mechanism of modulating arrestin conformation by GPCR phosphorylation. Nat Struct Mol Biol, 25 (6):538-545.

Shukla AK, Manglik A, Kruse AC, Xiao K, Reis RI, Tseng WC, Staus DP, Hilger D, Uysal S, Huang LY, Paduch M, Tripathi-Shukla P, Koide A, Koide S, Weis WI, Kossiakoff AA, Kobilka BK, Lefkowitz RJ. 2013. Structure of active beta-arrestin-1 bound to a G-protein-coupled receptor phosphopeptide. Nature, 497 (7447):137-141.

Shukla AK, Westfield GH, Xiao K, Reis RI, Huang LY, Tripathi-Shukla P, Qian J, Li S, Blanc A, Oleskie AN, Dosey AM, Su M, Liang CR, Gu LL, Shan JM, Chen X, Hanna R, Choi M, Yao XJ, Klink BU, Kahsai AW, Sidhu SS, Koide S, Penczek PA, Kossiakoff AA, Woods VL, Jr., Kobilka BK, Skiniotis G, Lefkowitz RJ. 2014. Visualization of arrestin recruitment by a G-protein-coupled receptor. Nature, 512 (7513):218-222.

Singer SJ, Nicolson GL. 1972. The fluid mosaic model of the structure of cell membranes. Science, 175 (4023):720-731.

Staus DP, Hu H, Robertson MJ, Kleinhenz ALW, Wingler LM, Capel WD, Latorraca NR, Lefkowitz RJ, Skiniotis G. 2020. Structure of the M2 muscarinic receptor-beta-arrestin complex in a lipid nanodisc. Nature, 579 (7798):297-302.

Sutkeviciute I, Vilardaga JP. 2020. Structural insights into emergent signaling modes of G protein-coupled receptors. J Biol Chem, 295 (33):11626-11642.

Teixeira LB, Parreiras ESLT, Bruder-Nascimento T, Duarte DA, Simoes SC, Costa RM, Rodriguez DY, Ferreira PAB, Silva CAA, Abrao EP, Oliveira EB, Bouvier M, Tostes RC, Costa-Neto CM. 2017. Ang-(1-7) is an endogenous beta-arrestin-biased agonist of the AT1 receptor with protective action in cardiac hypertrophy. Sci Rep, 7 (1):11903.

Tesmer VM, Kawano T, Shankaranarayanan A, Kozasa T, Tesmer JJ. 2005. Snapshot of activated G proteins at the membrane: the Galphaq-GRK2-Gbetagamma complex. Science, 310 (5754):1686-1690.

Thomsen ARB, Plouffe B, Cahill TJ, 3rd, Shukla AK, Tarrasch JT, Dosey AM, Kahsai AW, Strachan RT, Pani B, Mahoney JP, Huang L, Breton B, Heydenreich FM, Sunahara RK, Skiniotis G, Bouvier M, Lefkowitz RJ. 2016. GPCR-G Protein-beta-Arrestin Super-Complex Mediates Sustained G Protein Signaling. Cell, 166 (4):907-919.

Thul PJ, Akesson L, Wiking M, Mahdessian D, Geladaki A, Ait Blal H, Alm T, Asplund A, Bjork L, Breckels LM, Backstrom A, Danielsson F, Fagerberg L, Fall J, Gatto L, Gnann C, Hober S, Hjelmare M, Johansson F, Lee S, Lindskog C, Mulder J, Mulvey CM, Nilsson P, Oksvold P, Rockberg J, Schutten R, Schwenk JM, Sivertsson A, Sjostedt E, Skogs M, Stadler C, Sullivan DP, Tegel H, Winsnes C, Zhang C, Zwahlen M, Mardinoglu A, Ponten F, von Feilitzen K, Lilley KS, Uhlen M, Lundberg E. 2017. A subcellular map of the human proteome. Science, 356 (6340).

Torrecilla I, Spragg EJ, Poulin B, McWilliams PJ, Mistry SC, Blaukat A, Tobin AB. 2007. Phosphorylation and regulation of a G protein-coupled receptor by protein kinase CK2. J Cell Biol, 177 (1):127-137.

Tran TM, Friedman J, Qunaibi E, Baameur F, Moore RH, Clark RB. 2004. Characterization of agonist stimulation of cAMP-dependent protein kinase and G protein-coupled receptor kinase phosphorylation of the beta2-adrenergic receptor using phosphoserine-specific antibodies. Mol Pharmacol, 65 (1):196-206.

Vaidehi N, Kenakin T. 2010. The role of conformational ensembles of seven transmembrane receptors in functional selectivity. Curr Opin Pharmacol, 10 (6):775-781.

Venter JC, Adams MD, Myers EW, Li PW, Mural RJ, Sutton GG, Smith HO, Yandell M, Evans CA, Holt RA, Gocayne JD, Amanatides P, Ballew RM, Huson DH, Wortman JR, Zhang Q, Kodira CD, Zheng XH, Chen L, Skupski M, Subramanian G, Thomas PD, Zhang J, Gabor Miklos GL, Nelson C, Broder S, Clark AG, Nadeau J, McKusick VA, Zinder N, Levine AJ, Roberts RJ, Simon M, Slayman C, Hunkapiller M, Bolanos R, Delcher A, Dew I, Fasulo D, Flanigan M, Florea L, Halpern A, Hannenhalli S, Kravitz S, Levy S, Mobarry C, Reinert K, Remington K, Abu-Threideh J, Beasley E, Biddick K, Bonazzi V, Brandon R, Cargill M, Chandramouliswaran I, Charlab R, Chaturvedi K, Deng Z, Di Francesco V, Dunn P, Eilbeck K, Evangelista C, Gabrielian AE, Gan W, Ge W, Gong F, Gu Z, Guan P, Heiman TJ, Higgins ME, Ji RR, Ke Z, Ketchum KA, Lai Z, Lei Y, Li Z, Li J, Liang Y, Lin X, Lu F, Merkulov GV, Milshina N, Moore HM, Naik AK, Narayan VA, Neelam B, Nusskern D, Rusch DB, Salzberg S, Shao W, Shue B, Sun J, Wang Z, Wang A, Wang X, Wang J, Wei M, Wides R, Xiao C, Yan C, Yao A, Ye J, Zhan M, Zhang W, Zhang H, Zhao Q, Zheng L, Zhong F, Zhong W, Zhu S, Zhao S, Gilbert D, Baumhueter S, Spier G, Carter C, Cravchik A, Woodage T, Ali F, An H, Awe A, Baldwin D, Baden H, Barnstead M, Barrow I, Beeson K, Busam D, Carver A, Center A, Cheng ML, Curry L, Danaher S, Davenport L, Desilets R, Dietz S, Dodson K, Doup L, Ferriera S, Garg N, Gluecksmann A, Hart B, Haynes J, Haynes C, Heiner C, Hladun S, Hostin D, Houck J, Howland T, Ibegwam C, Johnson J, Kalush F, Kline L, Koduru S, Love A, Mann F, May D, McCawley S, McIntosh T, McMullen I, Moy M, Moy L, Murphy B, Nelson K, Pfannkoch C, Pratts E, Puri V, Qureshi H, Reardon M, Rodriguez R, Rogers YH, Romblad D, Ruhfel B, Scott R, Sitter C, Smallwood M, Stewart E, Strong R, Suh E, Thomas R, Tint NN, Tse S, Vech C, Wang G, Wetter J, Williams S, Williams M, Windsor S, Winn-Deen E, Wolfe K, Zaveri J, Zaveri K, Abril JF, Guigo R, Campbell MJ, Sjolander KV, Karlak B, Kejariwal A, Mi H, Lazareva B, Hatton T, Narechania A, Diemer K, Muruganujan A, Guo N, Sato S, Bafna V, Istrail S, Lippert R, Schwartz R, Walenz B, Yooseph S, Allen D, Basu A, Baxendale J, Blick L, Caminha M, Carnes-Stine J, Caulk P, Chiang YH, Coyne M, Dahlke C, Mays A, Dombroski M, Donnelly M, Ely D, Esparham S, Fosler C, Gire H, Glanowski S, Glasser K, Glodek A, Gorokhov M, Graham K, Gropman B, Harris M, Heil J, Henderson S, Hoover J, Jennings D, Jordan C, Jordan J, Kasha J, Kagan L, Kraft C, Levitsky A, Lewis M, Liu X, Lopez J, Ma D, Majoros W, McDaniel J, Murphy S, Newman M, Nguyen T, Nguyen N, Nodell M, Pan S, Peck J, Peterson M, Rowe W, Sanders R, Scott J, Simpson M, Smith T, Sprague A, Stockwell T, Turner R, Venter E, Wang M, Wen M, Wu D, Wu M, Xia A, Zandieh A, Zhu X. 2001. The sequence of the human genome. Science, 291 (5507):1304-1351.

Vilardaga JP, Romero G, Friedman PA, Gardella TJ. 2011. Molecular basis of parathyroid hormone receptor signaling and trafficking: a family B GPCR paradigm. Cell Mol Life Sci, 68 (1):1-13.

Vilardaga JP, Krasel C, Chauvin S, Bambino T, Lohse MJ, Nissenson RA. 2002. Internalization determinants of the parathyroid hormone receptor differentially regulate beta-arrestin/receptor association. J Biol Chem, 277 (10):8121-8129.

Vogel R, Mahalingam M, Ludeke S, Huber T, Siebert F, Sakmar TP. 2008. Functional role of the "ionic lock"--an interhelical hydrogen-bond network in family A heptahelical receptors. J Mol Biol, 380 (4):648-655.

White AD, Jean-Alphonse FG, Fang F, Pena KA, Liu S, Konig GM, Inoue A, Aslanoglou D, Gellman SH, Kostenis E, Xiao K, Vilardaga JP. 2020. Gq/11-dependent regulation of endosomal cAMP generation by parathyroid hormone class B GPCR. Proc Natl Acad Sci U S A, 117 (13):7455-7460.

Wiens MD, Campbell RE. 2018. Surveying the landscape of optogenetic methods for detection of protein-protein interactions. Wiley Interdiscip Rev Syst Biol Med, 10 (3):e1415.

Winstel R, Freund S, Krasel C, Hoppe E, Lohse MJ. 1996. Protein kinase cross-talk: membrane targeting of the beta-adrenergic receptor kinase by protein kinase C. Proc Natl Acad Sci U S A, 93 (5):2105-2109.

Xiao K, Liu H. 2016. "Barcode" and Differential Effects of GPCR Phosphorylation by Different GRKs. In: Gurevich V. GE, Tesmer J. , Hrsg. G Protein-Coupled Receptor Kinases. Methods in Pharmacology and Toxicology: Humana Press, New York, 75-120.

Xiao K, McClatchy DB, Shukla AK, Zhao Y, Chen M, Shenoy SK, Yates JR, 3rd, Lefkowitz RJ. 2007. Functional specialization of beta-arrestin interactions revealed by proteomic analysis. Proc Natl Acad Sci U S A, 104 (29):12011-12016.

Yang F, Yu X, Liu C, Qu CX, Gong Z, Liu HD, Li FH, Wang HM, He DF, Yi F, Song C, Tian CL, Xiao KH, Wang JY, Sun JP. 2015. Phospho-selective mechanisms of arrestin conformations and functions revealed by unnatural amino acid incorporation and (19)F-NMR. Nat Commun, 6:8202.

Yin W, Li Z, Jin M, Yin YL, de Waal PW, Pal K, Yin Y, Gao X, He Y, Gao J, Wang X, Zhang Y, Zhou H, Melcher K, Jiang Y, Cong Y, Edward Zhou X, Yu X, Eric Xu H. 2019. A complex structure of arrestin-2 bound to a G protein-coupled receptor. Cell Res, 29 (12):971-983.

Zhan X, Gimenez LE, Gurevich VV, Spiller BW. 2011. Crystal structure of arrestin-3 reveals the basis of the difference in receptor binding between two non-visual subtypes. J Mol Biol, 406 (3):467-478.

Zhang JH, Chung TD, Oldenburg KR. 1999. A Simple Statistical Parameter for Use in Evaluation and Validation of High Throughput Screening Assays. J Biomol Screen, 4 (2):67-73.

Zhao LH, Ma S, Sutkeviciute I, Shen DD, Zhou XE, de Waal PW, Li CY, Kang Y, Clark LJ, Jean-Alphonse FG, White AD, Yang D, Dai A, Cai X, Chen J, Li C, Jiang Y, Watanabe T, Gardella TJ, Melcher K, Wang MW, Vilardaga JP, Xu HE, Zhang Y. 2019. Structure and dynamics of the active human parathyroid hormone receptor-1. Science, 364 (6436):148-153.

Zhou XE, He Y, de Waal PW, Gao X, Kang Y, Van Eps N, Yin Y, Pal K, Goswami D, White TA, Barty A, Latorraca NR, Chapman HN, Hubbell WL, Dror RO, Stevens RC, Cherezov V, Gurevich VV, Griffin PR, Ernst OP, Melcher K, Xu HE. 2017. Identification of Phosphorylation Codes for Arrestin Recruitment by G Protein-Coupled Receptors. Cell, 170 (3):457-469 e413.

Zhu W, Tilley DG, Myers VD, Coleman RC, Feldman AM. 2013. Arginine vasopressin enhances cell survival via a G protein-coupled receptor kinase 2/beta-arrestin1/extracellular-regulated kinase 1/2-dependent pathway in H9c2 cells. Mol Pharmacol, 84 (2):227-235.

Zindel D, Engel S, Bottrill AR, Pin JP, Prezeau L, Tobin AB, Bunemann M, Krasel C, Butcher AJ. 2016. Identification of key phosphorylation sites in PTH1R that determine arrestin3 binding and fine-tune receptor signaling. Biochem J, 473 (22):4173-4192.